

# Uspostava modela eksplantata jetrenih metastaza duktalnog adenokarcinoma gušterače za istraživanja staničnih interakcija

---

Šutevski, Iva

Master's thesis / Diplomski rad

2021

Degree Grantor / Ustanova koja je dodijelila akademski / stručni stupanj: **University of Zagreb, Faculty of Science / Sveučilište u Zagrebu, Prirodoslovno-matematički fakultet**

Permanent link / Trajna poveznica: <https://um.nsk.hr/um:nbn:hr:217:446025>

Rights / Prava: [In copyright](#) / [Zaštićeno autorskim pravom.](#)

Download date / Datum preuzimanja: **2024-04-28**



Repository / Repozitorij:

[Repository of the Faculty of Science - University of Zagreb](#)



Sveučilište u Zagrebu  
Prirodoslovno-matematički fakultet  
Biološki odsjek

Iva Šutevski

**Uspostava modela eksplantata jetrenih metastaza  
duktalnog adenokarcinoma gušterače za istraživanja  
staničnih interakcija**

Diplomski rad



Zagreb, 2021.

University of Zagreb  
Faculty of Science  
Department of Biology

Iva Šutevski

**Establishment of a pancreatic ductal adenocarcinoma  
liver metastases explant model for cell interaction  
studies**

Master thesis

Zagreb, 2021.

This thesis was created in Marco Gerling's group at Karolinska Institutet in Stockholm, under the supervision of Dr. med. Marco Gerling, co-supervision of Dr Natalie Geyer, and Professor Nada Oršolić. The thesis is submitted for grading to the Department of Biology at the Faculty of Science, University of Zagreb, with the aim of obtaining a Master's degree in molecular biology.

Firstly, I would like to thank my mentor Marco Gerling for the opportunity to do a summer internship followed by master thesis research in his group at Karolinska Institute. The guidance and discussions together with supervisor Natalie Geyer helped plan and conduct the experiments. This was a priceless experience, through which I have learned a lot and become more independent with experiments. I am also grateful to Carlos Fernandez Moro for the help with vibratome sectioning and histology analysis, and to Arash Chitzasan for the daily scientific chats.

Furthermore, I am thankful to my co-mentor Nada Oršolić for all the advice and help with my thesis, and the knowledge passed on through the courses.

Finally, I thank my family for always believing in me, and my friends for all the support.

# TEMELJNA DOKUMENTACIJSKA KARTICA

---

Sveučilište u Zagrebu  
Prirodoslovno-matematički fakultet  
Biološki odsjek

Diplomski rad

## Uspostava modela eksplantata jetrenih metastaza duktalnog adenokarcinoma gušterače za istraživanja staničnih interakcija

Iva Šutevski

Rooseveltov trg 6, 10000 Zagreb, Hrvatska

Duktalni adenokarcinom gušterače (PDAC, engl. pancreatic ductal adenocarcinoma) karakterizira izrazito loša prognoza, te mali napredak u klinici u posljednjih 30 godina. U trenutku postavljanje dijagnoze, većina pacijenata već ima udaljene metastaze, koje su najčešći uzrok smrti. Glavno mjesto metastaziranja gastrointestinalnih tumora je jetra. Unatoč tome, malo se zna o interakcijama tumora i okolnih stanica kod PDAC jetrenih metastaza. Cilj ovog rada je bio uspostaviti model eksplantata PDAC jetrenih metastaza za istraživanje staničnih interakcija između tumora i okolnih stanica jetre kroz 1) optimizaciju odabranih uvjeta uzgoja, 2) karakterizaciju vijabilnosti, apoptoze i prisutnosti specifičnih tipova stanica te 3) primjenu modela za snimanje živih stanica. Za to su korišteni precizni tkivni prerezi koji nude nekoliko prednosti: sačuvana struktura i funkcija tkiva, reducirano korištenje životinja u istraživanju i potencijalna primjena u personaliziranoj medicini. MTT test, koji mjeri metaboličku aktivnost, je pokazao da su debljina tkiva od 300  $\mu\text{m}$  te Williamov medij E s 10% seruma, idealni uvjeti za uzgoj, posebice za okolno tkivo jetre. Kroz daljnje eksperimente je pokazano da model eksplantata PDAC jetrenih metastaza zadržava cjelovitost i morfologiju tijekom kultiviranja. U konačnici model je uspješno korišten u svrhu praćenja pojedinačnih stanica na dvo-fotonskom konfokalnom mikroskopu.

(78 stranice, 29 slika, 3 tablice, 95 literaturnih navoda, jezik izvornika: engleski)

Rad je pohranjen u Središnjoj biološkoj knjižnici

Ključne riječi: duktalni adenokarcinom gušterače, jetrene metastaze, kultura eksplantata

Voditelj: Dr. med. Marco Gerling

Suvoditelj: Prof. dr. sc. Nada Oršolić

Ocjenitelji: Prof. dr. sc. Nada Oršolić

Izv. prof. dr. sc. Inga Urlić

Doc. dr. sc. Romana Gračan

Izv. prof. dr. sc. Petra Peharec Štefanić (zamjena)

Rad prihvaćen: 27.05.2021.

## BASIC DOCUMENTATION CARD

---

University of Zagreb  
Faculty of Science  
Department of Biology

Master Thesis

### Establishment of a pancreatic ductal adenocarcinoma liver metastases explant model for cell interaction studies Iva Šutevski

Rooseveltova trg 6, 10000 Zagreb, Hrvatska

Pancreatic ductal adenocarcinoma (PDAC) has an extremely poor prognosis and little therapeutic progress has been made during the last 30 years. At the time of diagnosis, almost all patients already have distant metastases; the most common cause of death. Even though most gastrointestinal tumours metastasize to the liver, little is known about the tumour-stroma interactions in PDAC liver metastases. This study aims to establish an explant model of PDAC liver metastases for the investigation of cellular interactions between tumour and surrounding liver cells. This was performed through 1) optimization of selected culturing conditions, 2) characterisation of viability, apoptosis and persistence of specific cell types, and 3) model application in live-cell imaging. Precise tissue sections, as used in this thesis, offer several advantages: preserved tissue structure and function, reduced use of laboratory animals, and possible application in personalized medicine. The assay quantifying metabolic activity (MTT), revealed 300 µm thick sections cultured in William's Medium E with 10% serum, as optimal conditions, particularly for the surrounding liver. The optimised model maintained its tissue integrity, morphology and cellular heterogeneity during cultivation. Finally, individual cells inside the explant were successfully tracked using a two-photon confocal microscope.

(78 pages, 29 figures, 3 tables, 95 references, original in: English)

Thesis is deposited in Central Biological Library.

Keywords: pancreatic ductal adenocarcinoma, liver metastases, explant culture

Supervisor: Dr. med. Marco Gerling

Co-supervisor: Prof. Nada Oršolić

Reviewers: Prof. Nada Oršolić

Assoc. Prof. Inga Urlić

Asst. Prof. Romana Gračan

Assoc. Prof. Petra Peharec Štefanić (substitution)

Thesis accepted: 27.05.2021.

# Content

1. Introduction .....	1
1.1. Pancreatic ductal adenocarcinoma (PDAC).....	1
1.2. PDAC liver metastases (PCLM) .....	8
1.3. Cancer models .....	13
2. Aim of research .....	20
3. Materials and methods .....	21
3.1. Cell culture.....	21
3.2. Animals .....	22
3.3. Intrahepatic injection of KPC-T cells .....	22
3.4. Tissue extraction for explant culture.....	23
3.5. Cell viability assay on explant cultures .....	24
3.6. Hematoxylin&eosin (H&E) and immunohistochemistry (IHC).....	25
3.7. RNA in situ hybridization (ISH).....	26
3.8. Two-photon confocal live-cell imaging.....	27
4. Results .....	29
4.1. Tissue culture optimisation .....	29
4.2. Tissue culture characterisation: viability, apoptosis, and cell type heterogeneity .....	44
4.3. Two-photon live-cell imaging.....	52
5. Discussion.....	59
6. Conclusions .....	66
References .....	67



## List of abbreviations

ATP – adenosine triphosphate  
BS – blocking solution  
CAF – cancer-associated fibroblast  
CICasp3 – cleaved caspase 3  
DAB – diaminobenzidine  
DCC – disseminated cancer cell  
DMEM/F12 – Dulbecco's Modified Eagle Medium/Nutrient Mixture F-12  
DNA – deoxyribonucleic acid  
ECM – extracellular matrix  
EMT – epithelial to mesenchymal transition  
EtOH – ethanol  
FBS – fetal bovine serum  
GEMM – genetically engineered mouse model  
HBSS – Hanks' Balanced Salt Solution  
HGP – histopathological growth pattern  
H&E - hematoxylin and eosin  
IPMN – intraductal papillary mucinous neoplasm  
ISH – in situ hybridization  
KC – Kupffer cell  
KPC-T – murine pancreatic cancer cells (from *LSL-KrasG12D/+;LSL Trp53R172H/+;Pdx-1-Cre* mice crossed with *B6.Cg-Gt(ROSA)26Sortm9/CAG-tdTomato*Hze/J mice)  
MDSC – myeloid-derived suppressor cell  
MET – mesenchymal-to-epithelial transition  
MCN – mucinous cystic neoplasms  
MTT – 3-[4,5-dimethylthiazol-2-yl]-2,5-diphenyltetrazolium bromide  
PanIN – pancreatic intraepithelial neoplasia  
PBS – phosphate buffer saline  
PCLM – PDAC liver metastases  
PCTS – precision-cut tissue slices  
PDAC – pancreatic ductal adenocarcinoma  
PDX – patient-derived xenografts  
PEST – Penicillin/Streptomycin  
RNA – ribonucleic acid  
TME – tumour microenvironment  
TGF – transforming growth factor  
Tx-100 – Triton X-100  
WME – William's Medium E with GlutaMAX

# **1. Introduction**

## **1.1. Pancreatic ductal adenocarcinoma (PDAC)**

The pancreas is a key part of the digestive system (Paoli and Carrer, 2020), located next to and beneath the stomach (Hall, 2015). There are two major tissue types in the pancreas; the acini (connected to the intestine) and islets of Langerhans (connected to the vasculature) (Hall, 2015). Pancreatic acini are composed of acinar cells, intercalated ductal cells and centroacinar cells (Paoli and Carrer, 2020). They secrete various enzymes, including trypsin, chymotrypsin and carboxypolypeptidase (for the digestion of proteins), pancreatic amylase (for the digestion of carbohydrates), pancreatic lipase, cholesterol esterase and phospholipase (for the digestion of fat) (Hall, 2015). Langerhans' islands contain three cell types; alpha (25%), beta (60%) and delta (10%) (Hall, 2015). They secrete insulin, glucagon, and somatostatin (Paoli and Carrer, 2020) directly into the circulation (Hall, 2015).

Pancreatic ductal adenocarcinoma (PDAC) is the most common type of pancreatic cancers, a group of malignant diseases originating from the exocrine or endocrine pancreatic tissue (Lippi and Mattiuzzi, 2020; Sarantis et al., 2020).

### **1.1.1. Epidemiology of PDAC**

Despite the improvements in diagnostics and therapy, PDAC remains one of the most lethal malignancies (Søreide et al., 2019; Bazzichetto et al., 2020; Sarantis et al., 2020) with an overall 5-year survival rate of approximately 9% (Lippi and Mattiuzzi, 2020). Moreover, in the last ~ 25 years, pancreatic cancer incidence, prevalence and mortality have increased by 50-60%, while current projections point to an even higher rise in mortality by 2060-s (Lippi and Mattiuzzi, 2020). The predictions are that PDAC will become one of the leading causes of cancer-related death already in the next decade (Søreide et al., 2019).

The causes of the low survival rate for PDAC are multifaceted and include late detection, early distant metastases (Krempley and Yu, 2017; Lippi and Mattiuzzi, 2020; Sarantis et al., 2020) and limited treatment options (Costa-Silva et al., 2015; Søreide et al., 2019; Sarantis et al., 2020).

PDAC often remains undetected until the later stages of the disease because of the lack of severe signs and symptoms (Fokas et al., 2015; Hessmann et al., 2020; Lippi and Mattiuzzi, 2020; Sakamoto et al., 2020), its anatomical location (Yonezawa et al., 2008; Søreide et al., 2019; Hessmann et al., 2020) and lack of specific diagnostic markers (Krempley and Yu, 2017; Hessmann et al., 2020).

The most common PDAC symptoms, often occurring only after the disease has progressed and metastasized to distinct sites, are weight loss, abdominal pain and jaundice. In rarer cases, patients also develop diabetes and thromboembolic disease (Sarantis et al., 2020).

The location of the pancreas in the abdomen complicates its imaging and possible early detection of PDAC (Yonezawa et al., 2008; Søreide et al., 2019). Except for the imaging diagnostic technologies, other non-invasive tests have been proposed, such as liquid biopsies that can utilise potentially any bodily fluid for the detection of circulating cancer biomarkers. Several promising PDAC markers have been proposed in recent years, but with a rather low clinical impact (Søreide et al., 2019). However, the population that requires regular screening has not been determined yet, since no defined risk groups for PDAC exist (Søreide et al., 2019; Hessmann et al., 2020). Several genetic syndromes have been associated with a higher risk for PDAC (Lippi and Mattiuzzi, 2020), but are present in only a small minority of cases (Borazanci et al., 2017; Søreide et al., 2019). General risk factors include tobacco smoke, alcohol, obesity (Borazanci et al., 2017; Søreide et al., 2019; Lippi and Mattiuzzi, 2020), chemical exposure, diabetes, pancreatitis, *Helicobacter pylori* infections and age (Lippi and Mattiuzzi, 2020).

A major challenge in dealing with PDAC is its high aggressiveness and metastatic potential (Krempley and Yu, 2017; Lippi and Mattiuzzi, 2020; Mejia et al., 2020). Even small primary PDAC tumours with diameters less than 2 cm, frequently present distant metastases (Yonezawa et al., 2008). Therefore, in a high percentage of cases, at the moment of diagnosis, PDAC has already reached an advanced stage and is often incurable (Søreide et al., 2019; Lippi and Mattiuzzi, 2020). In fact, only 20% of PDAC cases are susceptible to surgical resection therapy with curative

potential, which is the only chance for long term survival (Krempley and Yu, 2017; Søreide et al., 2019; Garcia et al., 2020; Hessmann et al., 2020).

Another important characteristic of PDAC is its striking resistance to most standard therapies, including chemotherapy, radiotherapy and molecular targeting (Krempley and Yu, 2017; Søreide et al., 2019; Sarantis et al., 2020). A potential reason for this is the high level of genetic and epigenetic heterogeneity within both primary and metastatic sites. Furthermore, PDAC possesses a complex and dense tumour microenvironment (TME) that forms a passive and active barrier to the treatments (Krempley and Yu, 2017; Mejia et al., 2020). Therefore, the implementation of new medical therapeutics for PDAC into the clinic is slow, compared to other tumour types (Hessmann et al., 2020).

### **1.1.2. General biology of PDAC**

#### ***Preneoplastic lesions - precursors of PDAC***

PDAC can emerge from various noninvasive precursor lesions; including pancreatic intraepithelial neoplasia (PanIN) lesions, intraductal papillary mucinous neoplasms, and mucinous cystic neoplasms (MCN) (Iacobuzio-Donahue, 2012; Fokas et al., 2015; Ying et al., 2016; Søreide et al., 2019; Bazzicheto et al., 2020). The risk of cancerous transformation varies between different precursor lesions, with the highest being in PanIN and lowest in MCN lesions (Aguirre and Collison, 2017).

PanINs, microscopic intraductal lesions composed of cuboid and columnar mucinous cells (Bazzicheto et al., 2020), are the most common precursor lesions, found in over 80% of patients with invasive carcinoma (Iacobuzio-Donahue, 2012; Bazzicheto et al., 2020; Hessmann et al., 2020).

Based on increasing cellular and nuclear atypia of the duct lining cells, PanINs are classified into three histological stages (Morris et al., 2010; Iacobuzio-Donahue, 2012; Hessmann et al., 2020), before turning into aggressive PDAC; low-grade PanIN1 and PanIN2, and high-grade PanIN3 (Fokas et al., 2015; Ying et al., 2016). Low-grade lesions are common in the adult pancreas and do

not necessarily progress to PDAC, but high-grade lesions are specifically associated with PDAC (Brosens et al., 2015; Ying et al., 2016; Hessmann et al., 2020).

### ***Genetic background of PDAC***

There are four commonly mutated genes in PDAC that accompany the histopathological changes from precursor lesions to cancer *in situ* (Brosens et al., 2015; Fokas et al., 2015; Søreide et al., 2019). These genes include *Kras* (Kirsten rat sarcoma), *Cdkn2a/p16* (cyclin-dependent kinase inhibitor 2A), *Tp53* (tumour suppressor protein 53) and *Smad4* (SMAD family member 4) (Morris et al., 2010; Brosens et al., 2015; Ying et al., 2016; Søreide et al., 2019; Bazzichetto et al., 2020; Khan et al., 2021) (Tab. 1).

Activation mutation of the *Kras* oncogene is the most common mutation in PDAC. It is present already in low-grade PanIN lesions (Brosens et al., 2015; Fokas et al., 2015; Ying et al., 2016; Aguirre and Collison, 2017; Søreide et al., 2019; Bazzichetto et al., 2020), which makes it unique in comparison to other cancer types where *RAS* mutations appear later in the progression of the disease (Borazanci et al., 2017).

**Table 1.** Driver genes in PDAC. (adapted from Khan et al., 2021)

<b>Gene</b>	<b>Gene nature</b>	<b>Function</b>	<b>Mechanisms of genetic alteration</b>	<b>Chromosome</b>	<b>Mutational percentage</b>
<b><i>Kras</i></b>	Oncogene	Cell survival and proliferation, signal transduction and motility	Point mutation at G12, G13 and Q61 codon	Chromosome #12 (p12.1)	70-95%
<b><i>Cdkn2a</i></b>	Tumour suppressor	Cell cycle arrest in G1 to S phase, cyclin-dependent kinase inhibitor	Aberant methylation, homozygous deletion, intragenic mutation (single nucleotide polymorphism)	Chromosome #9 (p21)	49-98%
<b><i>Tp53</i></b>	Tumour suppressor	Cell cycle arrest, cellular metabolism, cellular senescence, cellular apoptosis, and DNA repair	Point mutation in codons 35, 105, 133, 213, 258 and 299, intragenic loss of one allele	Chromosome #17 (p13.1)	20-75%
<b><i>Smad4</i></b>	Tumour suppressor	Cell cycle arrest, apoptosis, wound healing, embryonic development, immune function	Intragenic mutation, homozygous deletion	Chromosome #18 (q21.1)	19-50%

Except for *Kras*, *Cdkn2a*, *TP53* and *Smad4*, a variety of other mutations with potential roles in tumour development have been found in PDAC, including *BRCA1* (Breast cancer type 1), *MLL3* (Mixed-lineage leukaemia protein 3), *TGF* (transforming growth factor), and *MKK4* (Mitogen-activated protein kinase kinase 4) (Haeno et al., 2012). It is important to highlight that majority of genes that are mutated in PDAC, belong to a certain number of, so-called “core signalling pathways”, including mitogen-activated protein kinase (MAPK), TGF- $\beta$ , Hedgehog (Hh), c-Jun N-terminal kinase (JNK), Wnt/Notch, GTPase dependent signalling pathways and pathways regulating DNA damage control, G1-S cell phase transition, apoptosis, homophilic cell adhesion, integrin signalling, chromatin remodelling and axon guidance (Iacobuzio-Donahue, 2012; Ying et al., 2016; Bazzichetto et al., 2020).

In recent years, it has been observed that epigenetic alterations also have a crucial role in PDAC progression (Brosens et al., 2015; Hessmann et al., 2020), more precisely in tumour cell plasticity and chemoresistance (Hessmann et al., 2020).

In fact, genes that are involved in the regulation of epigenetics, such as histone methyltransferases, histone demethylases, SWI/SNF-mediated chromatin remodelling complexes and bromodomain and extra terminal domain proteins, are frequently mutated in PDAC (Borazanci et al., 2017).

### ***PDAC progression model***

In the currently dominating model, PDAC arises gradually, from preneoplastic lesions, driven by initial *Kras* oncogene mutations, with progressive accumulation of new mutations (Iacobuzio-Donahue, 201). Progress to PanIN3 or PDAC depends on additional signalling and mutational events, including loss of *Cdkn2a*, *Tp53* and *Smad4* (Storz, 2017).

### **1.1.3. PDAC microenvironment**

The PDAC TME is composed of dense fibrotic stroma consisting of various cell types and extracellular matrix (ECM) components, that make up to 90% of tumour volume (Fokas et al., 2015; Ying et al., 2016; Aguirre and Collison, 2017; Søreide et al., 2019; Bazzichetto et al., 2020;

Sarantis et al., 2020; Sperb et al., 2020; Khan et al., 2021). It begins to form already around PanIN lesions (Hessmann et al., 2020) and has a key role in PDAC progression, invasion and chemoresistance (Aguirre and Collison, 2017; Søreide et al., 2019; Hessmann et al., 2020; Sperb et al., 2020; Khan et al., 2021).

It has been shown that normal stroma appears to prevent or even delay tumour growth, while abnormal stroma facilitates tumour progression (Fokas et al., 2015). However, it was recently revealed that a low concentration of stromal components correlates with a worse prognosis in PDAC patients (Mejia et al., 2020). Several studies conducted on murine PDAC models showed that removing the stroma led to a more aggressive tumour phenotype and decreased overall survival, suggesting a dual role of stroma (Krempley and Yu, 2017; Hessmann et al., 2020; Mejia et al., 2020).

### ***Non-cellular components of the PDAC microenvironment***

One of the main characteristics of the PDAC microenvironment is an extensive desmoplastic reaction (Whatcott et al., 2015; Khan et al., 2021), defined by dense fibrosis, inflammation, poor cellularity (Søreide et al., 2019), lack of nutrients and an immunosuppressive environment (Aguirre and Collison, 2017). Desmoplasia is largely a product of autocrine and paracrine communication between stromal cells, particularly pancreatic stellate cells, and PDAC cells (Bazzichetto et al., 2020).

This ECM rich stroma, present in PDAC, is composed of various fibrous proteins, including collagen, glycoproteins, proteoglycans, fibronectin, laminin and soluble factors such as cytokines, chemokines and growth factors (Fokas et al., 2015; Ying et al., 2016; Houg and Bijlsma, 2018; Lafaro and Melstrom, 2019; Bazzichetto et al., 2020; Tomás-Bort et al., 2020), that are mostly secreted by stromal cells, and to a lesser extent by PDAC cells (Shi et al., 2016; Mejia et al., 2020). All these components form a dynamic environment (Bazzichetto et al., 2020; Stopa et al., 2020) that provides mechanical support and a framework for cellular interactions (Fokas et al., 2015; Williamson et al., 2019) and so influences tumour cell behaviour, progression, metastasis and resistance to chemotherapy (Tomás-Bort et al., 2020).

By interacting with growth factors that promote cell migration and angiogenesis (Williamson et al., 2020), ECM can influence tumour cell invasiveness and metastatic potential (Fokas et al., 2015).

Furthermore, large amounts of ECM components, such as hyaluronic acid, make stroma a rigid barrier (Sarantis et al., 2020) and PDAC a physically hard tumour (Hessmann et al., 2020). A consequence of this is high interstitial tumour pressure that induces vascular dysfunction and compression, making PDAC extremely hypovascular, with up to 75% decrease in vessel density (Fokas et al., 2015; Whatcott et al., 2015; Ying et al., 2016). Impaired oxygen and nutrient delivery and altered immune cell infiltration lead to high tissue heterogeneity, therapy resistance and tumour progression (Fokas et al., 2015; Krempsey and Yu, 2017; Lafaro and Melstrom, 2019; Søreide et al., 2019; Sarantis et al., 2020).

Moreover, biomechanical cues can influence intracellular signalling pathways, usually through integrin aggregation into focal adhesion complexes, and increase tumour progression (Houg and Bijlsma, 2018). It was found that high matrix stiffness promotes invadopodia formation (Mejia et al., 2020), epithelial to mesenchymal transition and enhances cellular contractility through Rho/ROCK pathway (Houg and Bijlsma, 2018).

### ***Cellular components of the PDAC microenvironment***

Cellular components of the PDAC microenvironment include cancer-associated fibroblasts (CAF), myeloid and lymphoid immune cells, endothelial cells and neurons (Ying et al., 2016; Aguirre and Collison, 2017; Bazzichetto et al., 2020; Hessmann et al., 2020; Sarantis et al., 2020; Stopa et al., 2020). PDAC cells educate both infiltrating and resident immune cells, including tumour associated macrophages (TAMs), myeloid-derived suppressor cells (MDSC) and regulatory T cells (Tregs) towards an immunosuppressive state (Lafaro and Melstrom, 2019; Mejia et al., 2020; Sperb et al., 2020). Other immune cells, such as CD8<sup>+</sup> effector T lymphocytes, natural killer (NK) cells and dendritic cells, exert anti-tumorigenic effects. However, they are usually depleted during tumour progression (Mejia et al., 2020).

These different cell types in the PDAC TME form a unique and complex signalling network that makes it difficult to predict biological responses to, for instance, certain therapies (Hessmann et al., 2020).



## **1.2. PDAC liver metastases (PCLM)**

### **1.2.1. Cancer metastases**

Cancer metastases are a major challenge to the successful management of malignant disease (Brodt, 2016) since they are, in many cases as well as in PDAC, the main cause of cancer-related deaths (Whatcott et al., 2015; Shi et al., 2016; Aguirre and Collison, 2017; Van Dam et al., 2017).

#### ***Metastatic cascade***

Metastases formation happens through a complex multi-step process, that includes the epithelial-to-mesenchymal transition (EMT) of cells within the primary tumour, intravasation into the circulation, extravasation from the circulation and colonization of a distant organ that requires mesenchymal-to-epithelial transition (MET) (Clark et al., 2016; Houg and Bijlsma, 2018). Disseminated cancer cells (DCC) can stay in a dormant state for years to decades before forming clinically detectable metastases (Clark et al., 2016).

EMT enables cells to detach from the surroundings and gain pro-metastatic traits (Clark et al., 2016; Ayres Pereira and Chio, 2019). Through EMT, cells lose their epithelial characteristics, such as apical-basal polarity and cell-cell adhesions and transform into a more motile mesenchymal state (Zheng et al., 2015; Ayres Pereira and Chio, 2019), with spindle-like shape and enhanced migratory capacity, invasiveness, increased resistance to apoptosis and elevated production of ECM components (Houg and Bijlsma, 2018; Bulle and Lim, 2020).

The dissemination of cancer cells is the main rate-limiting step for metastases formation (Mielgo and Schmid, 2020). Even though ~68% of PDAC cells are capable of EMT, only 0.01% of cells establish metastases (Houg and Bijlsma, 2018). Dissemination can occur through blood or lymphatic vasculature, in form of single cells or clusters of cells (Ayres Pereira and Chio, 2019). In the vasculature, tumour cells are exposed to immune surveillance and host-tissue defence (Mielgo and Schmid, 2020) and therefore, tumour clusters usually have a higher metastatic potential than single cells (Ayres Pereira and Chio, 2019).

When DCCs reach a distant organ, they first need to migrate through the endothelial layer to reach the stroma. This process, called extravasation, relies on cellular interactions between DCCs and endothelial cells (Barbazán et al., 2017).

Finally, DCCs that have reached a distant organ can grow into clinically observable metastases only if the environment enables their survival and proliferation. Growing evidence shows that certain immune cells, like neutrophils, have an important role in homing the metastatic environment (Kos and Visser, 2021).

### ***Sites of metastases***

DCCs require a host microenvironment that enables their proliferation (Williamson et al., 2019). PDAC metastasizes most frequently to the liver (Houg and Bijlsma, 2018).

A growing body of evidence supports the idea of a premetastatic niche, which is a secondary organ microenvironment made more permissive to metastases before the arrival of DCCs (Brodt, 2016; Milette et al., 2017; Houg and Bijlsma, 2018; Mielgo and Schmid, 2020; Vidal-Vanaclocha et al., 2020). However, it is difficult to verify the dependency of metastases on the presence of pre-metastatic niches (Mielgo and Schmid, 2020) and clinical evidence for this is still lacking (Vidal-Vanaclocha et al., 2020)

### **1.2.2. Liver metastases**

#### ***Liver architecture and microenvironment***

The liver is the largest internal organ in the human body and the only organ with a dual blood supply, receiving oxygenated blood from the hepatic artery (~25% of blood influx) and nutrient-rich blood from visceral circulation (~75% of blood influx) (Mielgo and Schmid, 2020).

The liver is mostly composed of parenchymal hepatocytes and cholangiocytes that have glandular, metabolic and detoxification function (Mielgo and Schmid, 2020). Hepatocytes also have an important role in innate and adaptive immunity. They can detect microbial signals, communicate

with various immune cells, sense cytokine injury signals, and respond by producing acute-phase proteins (Stamataki and Swadling, 2020).

The remaining nonparenchymal cells are hepatic stellate cells and liver sinusoidal endothelial cells (Williamson et al., 2019; Mielgo and Schmid, 2020; Ciner et al., 2021). The liver is also rich in immune cells (Mielgo and Schmid, 2020), such as liver-resident macrophages called Kupffer cells (KCs), bone marrow-derived macrophages, dendritic cells, neutrophils, and MDSC (Williamson et al., 2019; Ciner et al., 2021).

### ***Prevalence of liver metastases***

After the locoregional lymph nodes, the liver is the most frequent site of metastasis and is the most common metastatic site for tumours originating from the gastrointestinal tract and pancreas (Brodt, 2016; Clark et al., 2016; Van Dam et al., 2017; Mielgo and Schmid, 2020; Ciner et al., 2021). It is interesting to mention that liver metastases are even more common than primary liver tumours (Mielgo and Schmid, 2020).

In many cases, the high frequency of liver metastases can be explained by hematogenic spread, since many intra-abdominal organs have their primary blood drainage to the liver. This is especially the case in gastrointestinal cancers, including pancreatic cancers (Williamson et al., 2019; Mielgo and Schmid, 2020).

However, there are also some unique organ-specific characteristics of the liver that make it more susceptible to metastases, including its architecture, vascularization, specific endothelial cells that line the liver capillaries, regenerative capabilities and regional immune suppression (Clark et al., 2016; Mielgo and Schmid, 2020). All these features are crucial for the liver's role in blood detoxification, but also enable the extravasation of DCCs (Mielgo and Schmid, 2020).

With the dual blood supply, the liver has a significant role in the circulatory system (Clark et al., 2016; Milette et al., 2017). But this slow and tortuous microcirculation allows DCCs easier access to the liver microenvironment (Clark et al., 2016). Furthermore, cells lining up the hepatic capillaries express various surface molecules that cancer cells can attach to (Clark et al., 2016), while LSECs form a discontinuous lining of the hepatic sinusoids, due to their fenestrations and lack of a subendothelial basement membrane (Mielgo and Schmid, 2020).

The liver possesses high regenerative capabilities and the cellular mechanisms involved in self-renewal and tissue reconstruction can be used by cancer cells to produce an environment that promotes survival and growth (Clark et al., 2016).

Moreover, the liver is continuously exposed to food-derived and microbial antigens from the gut, such as lipopolysaccharides, peptidoglycans and flagellin that can serve as inflammatory stimuli (Vidal-Vanaclocha et al., 2020). The liver needs to maintain the capacity to respond to life-threatening pathogens (Ciner et al., 2021) but also block the unwanted immune responses for harmless molecules such as food antigens (Stamataki and Swadling, 2020). To achieve this balance, the liver possesses specific responses of antigen-presenting cells (APC), that induce immune tolerance under non-pathogenic conditions (Stamataki and Swadling, 2020). However, in general, antigen responses in the liver are suppressed compared to other organs (Clark et al., 2016; Stamataki and Swadling, 2020; Ciner et al., 2021). And this, in turn, results in a relatively immunotolerant microenvironment that allows DCCs survival and growth (Clark et al., 2016).

Additionally, premetastatic niche formation has also been reported in liver metastases (Mielgo and Schmid, 2020). The liver reacts in an acute and proinflammatory way in response to circulating tumour-derived soluble factors (Vidal-Vanaclocha et al., 2020). Recent studies by Costa-Silva and colleagues have shown that PDAC-derived exosomes can interact with KCs through integrin  $\alpha\text{v}\beta 5$  and consequently induce the formation of a pre-metastatic niche. More specifically, the macrophage migration inhibitory factor contained in the exosomes induces KCs to express TGF $\beta$ , a key mediator in fibrosis. It activates hepatic stellate cells to produce fibronectin, an important ECM component of a pro-inflammatory environment. Moreover, this fibrotic reaction induces an arrest of bone marrow-derived macrophages and neutrophils that also participate in pre-metastatic niche preparation (Costa-Silva et al., 2015; Houg and Bijlsma, 2018).

### ***Growth patterns of liver metastases***

There are three major histopathological growth patterns (HGP) found in liver metastases; desmoplastic, pushing and replacement, that differ in the cellular composition and morphology at the interphase between the tumour and surrounding liver tissue (Brodts, 2016; Van Dam et al., 2017).

In the desmoplastic HGP, metastasis is separated from the liver by a rim of desmoplastic tissue, preventing direct contact between cancer cells and hepatocytes. In this HGP, new blood vessels are formed by sprouting angiogenesis and there is often a dense lymphocytic infiltrate at the interface of the desmoplastic and liver tissue. Ductular reaction, a proliferation of bile ducts, can sometimes be observed around the desmoplastic metastasis (Van Dam et al., 2017).

In the pushing HGP, there is no desmoplastic rim around the metastases and tumour tissue pushes away and compresses the liver cells that surround it (Van Dam et al., 2017).

In the replacement HGP, cancer cells replace hepatocytes by forming cell plates in continuity with the liver cell plates. Furthermore, this enables cancer cells to co-opt the sinusoidal blood vessels at the metastasis-liver interface, so they do not rely on sprouting angiogenesis (Van Dam et al., 2017).

There is a link between a type of primary cancer and its liver metastases HGPs. For instance, almost all breast cancer liver metastases have replacement HGPs. Furthermore, there is a correlation between HGPs and patient prognosis, with desmoplastic HGP having a superior overall survival. However, molecular differences that drive different HGPs are unknown (Van Dam et al., 2017).

### ***Liver metastatic cascade***

After the formation of a pre-metastatic niche in response to factors released from the primary tumour, the processes of liver metastases can be separated into four key phases: (1) microvascular phase, (2) extravascular/proangiogenic phase (extravasation into the space of Disse), (3) angiogenic phase, and (4) growth phase (expansion of metastasis) (Brodt, 2016; Milette et al., 2017; Mielgo and Schmid, 2020; Ciner et al., 2021). The microvascular phase involves DCCs arrest in the sinusoidal vessels and can lead to tumour cell death or extravasation. During extravasation or the so-called pre-angiogenic phase, stromal cells and myeloid cells colonize avascular micrometastases. In the angiogenic phase, cancer cells recruit endothelial cells and become vascularized. Finally, clinically observable metastases are formed during the growth phase (Clark et al., 2016; Ciner et al., 2021).

During the metastatic cascade, cancer cells encounter a complex microenvironment of various cellular and non-cellular components, communicating through soluble factors, proteolytic enzymes and receptor-mediated contacts. Each cell type is involved in different metastatic stages and can

execute both tumoricidal and/or tumour promoting roles (Clark et al., 2016). Whether they play anti- or pro-tumorigenic roles depends on the stage of the metastatic cascade, tumour antigen load and interactions with other immune cells (Mielgo and Schmid, 2020).

### **1.3. Cancer models**

A major challenge in understanding the biology of the disease (Garcia et al., 2020; Nelson et al., 2020) and in developing effective therapies for solid tumours, including PDAC, is the lack of appropriate models that match cancer complexity (Sivakumar et al., 2019; Garcia et al., 2020; Nelson et al., 2020; Yu et al., 2021).

Various models, including immortalized cell lines, genetically engineered mouse models, xenografts (Krempley and Yu, 2017; Lim et al., 2018; Misra and Moro et al., 2019; Garcia et al., 2020; Tomás-Bort et al., 2020) and 3D models (Garcia et al., 2020) that are currently used in preclinical studies, do not generate translatable results (Tomás-Bort et al., 2020).

An ideal cancer model of PDAC should have a similar pathophysiological development and malignant phenotype as human cancer (Kong et al., 2020). It needs to match all the heterogeneity in terms of PDAC subclones (Yu et al., 2021) and the tumour microenvironment (Hessmann et al., 2020). Lastly, it should be cost-efficient, easy and fast to establish, stable and reproducible (Hessmann et al., 2020; Kong et al., 2020).

#### **1.3.1. Cell lines**

The most common method used to study PDAC biology (Bulle and Lim, 2020) and to develop and test chemotherapeutics (Nelson et al., 2020) is the traditional monolayer cell culture (Deer et al., 2010; Hwang et al., 2016; Kong et al., 2020).

In addition to traditional 2D cultures, new cell lines could be established from PDAC patient samples (Garcia et al., 2020). Early passages of such primary PDAC cell lines show higher heterogeneity, as they can contain CAFs (Garcia et al., 2020; Nelson et al., 2020). However, these cultures only offer a snapshot of the tumour at the time of biopsy and lead to therapies that target only certain most aggressive clones (Hwang et al., 2016; Krempley and Yu, 2017).

Furthermore, PDAC cancer cells can be cultured with certain stromal cells, such as CAFs, either in direct contact (by layering cells in a fixed ratio one on top of the other or by mixing them) or without direct contact (by placing cells in separate chambers so the communications occur only through diffusion) (Bulle and Lim, 2020). Such co-cultures can be used to investigate tumour-stroma crosstalk (Yu et al., 2021).

Traditional monolayer cell lines provide several practical advantages (Hwang et al., 2016; Krempsey and Yu, 2017) and have proven useful over the past decades (Søreide et al., 2019). They are low-cost, reproducible, homogeneous and easy to propagate. Therefore, they are suitable for high-throughput bioinformatics studies (Hwang et al., 2016; Krempsey and Yu, 2017; Garcia et al., 2020; Yu et al., 2021) and proof-of-concept studies (Nelson et al., 2020).

On the other hand, 2D cell lines are very limited. They select for phenotypes that are more preferable in monolayer (Hwang et al., 2016; Krempsey and Yu, 2017) and so adapt to the growth in culture (Haykal et al., 2020). Consequently, they differ significantly from the initial tumour by many aspects including polarity, microenvironment (Sivakumar et al., 2019; Frappart and Hofmann, 2020; Garcia et al., 2020), cell metabolism, gene expression (Hwang et al., 2016; Clarke and Fisher, 2020; Frappart and Hofmann, 2020; Haykal et al., 2020), structural complexity, tissue architecture (Ayres Pereira and Chio, 2019; Haykal et al., 2020; Yu et al., 2021) and tumour heterogeneity (Yu et al., 2021). Additionally, during passaging, cell lines undergo genetic modifications associated with immortalization (Garcia et al., 2020; Nelson et al., 2020) and this poor consistency between passages lowers the predictive powers of the model (Yu et al., 2021). Even though PDAC cell lines could serve as an important starting point, additional models that better mimic PDAC biology, are needed (Hwang et al., 2016).

### **1.3.2. Organoids**

Organoids are 3D cultures in which cells spontaneously self-organize into structures that resemble the *in vivo* state in terms of tissue architecture, function, cellular make-up (Krempsey and Yu, 2017; Sivakumar et al., 2019; Frappart and Hofmann, 2020; Nelson et al., 2020) and molecular characteristics (Hessmann et al., 2020). Organoids have been developed for various research

approaches and from different organs, including the intestine, kidney, brain, liver, pancreas, ovary and lung (Haykal et al., 2020). Importantly, they can also be established from small amounts of patient tissue, such as a fine needle biopsy (Krempley and Yu, 2017; Søreide et al., 2019; Garcia et al., 2020), in 2-4 weeks (Søreide et al., 2019).

Organoids can be derived from either embryonic, pluripotent, adult organ restricted stem cells (Krempley and Yu, 2017; Nelson et al., 2020) or tumour cells (Frappart and Hofmann, 2020; Garcia et al., 2020; Nelson et al., 2020).

For the formation of organoids, the tissue of interest is mechanically dissociated and exposed to enzymatic digestion (Frappart and Hofmann, 2020). Dissociated cells are then embedded into a collagen or matrigel based matrix (Hessmann et al., 2020), that resembles a basement membrane, so they remain suspended and do not attach to the bottom of the culture dish (Garcia et al., 2020). Furthermore, they are exposed to specific growth and differentiation factors (Hessmann et al., 2020; Nelson et al., 2020) that mimic the *in vivo* microenvironment (Hwang et al., 2016; Nelson et al., 2020). For instance, PDAC organoids are embedded in Matrigel and cultured in media supplemented with mitogens and growth factors that influence various signalling pathways, such as R-spondin-1 (enhances Wnt signalling) and Noggin (inhibits BMP signalling).

As well as 2D cultures, organoids can also be co-cultured to contain multiple cell types, such as tumour and stromal components (Garcia et al., 2020). To study the cellular crosstalk and roles of immune cells in cancer, many laboratories employ PDAC organoids co-cultured with CAFs in Matrigel ECM and media containing immune cells (Frappart and Hofmann, 2020; Garcia et al., 2020), that mimic PDAC biology more closely (Frappart and Hofmann, 2020).

Organoids are exposed to a complex and heterogeneous environment containing oxygen and nutrient-rich and poor regions, proliferating, non-proliferating and necrotic cells (Haykal et al., 2020; Nelson et al., 2020). Furthermore, the number of cellular interactions is exponentially increased by the addition of the third dimension (Krempley and Yu, 2017; Sivakumar et al., 2019). They mimic cell polarity, cell-cell and cell-ECM interactions (Ayres Pereira and Chio, 2019), gene expression and metabolism profiles (Frappart and Hofmann, 2020). Moreover, organoids preserve heterogeneity of *in vivo* tumours (Krempley and Yu, 2017; Hessmann et al., 2020; Nelson et al., 2020) and are genetically stable over serial passages (Frappart and Hofmann, 2020). PDAC



organoids can re-create PanIn-like structures (Krempley and Yu, 2017) and in later steps mimic PDAC tissue characterised by desmoplasia and poor vascularization (Hessmann et al., 2020). They preserve the proteomic and transcriptomic features (Bulle and Lim, 2020) and some tumour-stroma interactions (Søreide et al., 2019). Therefore, organoids possess a morphology and physiology that is more similar to the *in vivo* situation (Haykal et al., 2020; Nelson et al., 2020).

Organoids are still quite an artificial model (Hessmann et al., 2020). Even though patient derived organoids capture key phenotypic and genetic characteristics of tumours, important differences in somatic mutations have been observed compared to matched patient tumours (Clarke and Fisher, 2020). Also, organoids cannot completely model the complexity of the TME *in vivo* (Garcia et al., 2020). Compared to 2D cultures, organoids take weeks or months to generate (Sivakumar et al., 2019; Bulle and Lim, 2020), they are more costly due to matrices and heavily supplemented media needed (Hessmann et al., 2020) and have lower through-put capabilities (Sivakumar et al., 2019).

### **1.3.3. Mouse models**

Genetically engineered mouse models (GEMMs) for cancer research are created by introducing specific oncogene or tumour suppressor gene mutations (Krempley and Yu, 2017) by using transgenic, gene knock-in, gene knock-out (Fokas et al., 2015; Kong et al., 2020) or conditional/inducible (Fokas et al., 2015) techniques. A great breakthrough was the development of the Cre/LoxP strategy (Garcia et al., 2020), which was later utilised by the Tuveson laboratory to localise the expression of a mutant *Kras* allele specifically in pancreatic progenitor cells (Hingorani et al., 2005). The principle of this strategy is that the oncogenic *Kras* mutant is silenced by a loxP-flanked stop element, which can be removed in cells upon expression of a Cre recombinase (Garcia et al., 2020). In PDAC mouse models, Cre recombinase is expressed under pancreas-specific promoters, such as *Ptf1a* or *Pdx1* (Rampetsreiter et al., 2011).

GEMMs with modified expression of genes involved in PDAC development, either involving oncogene activation or tumour suppressor inactivation, can successfully recapitulate PDAC disease phenotypes (Fokas et al., 2015; Kong et al., 2020). Over the years, a plethora of multi-genetic

models have been described that target key drivers of PDAC development (Hessmann et al., 2020), including *Kras*, *Tp53*, *Cdkn2a* and *Smad4* (Kong et al., 2020).

The commonly used *LSL-Kras*<sup>G12D/+</sup>;*LSL-Trp53*<sup>R172H/+</sup>;*Pdx-1-Cre* (KPC) model harbours oncogenic *KRAS* (*Kras*G12D) and tumour suppressor *Tp53* (*Trp53*R172H) mutations, driven by *Pdx1-Cre* transgene (Krempley and Yu, 2017; Hessmann et al., 2020; Yu et al., 2021). It recapitulates many features of human malignancy (Krempley and Yu, 2017); both clinical and histopathological (Hessmann et al., 2020). It also mimics autologous TME and is often used for developing therapies that target tumour stroma (Yu et al., 2021).

Since GEMMs show many characteristics of human disease (Krempley and Yu, 2017), they greatly accelerated the study and understanding of PDAC biology (Bulle and Lim, 2020). They have been used in the research of predisposing PDAC risk factors, identifying potential biomarkers of early disease and for the discoveries of novel therapies. Since GEMMs have an intact immune system, they offer a useful tool for the investigation of immune responses (Krempley and Yu, 2017).

Still, GEMMs have several limitations. The breeding and maintenance of GEMMs are expensive, time-consuming (Krempley and Yu, 2017; Hessmann et al., 2020; Tomás-Bort et al., 2020; Yu et al., 2021), labour-intensive (Bulle and Lim, 2020) and ethically questionable (Haykal et al., 2020). This limits their usage in large-scale drug or genetic screenings (Bulle and Lim, 2020; Yu et al., 2021). Furthermore, it is difficult to evaluate the presence and volume of tumours at the beginning of an experiment, due to high variability in tumour onset between animals, ranging from 47 to 355 days (Hessmann et al., 2020). Finally, because of the interspecies differences in cytokines and metabolism, GEMMs do not completely mimic human diseases (Clark et al., 2016). As a consequence, most drugs tested on mice are not applicable to humans (Rampetsreiter et al., 2011).

#### **1.3.4. Transplantational models**

Transplantation models are established by implanting cancer cells or tissue from human or murine origin into recipient mice (Hwang et al., 2016; Ayres Pereira and Chio, 2019). They eventually develop tumours with 3D architecture and a complex microenvironment composed of host stromal components (Hwang et al., 2016). Transplantation models can also be established using organoids

(Krempley and Yu, 2017; Hessmann et al., 2020). Implantation can be orthotopic (organ matching implanted cells), heterotopic (subcutaneous, intraperitoneal, intravenous, intra-splenic, intra-cardiac) and intravenous (Ayres Pereira and Chio, 2019). Subcutaneous transplants are inexpensive, allow rapid screening and easy assessment of tumour size. Consequently, they are often used by pharmaceutical companies for drug development (Krempley and Yu, 2017). However, they are less biologically faithful, compared to orthotopic transplants, which are more costly and challenging to utilise in research (Krempley and Yu, 2017; Garcia et al., 2020; Hessmann et al., 2020; Yu et al., 2021). For tumour metastases models, orthotopic transplants can be used to study the whole metastatic cascade from the primary tumour, while intravenous injections allow the study of dissemination, extravasation, and colonization steps (Ayres Pereira and Chio, 2019).

Transplantation models can be syngeneic (allograft) or xenogeneic (xenograft) (Ayres Pereira and Chio, 2019; Hessmann et al., 2020). Allografts are prepared by injecting endogenous murine cell lines into healthy immunocompetent mice (Krempley and Yu, 2017; Hessmann et al., 2020). Such models are time- and cost-effective (Ayres Pereira and Chio, 2019) and suitable for the studies of immunotherapies (Krempley and Yu, 2017). Xenografts are prepared by injecting tumour tissue or cell lines into immune-deficient mice (Hwang et al., 2016; Krempley and Yu, 2017; Ayres Pereira and Chio, 2019; Garcia et al., 2020; Hessmann et al., 2020; Kong et al., 2020). Patient-derived xenografts (PDXs) have recently emerged as an important preclinical model (Nelson et al., 2020). They recapitulate genetics, histopathology, morphology, heterogeneity and metastatic potential of patient tumours (Fokas et al., 2015; Ayres Pereira and Chio, 2019; Garcia et al., 2020) and are used to study therapeutic responses (Hwang et al., 2016).

The PDX model has several limitations. A significant caveat is that they are used in immunocompromised mice. The tumours, therefore, develop without the pressure of a mature immune system (Krempley and Yu, 2017) and they are not able to truly recapitulate the TME (Garcia et al., 2020). Furthermore, PDX models are labour intensive to establish, costly (Garcia et al., 2020; Haykal et al., 2020; Nelson et al., 2020) and ethically questionable (Haykal et al., 2020). Successful engraftment is still difficult (Hwang et al., 2016; Krempley and Yu, 2017), and is usually around 60-70% (Hessmann et al., 2020). Risks of complications, such as infections, abdominal bleeding, disruption of the pancreatic capsule and intra-abdominal tumour cell spillage

are especially high in orthotopic models (Fokas et al., 2015). The process of PDX model development can take up to 6 months (Hwang et al., 2016; Krempsey and Yu, 2017) and then a significant period is needed for the first passage (Hwang et al., 2016; Garcia et al., 2020). The application of PDX models in the clinic is limited since only part of PDAC patients is eligible for surgery (Hwang et al., 2016; Garcia et al., 2020) and the model also requires a large piece of tissue (Hwang et al., 2016; Krempsey and Yu, 2017). Lastly, during the passages, the human stroma is lost and replaced with murine stromal components (Ayres Pereira and Chio, 2019; Garcia et al., 2020; Haykal et al., 2020; Nelson et al., 2020; Yu et al., 2021).

### **1.3.5. Precision-cut tissue slices (PCTS)**

Precision-cut tissue slices (PCTS), or organotypic tissue slice cultures/explant cultures, is an *ex vivo* model that has been used for the study of various subjects (Kenerson et al., 2020), including immunotoxicity (Sewald et al., 2013), fibrosis (Westra et al., 2013), cirrhosis (Jain et al., 2020), repair and injury (Vickers et al., 2018). Furthermore, they have been successfully produced from several tumour types, including head, neck, gastric tumours (Lim et al., 2018), pancreatic cancer (Misra and Moro et al., 2019), breast cancer (Naipal et al., 2016) etc.

PCTS preserve tissue architecture (Jiang et al., 2017), a partially intact microenvironment, native ECM (Sivakumar et al., 2019) and tumour-stroma interactions (Lim et al., 2018). Ghaderi and colleagues performed genome-wide transcriptome sequencing on PDAC explants and found only a limited number of changes, mostly upregulation of pathways related to cell death/apoptosis (Ghaderi et al., 2020). Importantly, explant cultures offer a personalized patient model for drug testing (Lim et al., 2018).

## **2. Aim of research**

The aim of my master thesis is to establish a PDAC liver metastases (PCLM) explant model using murine precision-cut tissue slices (PCTS). This model could potentially be used for the study of cellular interactions between tumour and liver parenchyma, and the assessment if these interactions could be manipulated to reduce tumour growth. Eventually, this model could increase our current understanding of the intricate networks of interactions inside the tumour microenvironment of PDAC metastases in the liver.

Specific aims of my master thesis are:

1. to determine optimal tissue sectioning and culturing conditions (including serum concentration and culturing medium) for a novel, murine PCLM explant model
2. to validate the model based on histology, cell survival, and cellular heterogeneity in the optimised murine PCLM explant model
3. to optimise the model for, and perform live-cell imaging on the established murine PCLM explant model in order to visualize tumour cell migration at the tumour-liver interphase

### 3. Materials and methods

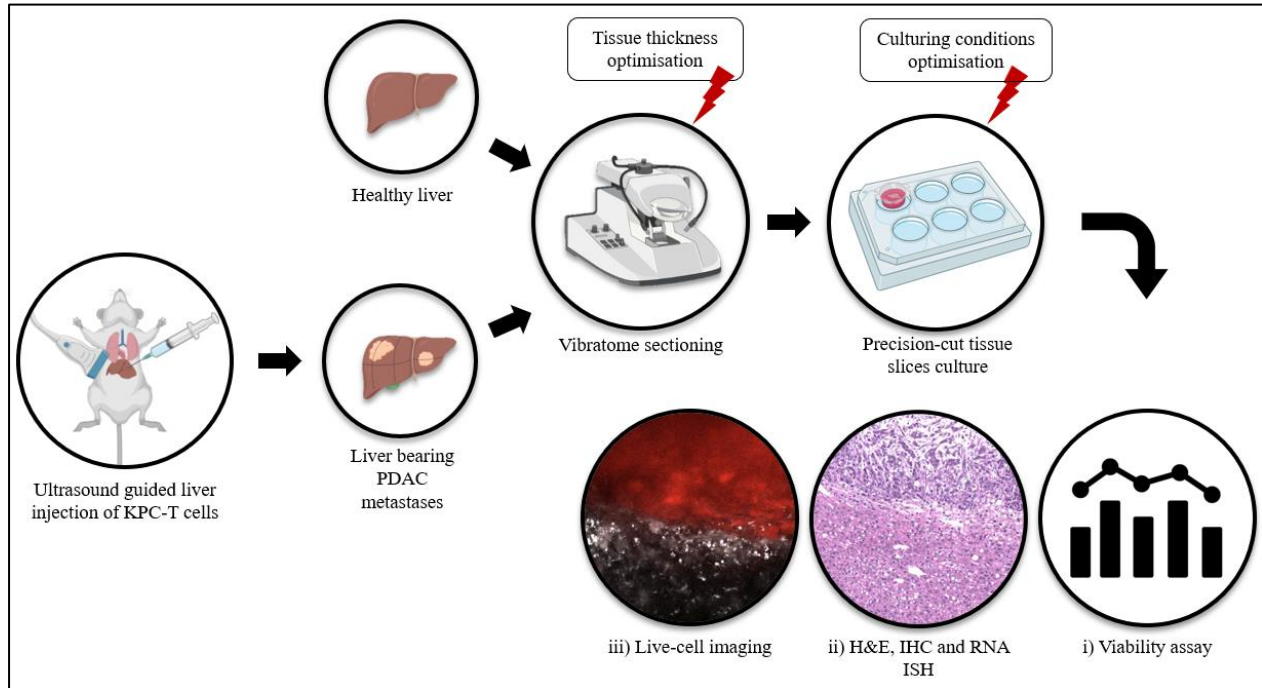


**Figure 1.** Experimental plan flow chart for the PCLM explant culture establishment. PCLM were induced by ultrasound-guided intrahepatic injection of murine PDAC cells into C57BL/6J mice. PCLM were extracted after approximately four weeks, sliced and cultivated for up to five days. Explant culture was optimized regarding tissue thicknesses and culturing media by assessing cell viability (i) and tissue histology (ii). Cell movement at the invasion front of PCLM was analyzed by live-cell imaging (iii).

#### 3.1. Cell culture

Murine pancreatic cancer cells (“KPC-T”) were derived from *LSL-KrasG12D/+;LSL-Trp53R172H/+;Pdx-1-Cre* mice, which were crossed with *B6.Cg-Gt(ROSA)26Sortm9/CAG-tdTomato*<sup>Hze/J</sup> mice expressing the red fluorescent protein tdTomato specifically in cells bearing *Kras* and *Tp53* mutations.

Cells were cultured in Dulbecco's Modified Eagle Medium/Nutrient Mixture F-12 (DMEM/F12) (Gibco, REF 11320), supplemented with 10% fetal bovine serum (FBS) (Sigma-Aldrich, F9665) and 1% of Penicillin-Streptomycin (PEST) antibiotics (Cytiva, HyClone™, Cat No: SV30010), at 37 °C in 5% CO<sub>2</sub> in a humidified atmosphere.

When passaging, cells were washed with phosphate buffer solution (PBS) (Gibco, REF 18912-014) and detached by 5 min incubation in TrypLE™ Express (Gibco, REF 12605) at 37 °C. Trypsin was subsequently inactivated by the addition of PBS. Cells were centrifuged for 5 min at 300 g, resuspended in culture medium and seeded into a new flask.

### **3.2. Animals**

C57BL/6J mice were obtained from Scanbur (Sollentuna, Sweden). Animal experiments and breedings were approved by the Swedish Board of Agriculture (Jordbruksverket, ethical permit number ID625, 2017). Animals were housed in Karolinska Institutet's animal facility in pathogen-free conditions with 12 hours night-day cycles. Water and standard chow diet were provided ad libitum. Experiments were conducted on animals of both sexes, aged between 7 and 10.5 months. In total, tissue from one healthy mouse and twelve mice with PCLM were used for this study.

### **3.3. Intrahepatic injection of KPC-T cells**

To induce murine PCLM, intrahepatic ultrasound-guided injections of KPC-T cells were performed on C57BL/6J mice. Around 90%-confluent KPC-T cells, passages 20 to 23, were washed with PBS, harvested as described in chapter 3.2 and resuspended in cold PBS. Cells were counted using a Bürker chamber and resuspended in PBS at a density of  $2 \times 10^6$  cells/mL. Cell suspensions were stored on ice until injected.

Mice were anaesthetized with 2-3% (v/v) of Isoflurane (Baxter, FDG9623) in an induction chamber, and anaesthesia was maintained at 1-2% (v/v). To relieve pain from the injection, 5 mg/kg of the analgesic drug Carprofene (Rimadyl, Orion Pharma Animal Health, Vnr 462986) was subcutaneously administered, and protective eye ointment was applied. The hair was removed from the upper abdominal skin and liver lobes were localized with the ultrasound probe using a Vevo LAZR-X (FujiFilm VisualSonics) imaging platform. 50 µL of the KPC-T cell suspension, containing  $10^5$  cells, was brought to room temperature and injected into the liver using a 30-gauge needle. Following the injection, mice were transferred to their cage and monitored until fully recovered.

Tumour development was monitored by ultrasound and through assessment of the general health status of the injected mice (including signs of distress or pain, bodyweight). Mice were sacrificed for tissue extraction ~ 4 weeks after tumour cell injection when tumor had developed according to ultrasound assessments, or when reaching a humane endpoint as defined in the body condition scoring guidelines from Karolinska Institutet, which included assessments of the general condition, porphyrin staining of the eyes, movement and posture, piloerection, skin, weight, intestinal and urinary function, and an estimation of respiration frequency. In the category weight, for example, the humane endpoint was reached when mice showed > 15% weight loss.

### **3.4. Tissue extraction for explant culture**

PCLM tissue with adjacent liver, unaffected liver lobes distant from PCLM, as well as liver tissue from healthy animals was extracted for explant culture. Mice were anaesthetized in a pre-filled induction chamber with 5% (v/v) Isoflurane (Baxter, FDG9623) and subsequently sacrificed by cervical dislocation. After death was confirmed, the abdominal cavity and peritoneum were opened, and the liver was extracted to PBS (Gibco, REF 18912-014) or Hanks' Balanced Salt Solution (HBSS, Gibco, REF 14175-053) with 1% PEST (Cytiva, HyClone™, Cat No: SV30010). From here on, tissue was kept ice-cold until entirely cut and transferred to the culture medium. Extracted tissue was rinsed in PBS and trimmed with a scalpel. In initial experiments, approximately 1 mm thick tissue sections were cut manually using a scalpel, washed in PBS and transferred to DMEM/F12 medium supplemented with 10% FBS and 1% PEST for cultivation. In the following experiments, tissue pieces were embedded in 4% (w/v) low melting point agarose (Sigma-Aldrich, A4018), prepared in PBS, using embedding moulds (Sigma-Aldrich, E6032). Embedded tissue was stored in PBS, attached to the vibratome tray with 3M Vetbond Tissue Adhesive and submerged in ice-cold HBSS. PCTS of 300 µm and 400 µm thickness were prepared using a vibrating-blade microtome (VT1200S, Leica, Germany), equipped with a razor blade with the following settings: 0.14-0.18 mm/s speed and 1.3 mm amplitude. Tissue slices were transferred with a thin brush to a 24-well plate with ice-cold HBSS containing 1% PEST for transportation. The duration of the slicing procedure varied between 1 and 3 h, depending on the number of samples.



Tissue sections used in explant culture optimisation and characterisation experiments were cultured in 6-well plates with 0.4  $\mu\text{m}$  pore size membrane culture inserts (Millipore Corporation, Merck, REF PICM03050) or in 60 mm diameter TC dishes (Sarstedt, REF 83.3901) embedded in collagen/low melting point agarose for live-cell imaging in a humidified incubator at 37 °C in 5% CO<sub>2</sub> for up to 5 days. Culturing medium was DMEM/F12 or William's Medium E with GlutaMAX (WME) (Gibco, REF 32551) supplemented with 10% or 5% FBS and 1% PEST. The medium was exchanged a few hours after culture initiation (preincubation step) and every 24 hours thereafter.

### **3.5. Cell viability assay on explant cultures**

The 3-[4,5-dimethylthiazol-2-yl]-2,5-diphenyltetrazolium bromide (MTT) assay was used to assess cell viability within the tissue (Sasaki et al., 2019). First, tissue sections were rinsed in PBS and cut into smaller pieces using a scalpel. Excess liquid was removed from the tissue and it was transferred into a 96-well plate with 100  $\mu\text{L}$  of culturing medium and 10  $\mu\text{L}$  of MTT solution (from Cell Proliferation Kit I (MTT), Roche, REF 11465007001) per well and incubated for 4 hours at 37 °C. Tissue sections were dried briefly, weighed, and transferred into an Eppendorf tube with 200  $\mu\text{L}$  of isopropanol (Sigma-Aldrich, REF 278475). They were homogenized using Tissue Rupter homogenizer (Qiagen) on ice and incubated in isopropanol overnight at 4 °C. 140  $\mu\text{L}$  were transferred to a 96-well plate and the absorbance was measured at 565 nm with the NanoQuant microplate reader (infinite M200 pro, Tecan) using Tecan's i-control 1.10 software. The reference wavelength was 660 nm.

The measured optical density (OD) values were normalized to slice weight. MTT assay results were analysed using GraphPad Prism Version 8. The values were first transformed as a percentage of the mean of a certain condition (300  $\mu\text{m}$  thickness – in case of tissue thickness comparison, and DMEM F12 medium with 10% FBS – in case of culturing condition comparison). Those values were afterwards analysed using the t-test (in cases with two groups of values) or one-way ANOVA (in cases with more than two groups of values). These experiments were performed on tissue sections from 2-5 animals, including a minimum of 3 tissue sections from each animal. Each tissue section was considered a biological replicate.

### **3.6. Hematoxylin&eosin (H&E) and immunohistochemistry (IHC) staining**

Hematoxylin&eosin (H&E) staining was performed to assess general tissue morphology. Immunohistochemistry (IHC) staining was utilised to test for the presence of proliferating cells (by detecting Ki67), apoptotic cells (by detecting ClCasp3) and stromal cells (by detecting Desmin protein marker).

Tissue was fixed by incubation in 4% paraformaldehyde (PFA, Sigma-Aldrich, P6148), at room temperature for 20-24 h. Fixed samples were stored in 70% ethanol (EtOH, VWR, 20821.310) at 4 °C. Paraffin embedding, microtome sectioning into 3 µm thick sections and H&E staining were performed by ZeMac histoanalysis AB (Stockholm, Sweden) or Histology Core Facility (Karolinska Institutet, Solna, Sweden).

For IHC, sections were baked for 1 h at 60 °C. Deparaffinisation and rehydration was done by incubating in xylene (Sigma-Aldrich, 214736) for 2 min (x3) and 99.5%, 99.5%, 95%, 70%, 50% EtOH for 1 min each. Slides were washed in Milli-Q water for 2 min and PBS for 2 min (x3). Heat mediated antigen retrieval was performed by cooking the slides in DIVA Decloaker (Biocare, REF DV2004MX) with a steam cooker (Retriever 2010) for 30-40 min. Samples were allowed to cool down for 20 min and washed with PBS. To block endogenous peroxidases, samples were incubated in 3% (v/v) hydrogen peroxide solution (Sigma-Aldrich, H1009) for 15 min and washed in PBS for 2 min (x3). Slides were incubated in blocking solution (BS) (Tab. 2.) with 5 % serum (Tab. 3.) and 4 drops/mL avidin (Vector Laboratories, SP-2001) for 30 min and washed in PBS for 2 min (x3). Slides were incubated in primary antibody (Tab. 3.) diluted in BS 5 % serum and with 4 drops/mL biotin (Vector Laboratories, SP-2001) overnight at 4 °C. Slides were washed in PBS with 0.1% of Triton X-100 (Tx-100) for 5 min and PBS for 5 min (x2). Slides were incubated in secondary antibody (Tab. 3) diluted in BS for 30 min, washed in PBS with 0.1% Tx-100 for 5 min and in PBS for 5 min (x2). Slides were incubated with horseradish peroxidase-conjugated streptavidin (Invitrogen, REF 50209Z) for 20 min at room temperature. Slides were washed in PBS with 0.1% Tx-100 for 5 min and in PBS for 5 min (x2). Diaminobenzidine (DAB) substrate (Invitrogen D22187 or Metal Enhanced DAB Substrate Kit, producer, REF 34065) was added and staining density was monitored under a light microscope. After 1-2 min slides were washed in Milli-Q water (x3), counterstained with 50% Hematoxylin solution (Sigma-Aldrich, REF GHS132)

for 1-2 min, thoroughly washed under tap water, rinsed in PBS and mounted using Aqua poly mount (Polyscience, Inc., Cat# 18606).

IHC stainings were visualized by brightfield microscopy. Detection and quantification of positive cells was done with the help of QuPath (Bankhead et al., 2017) software (Version 0.1.2, Build time: 2016-12-31, Copyright (C) 2014 - 2016 The Queen's University of Belfast, Northern Ireland).

**Table 2.** Composition of blocking solution used for immunohistochemistry stainings.

Components of blocking solution (in PBS)	Producer and reference number
1% bovine serum albumin (BSA)	Sigma-Aldrich, A9418
0.2% cold fish skin gelatin (CFSG)	Sigma, 900-70-8
0.1% Tx-100	Sigma-Aldrich, T8787
0.1% sodium azide	Sigma-Aldrich, S2002

**Table 3.** Primary antibodies, secondary antibodies and serum used for immunohistochemistry stainings.

Primary antibody	Secondary antibody	Serum
Ki67 (D3B5, Cell Signalling #12202, rabbit), diluted 1:400	biotinylated goat anti-rabbit secondary antibody (Vector Laboratories, BA-1000), diluted 1:200	normal goat serum (Sigma-Aldrich, G9023)
ClCasp3 (Asp175, 5A1E, Cell Signalling #9664, rabbit), diluted 1:1500	biotinylated goat anti-rabbit secondary antibody (Vector Laboratories, BA-1000), diluted 1:150	normal goat serum (Sigma-Aldrich, G9023)
Desmin (Y-20, Santa Cruz Biotechnology, sc-7559, goat), diluted 1:50	biotinylated rabbit anti-goat (Vector Laboratories, BA-5000), diluted 1: 200	normal rabbit serum (Sigma-Aldrich, R4505)

### 3.7. RNA in situ hybridization (ISH)

The RNA in situ hybridization (ISH) was utilised to detect the presence of differentiated tumour cells based on the presence of *Alpi* mRNA marker.

The RNAscope 2.5 HD Duplex Detection Reagent Kit (Bio-Techne Ltd, UK, REF 322500) was used for RNA ISH according to the manufacturer's instructions. In brief, slides were incubated at 60 °C for 1 h. For deparaffinization, slides were incubated in xylene for 5 min (x2), in 100% EtOH for 1 min (x2) at room temperature and subsequently air-dried for 5 min. Slides were covered with

RNAscope Hydrogen peroxide solution and incubated for 10 min at room temperature. Slides were washed in Milli-Q water (x2) and slowly submerged into boiling 1x RNAscope Target Retrieval solution (ACD Advanced Cell Diagnostics, REF 322000) and incubated for 15 min. Slides were washed in Milli-Q water (x3), following 100% EtOH and air-dried. A liquid barrier was drawn around tissue sections with the Immedge Hydrophobic barrier pen and slides were placed in the HybEZ humidity tray. Slides were covered with RNAscope Protease Plus solution, incubated in the HybEZ oven at 40 °C for 30 min and subsequently washed in Milli-Q water (x3). Slides were covered with RNA ISH Alpi probe (ACD, Cat No. 436788) and incubated in the HybEZ oven at 40 °C for 2 h. Positive controls included tissue control - small intestine, and probe control from the RNAscope kit - murine UBC probe (ACD, REF 310771). As a negative control, a murine DapB probe (ACD, REF 310043) from the RNAscope kit was used. Slides were washed in 1x RNAscope Wash Buffer (ACD Advanced Cell Diagnostics, REF 310091) for 2 min (x2) and stored in 5x saline-sodium citrate (SSC) buffer overnight. Slides were washed in 1x Wash Buffer for 2 min (x2) and signal amplification with RNAscope Amp1-Amp10 reagents was performed according to the manufacturer's instructions. Each amplification step included removal of excess liquid, incubation with Amp reagent at 40 °C in HybEZ oven or room temperature and washing in 1x Wash buffer for 2 min (x2). After incubation with Amp6 and Amp10 reagent, samples were incubated for 10 min with freshly prepared RNAscope RED and RNAscope Green solution, respectively. From incubation with RNAscope RED on, slides were kept in dark. After amplification, slides were washed in 1x Wash buffer for 5 min and Milli-Q water for 30 sec at room temperature. Slides were counterstained with 50% Hematoxylin solution for 30 sec at room temperature, thoroughly washed under tap water and dried at 60 °C for 20 min. Slides were cooled at room temperature for 5 min, mounted with VectaMount Permanent mounting medium (Vector Laboratories, H-5000), air-dried for 5 min and stored in the dark at 4 °C.

### **3.8. Two-photon confocal live-cell imaging**

Two-photon confocal live-cell imaging was performed at the Live Cell Imaging Facility at Karolinska Institutet (Flemingsberg, Sweden) on an upright Zeiss LSM710-NLO microscope with an in-built full-size incubator, using a 20x dipping objective (Zeiss, n 1.33, NA 1.00, WD mm 1.5). PCLM sections were embedded in 80% collagen and/or 4% low melting point agarose, and cultured

in either DMEM/F12 or WME media, for the imaging. During time-lapse imaging, the temperature was maintained at 37 °C and CO<sub>2</sub> concentration at 5%.

Live-cell imaging of a region of interest was conducted at 1020 nm laser wavelength, 90% laser power, 6-10 µm z-stacks, 1-4 tiles (fields of view), and 30-35 min time intervals for up to 20 h. TdTomato expressing cancer cells were detected through the NDD R1 channel (565-610 nm detection wavelengths, 1.57 µm depth of focus), while the liver parenchyma tissue and surrounding collagen were imaged using second harmonic generation through the NDD R2 channel (500-550 nm detection wavelengths, 1.4 µm depth of focus). Time-lapse videos were processed using ImageJ (Schneider et al., 2012) software (ImageJ 1.52a, Wayne Rasband, National Institutes of Health, USA), by combining channels and using the maximum intensity projection function for 2-4 z-stacks at a time.

## **4. Results**

### **4.1. Tissue culture optimisation**

Murine PCLM explant culture optimisation included initial experiments on manually cut explants to test the feasibility of the general approach and determining an optimal tissue slice thickness as well as optimal culturing conditions on PCTS.

Firstly, two tissue thicknesses, 300  $\mu\text{m}$  and 400  $\mu\text{m}$ , chosen based on the literature review and preliminary experiments, were compared on tumour and unaffected liver sections that were cultured in DMEM/F12 medium with 10% FBS and 1% PEST at 37 °C in 5% CO<sub>2</sub> (standard condition 1). The MTT (3-(4,5-dimethylthiazol-2-yl)-2,5-diphenyl-2H-tetrazolium bromide) assay was used as a validation method for metabolic activity in tumour sections, also reflecting cell viability. Validation methods used for unaffected liver sections included 1) MTT assay, 2) H&E staining for the analysis of general tissue morphology, and 3) IHC staining for Ki67 (proliferation marker) and clCasp3 (cleaved caspase 3, apoptosis marker) to assess the presence of proliferating and apoptotic cells in the tissue, respectively.

In subsequent culture optimisation experiments, two culturing media, WME (Gibco, REF 32551) and DMEM/F12 (Gibco, REF 11320), chosen based on the literature review, with two FBS concentrations, 10% and 5%, were compared on 300  $\mu\text{m}$  thick tumour and unaffected liver sections. Validation methods were as in the previous step.

#### **4.1.1. Manually cut PDAC liver metastases explants**

Initial experiments were performed on manually cut PCLM explants cultured in standard condition 1. The experiments included 1) tumour tissue growth measurement over eight days in culture using stereo microscope imaging and 2) histology (H&E staining, Ki67 and clCasp3 IHC stainings) on directly fixed (0-time point) explants as well as explants fixed after 7, 24 and 96 h in culture.

The measurements of tumour tissue surface area (Fig. 3) from the stereo fluorescence microscope images of PCLM explants (Fig. 2) revealed no significant tumour tissue growth during eight days of culturing. However, there was cancer cell outgrowth into the collagen, especially noticeable at later time points (five and eight days) (Fig. 2).

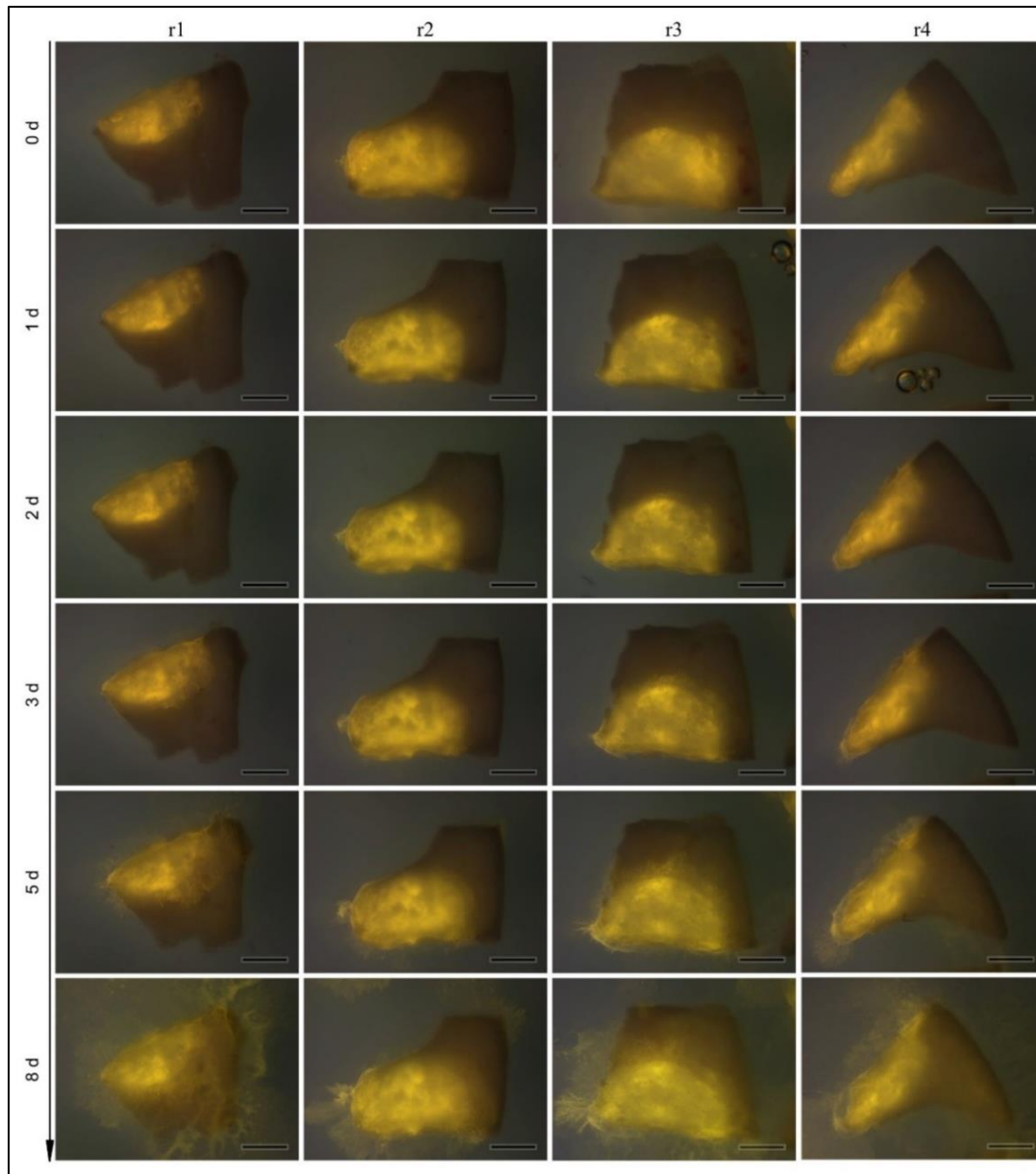


**Figure 2.** Time-lapse stereo microscope images of manually cut PCLM explants, embedded in 80% collagen, cultured in standard condition 1 for up to eight days (d). Tumour tissue is shown in yellow (number of animals,  $n = 1$ , number of sections from one animal,  $r = 4$ , scale bar = 5 mm).

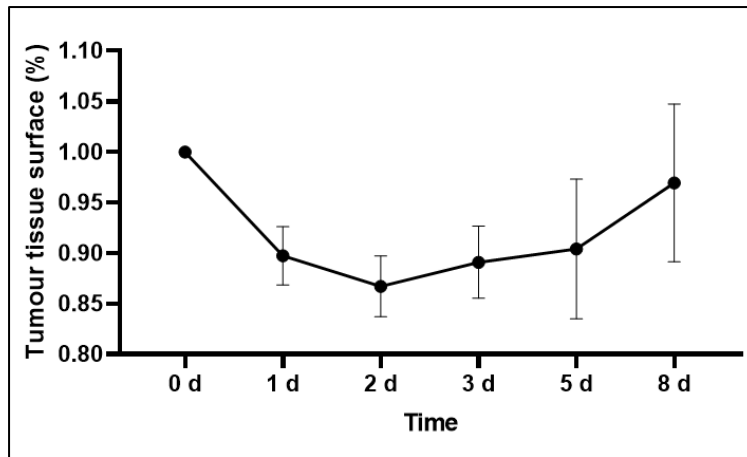


**Figure 3.** Tumour tissue surface area of PCLM explants (shown in Fig. 2) cultured over eight days in standard condition 1, presented as a percentage of the tumour tissue surface on day 0. The surface was measured manually in ImageJ software ( $n = 1$ ,  $r = 4$ ).

The histological morphology of liver tissue in the PCLM explants was generally similar throughout 96 hours of culturing without major changes in the tissue structure (Fig. 4). In general, tumour tissue was heterogeneous, containing regions of cells with differences in differentiation, but also necrotic areas. This structure was preserved in all the time points analysed (Fig. 4).

In some samples (Fig. 4 – 0 h and 7 h time points) tumour and liver tissue separated artificially, during the manual cutting procedure.



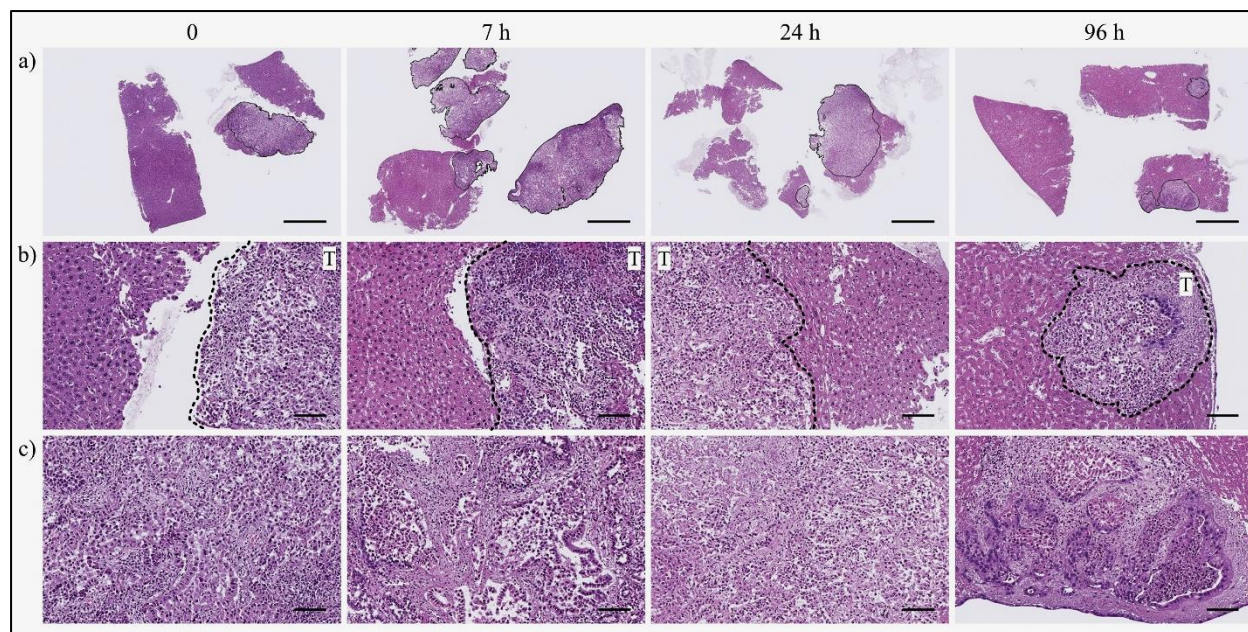


**Figure 4.** Representative images of H&E staining of manually cut PCLM explants cultured in standard condition 1 for 0, 7, 24 and 96 h. (a) Whole explants (scale bar = 1000 µm). (b) Invasion front between tumour (T) and liver parenchyma (scale bar = 100 µm). Tumour tissue is encircled with a black dashed line (a, b). (c) Tumour tissue from the centre (scale bar = 100 µm).

The presence of proliferating and apoptotic cells differed between liver and tumour tissue in the PCLM explants. There were almost no proliferating cells as detected with Ki67 IHC staining (Fig. 5) and no apoptotic cells, as detected with cIcasp3 IHC staining (Fig. 6) in the liver tissue. Tumour tissue contained both proliferating (Fig. 5) and apoptotic cells (Fig. 6) at all analysed time points.

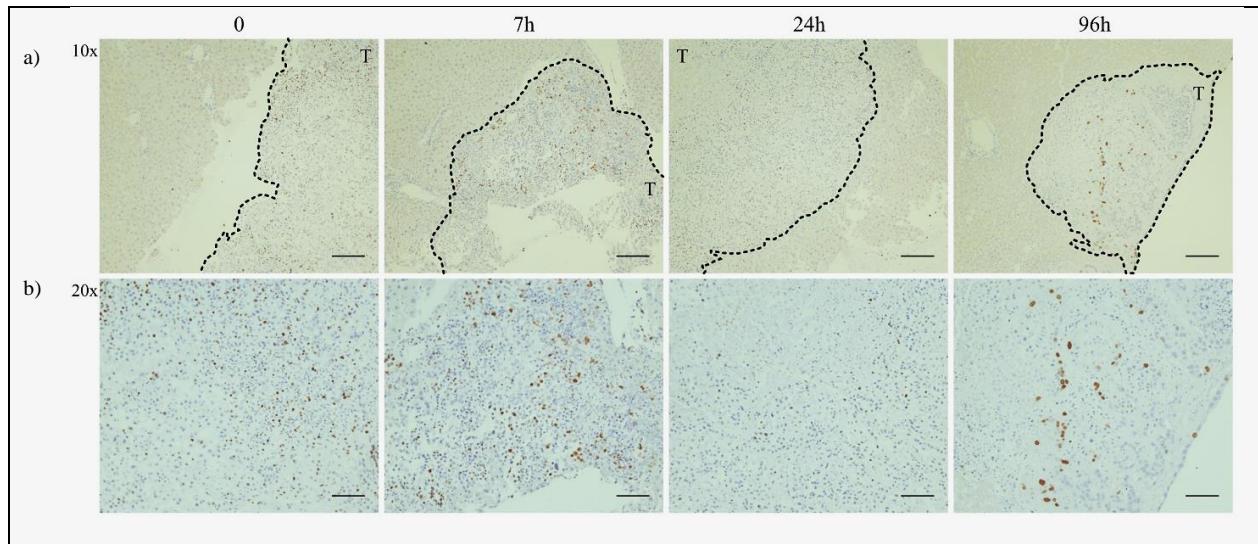


**Figure 5.** Ki67 (marker of proliferation) immunohistochemistry staining of manually cut PCLM explants cultured in standard condition 1 for 0, 7, 24 and 96 h. Positive cells show a brown nuclear pattern. (a) Invasion front between tumour (T) and liver parenchyma (10x magnification, scale bar = 100  $\mu$ m). Tumour tissue is encircled with a black dashed line. (b) Tumour tissue (20x magnified, scale bar = 50  $\mu$ m).

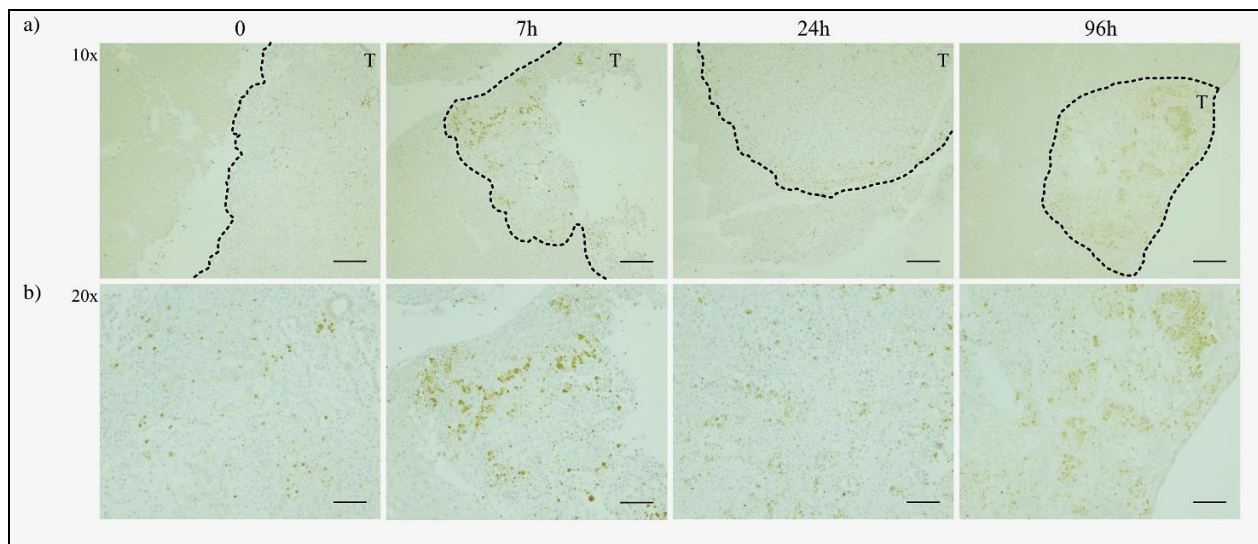


**Figure 6.** Cleaved Caspase-3 (clCasp3) (marker of apoptosis) immunohistochemistry staining of manually cut PCLM explants cultured in standard condition 1 for 0, 7, 24 and 96 h. Positive cells show a brown cytoplasmic pattern. (a) Invasion front between tumour (T) and liver parenchyma (10x magnification, scale bar = 100  $\mu$ m) Tumour tissue is encircled with a black dashed line. (b) Tumour tissue (20x magnified, scale bar = 50  $\mu$ m).

Manually cut PCLM sections exhibited structural integrity, maintained proliferation, comparable levels of apoptosis, and cellular heterogeneity. However, it was observed that manual cutting procedure can result in artefacts, such as separation between the tumour and liver tissue.

#### **4.1.2. Determining optimal tissue thickness**

After initial experiments on manually cut explants, the murine PCLM explant culture was optimised in order to facilitate live-cell imaging of sections of defined thickness. To this end, PCTS were prepared using a vibrating-blade microtome. In order to define the optimal tissue thickness for the explant culture, both unaffected liver and tumour tissue were sectioned into 300  $\mu\text{m}$  and 400  $\mu\text{m}$  thick PCTS and cultured in standard condition 1 for two and five days. Their metabolic activity was analysed with the MTT assay (Figs. 7, 8, 12, 13). Unaffected liver viability was analysed using H&E staining, Ki67 and cIcasp3 IHC staining. Representative images are shown in Figs. 9, 10, 11, 14, 15, 16.

Based on the MTT assay results, 300  $\mu\text{m}$  thick unaffected liver tissue sections showed higher metabolic activity than 400  $\mu\text{m}$  thick sections cultured in the same conditions for two and five days (Fig. 7).

There was no statistically significant difference between the 300  $\mu\text{m}$  and 400  $\mu\text{m}$  thick tumour tissue sections cultured for two and five days in the same culturing conditions (Fig. 8).

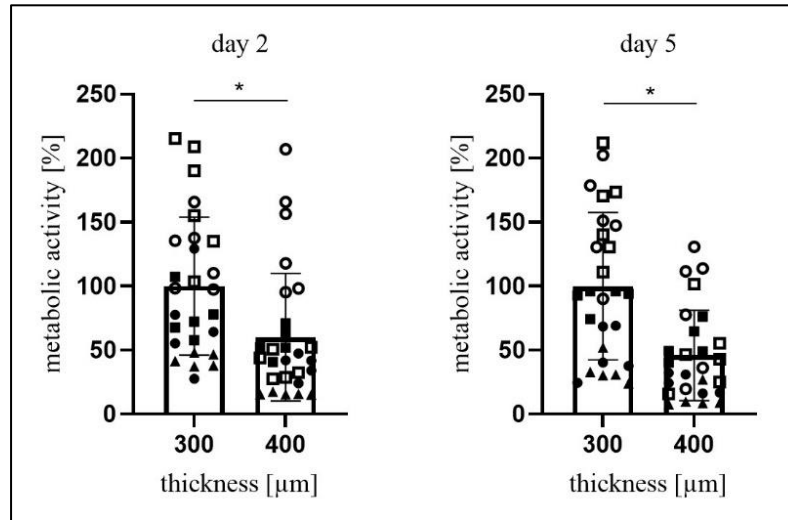


**Figure 7.** Metabolic activity in 300 μm and 400 μm thick liver tissue explants (from 5 mice bearing PDAC metastases) cultured for two (left) and five (right) days in standard condition 1. Each tissue section was considered a biological replicate. Asterisk indicates a statistically significant difference ( $p \leq 0.05$ ) based on an unpaired t-test. Different shapes represent samples from individual animals ( $n = 5$ ,  $r = \min. 3$ ).

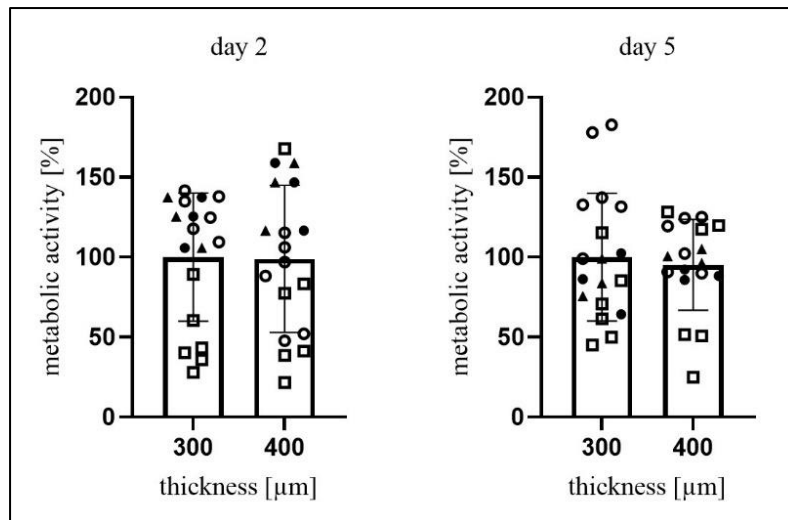


**Figure 8.** Metabolic activity in 300 μm and 400 μm thick tumour tissue explants (from 5 mice bearing PDAC metastases) cultured for two (left) and five (right) days in standard condition 1. Each tissue section was considered a biological replicate. Different shapes represent samples from individual animals ( $n = 5$ ,  $r = \min. 3$ ).



The structural integrity of both 300  $\mu\text{m}$  and 400  $\mu\text{m}$  thick unaffected liver tissue sections was intact after two days in culture, however, they started to show signs of damage, such as tissue breakage, after five days of culturing (Fig. 9).

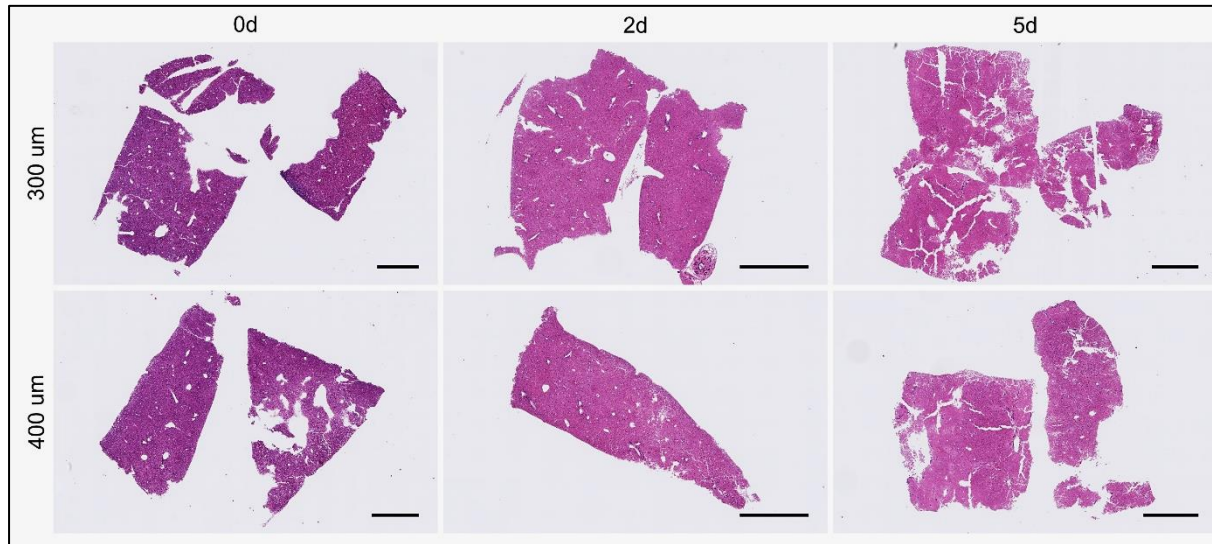


**Figure 9.** H&E staining on 300  $\mu\text{m}$  and 400  $\mu\text{m}$  thick unaffected liver tissue (of PDAC metastases) explants cultured for zero, two and five days in standard condition 1 (scale bar = 1000  $\mu\text{m}$ ).

Both Ki67 (Fig. 10) and cIcasp3 (Fig. 11) stainings had strong background signal, likely due to artefactual staining of hepatocytes, and a limited number of cells showed strong, specific staining. There was no overt difference in Ki67 expression in unaffected liver tissue sections when comparing 300  $\mu\text{m}$  and 400  $\mu\text{m}$  thickness. Directly fixed samples had the highest number of positive cells for both Ki67 and cIcasp3, compared to samples cultured for two and five days.

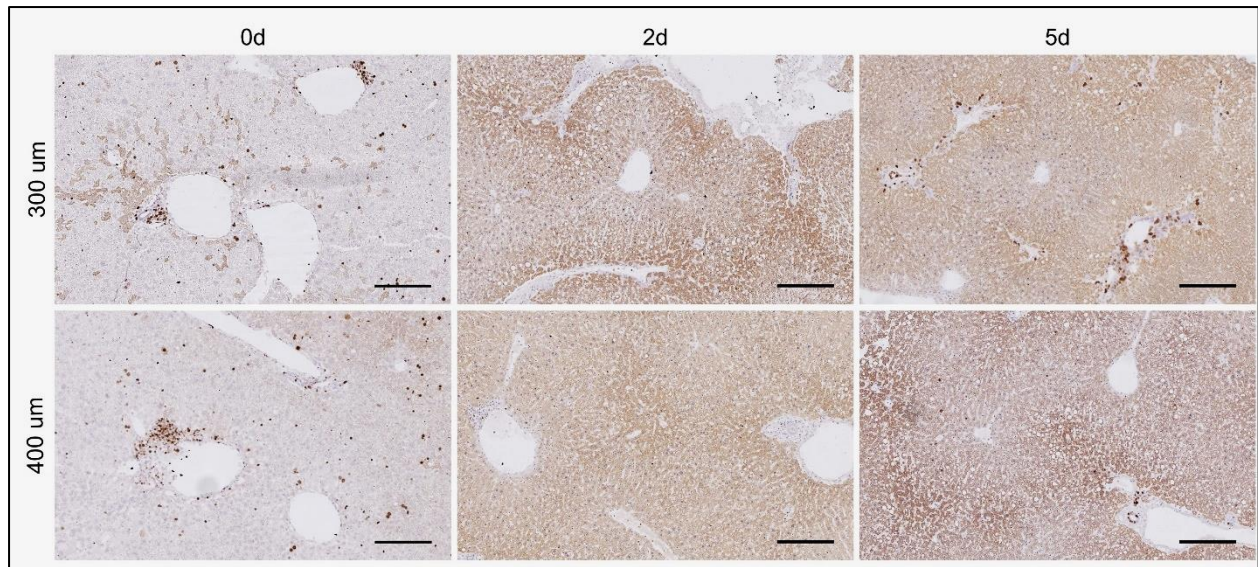


**Figure 10.** Ki67 (proliferation marker) immunohistochemistry staining of 300  $\mu\text{m}$  and 400  $\mu\text{m}$  thick unaffected liver tissue (of PDAC metastases) explants cultured for zero, two and five days in standard condition 1. Positive cells show a brown nuclear pattern (scale bar = 200  $\mu\text{m}$ ).

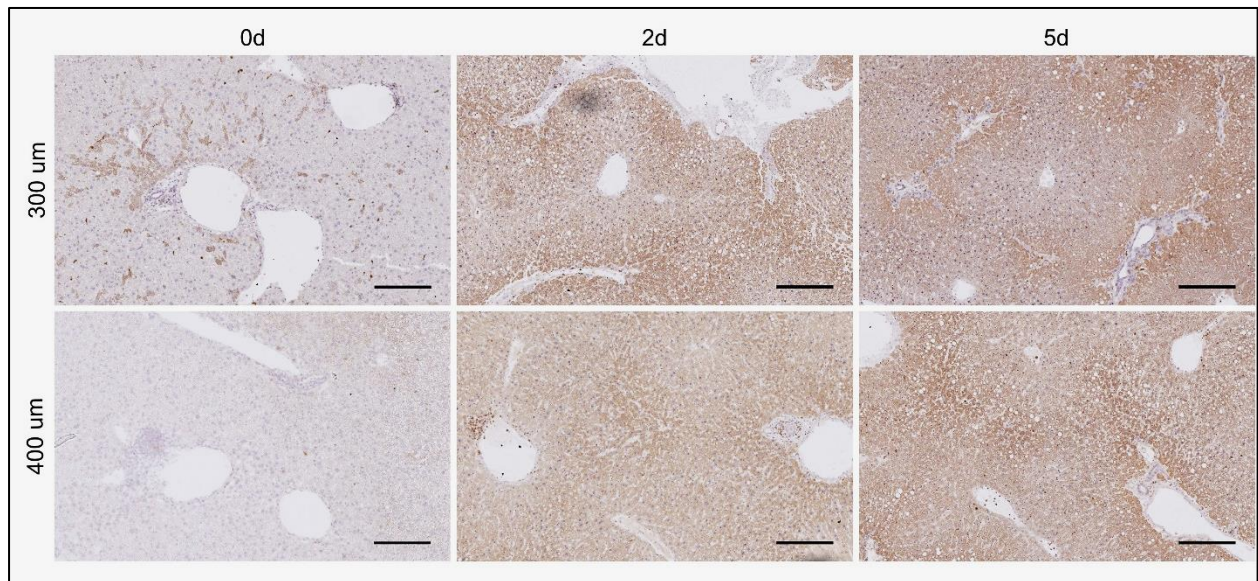


**Figure 11.** ClCasp3 (apoptosis marker) immunohistochemistry staining of 300  $\mu\text{m}$  and 400  $\mu\text{m}$  thick unaffected liver tissue (of PDAC metastases) explants cultured for zero, two and five days in standard condition 1. Positive cells show a brown cytoplasmic pattern (scale bar = 200  $\mu\text{m}$ ).

In conclusion, 300  $\mu\text{m}$  thick unaffected liver tissue sections showed higher metabolic activity, as measured by the MTT assay, compared to 400  $\mu\text{m}$  thick section. No significant difference was observed in IHC stainings for proliferation and apoptosis markers. Furthermore, tumour tissue sections of different thicknesses showed no overt difference in any of the experiments.

#### **4.1.3. Determining optimal culturing conditions**

For the establishment of optimal culturing conditions, 300  $\mu\text{m}$  thick liver and tumour tissue sections were cultured in DMEM/F12 medium supplemented with 10% FBS or 5% FBS and 1% PEST or in WME supplemented with 10% or 5% FBS and 1% PEST for two and five days. Metabolic activity in the slices was tested using an MTT assay (Figs. 12, 13). Unaffected liver tissue structural integrity (at light microscopic level), cellular proliferation and apoptosis were analysed using H&E staining, Ki67 and clCasp3 IHC staining, respectively. Representative images are shown in Figs. 14, 15, 16 respectively.

300  $\mu\text{m}$  thick unaffected liver tissue sections showed higher metabolic activity when cultured in WME with 10% FBS compared to DMEM/F12 medium with 10% FBS, after two and five days in culture (Fig. 12). Compared to 10% FBS, 5% FBS reduced the metabolic activity in both culture media.

There was no difference in metabolic activity between tumour tissue sections cultured in the investigated media for two and five days (Fig. 13)

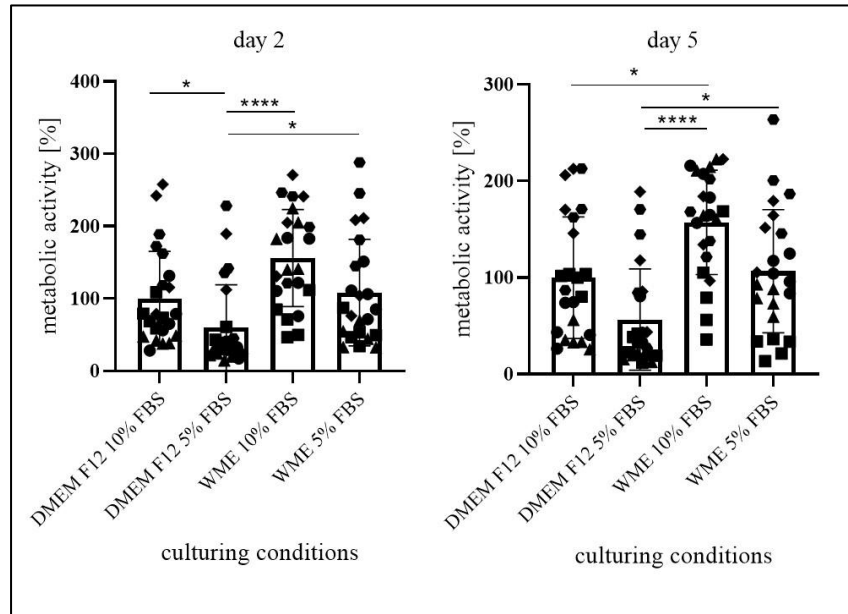


**Figure 12.** Metabolic activity in 300  $\mu$ m thick unaffected liver tissue explants (from 5 mice bearing PDAC metastases) cultured for two (left) and five (right) days at 37  $^{\circ}$ C in 5%  $\text{CO}_2$  in different culturing media; as indicated in the figures. Each tissue section was considered a biological replicate. Asterisks indicate a statistically significant difference with  $p \leq 0.05$  (\*) and  $p \leq 0.0001$  (\*\*\*\*), based on Kruskal-Wallis test with Dunn's multiple comparison test. Different shapes represent samples from individual animals ( $n = 5$ ,  $r = \text{min. } 3$ ).



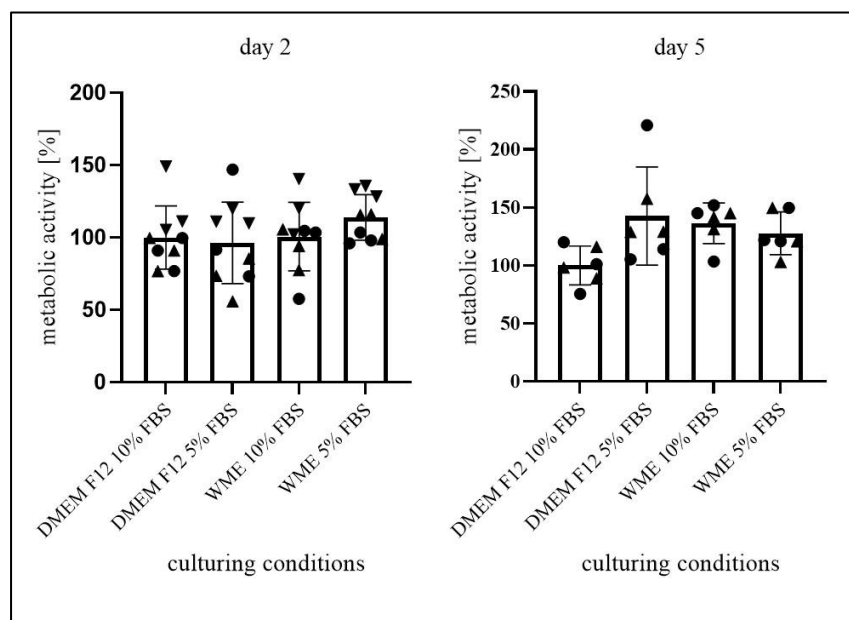


**Figure 13.** Metabolic activity in 300 µm thick tumour tissue explants (from 2-3 mice bearing PDAC metastases) cultured for two (left) and five (right) days at 37 °C in 5% CO<sub>2</sub> in different culturing media; as indicated in the figures. Each tissue section was considered a biological replicate. Different shapes represent samples from individual animals (n = 2-3, r = min. 3).

The morphology and integrity of unaffected liver tissue sections were similar between different culture conditions after two and five days of culturing. However, after five days of culturing, the amount of tissue damage, such as tissue folding and breakage, increased in all the culturing conditions (Fig. 14).

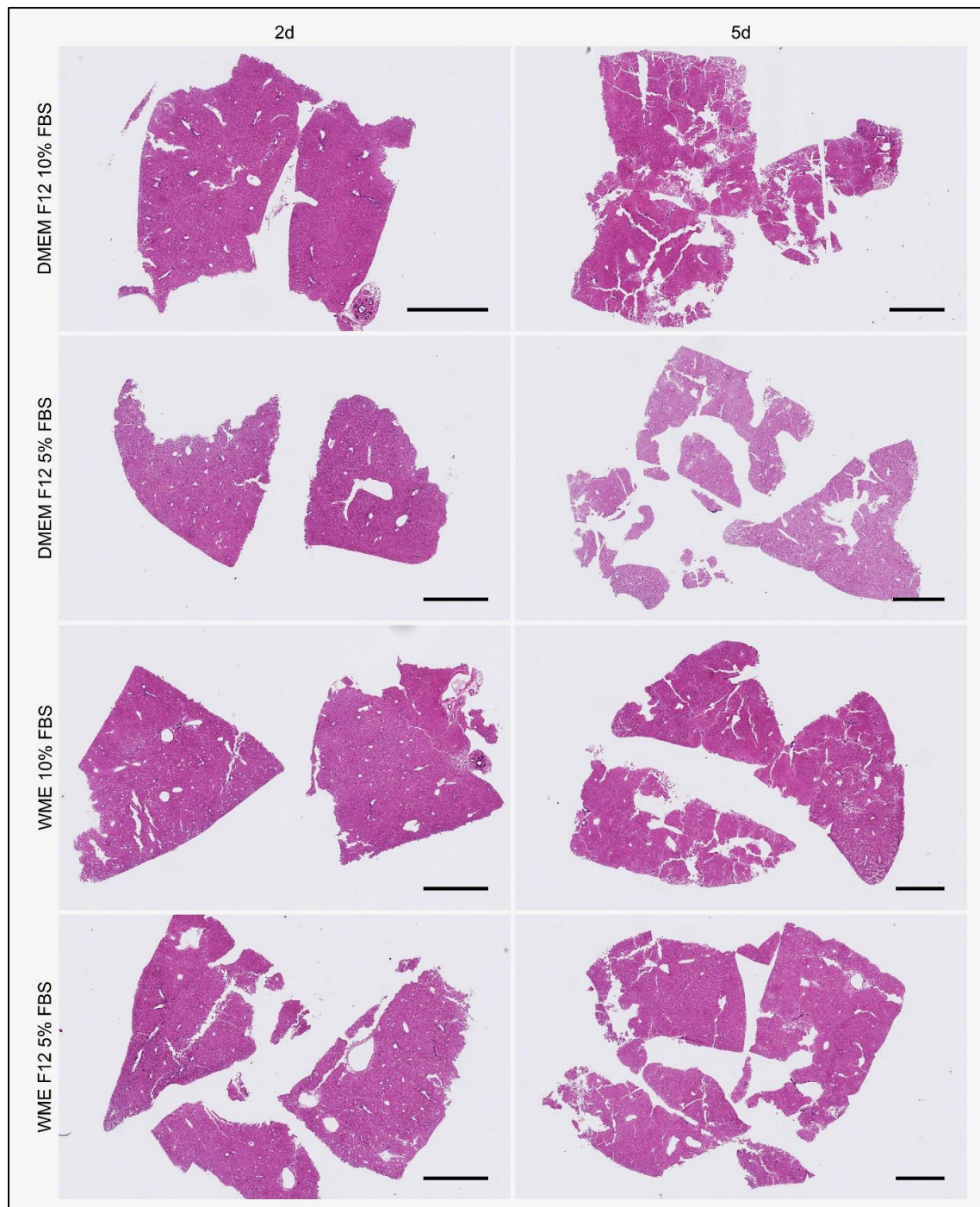


**Figure 14.** H&E staining on 300 μm thick unaffected liver tissue (of PDAC metastases) explants cultured for two and five days at 37 °C in 5% CO<sub>2</sub> in different culturing media; DMEM/F12 supplemented with 10% or 5% FBS and 1% PEST, WME supplemented with 10% or 5% FBS and 1% PEST (scale bar = 1000 μm).

Both Ki67 and cIcasp3 IHC stainings resulted in high background and scarce specific signal. Furthermore, no significant difference was observed in the proliferation or apoptosis rate between 300  $\mu\text{m}$  thick unaffected liver explants cultured in different media and serum concentrations (Figs. 15, 16).

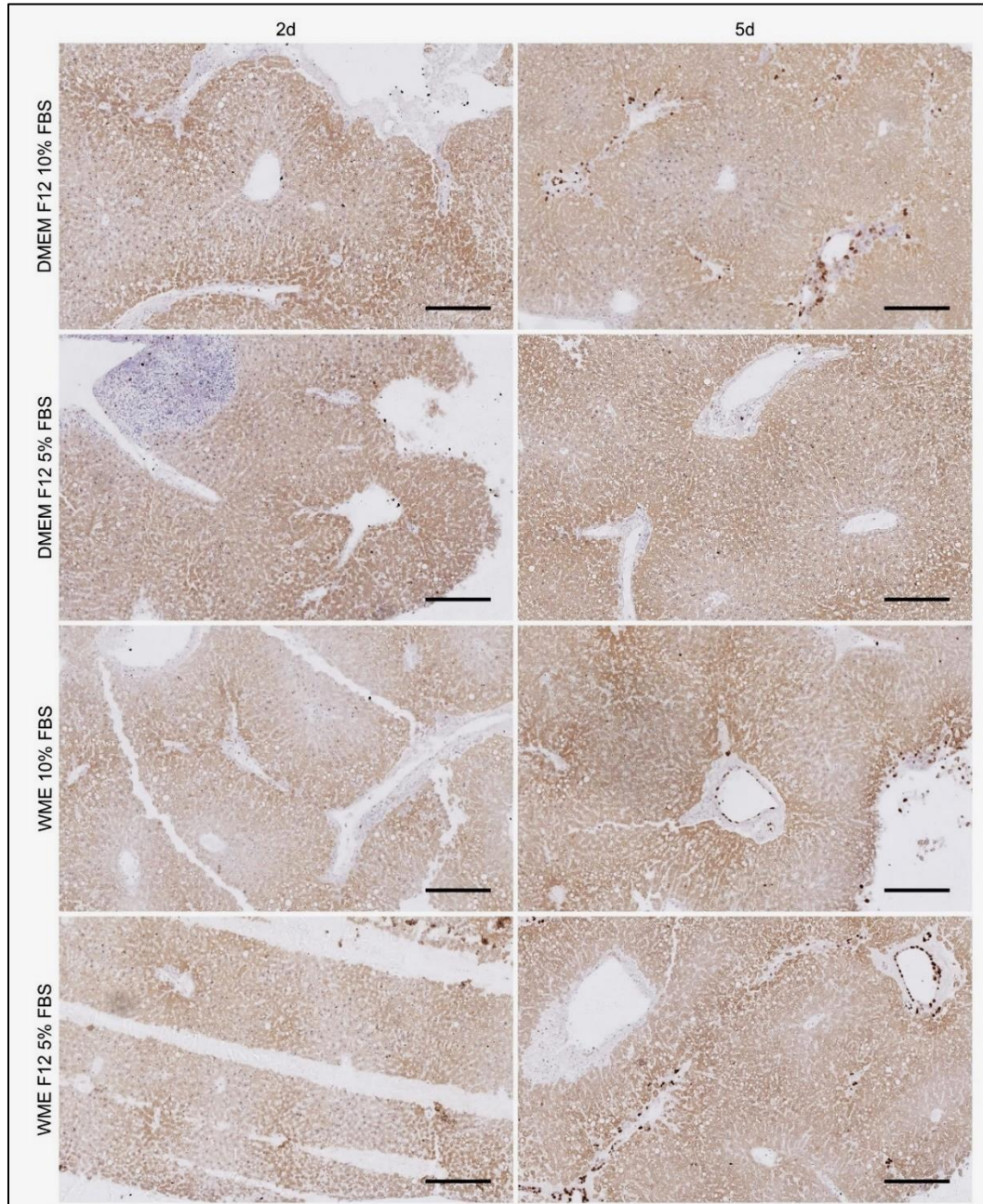


**Figure 15.** Ki67 (proliferation marker) immunohistochemistry staining on 300  $\mu\text{m}$  thick unaffected liver tissue (of PDAC metastases) explants cultured for two and five days at 37  $^{\circ}\text{C}$  in 5%  $\text{CO}_2$  in different culturing media; DMEM/F12 supplemented with 10% or 5% FBS and 1% PEST, WME supplemented with 10% or 5% FBS and 1% PEST. Positive cells show a brown nuclear pattern (scale bar = 200  $\mu\text{m}$ ).



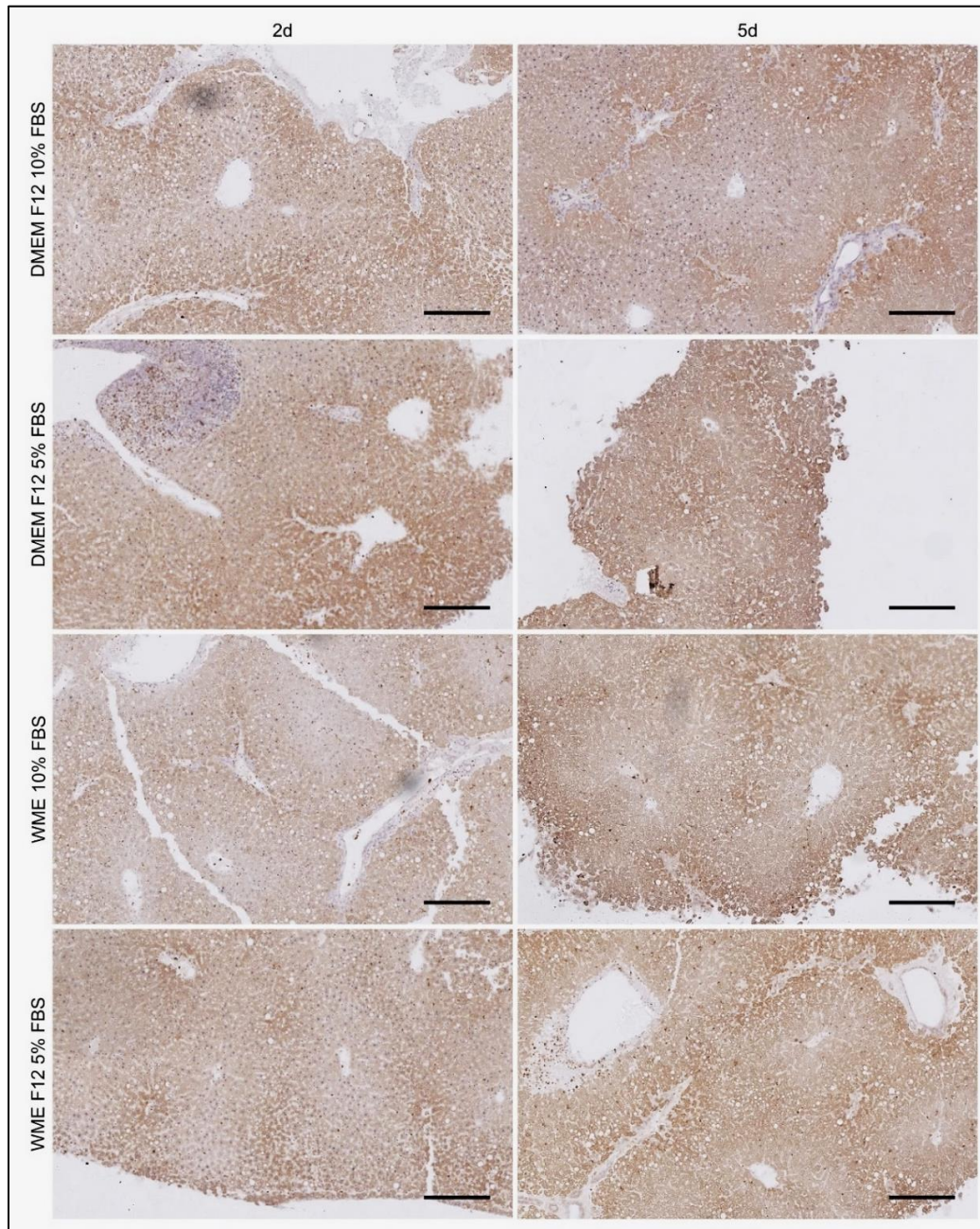


**Figure 16.** ClCasp3 (apoptosis marker) immunohistochemistry staining on 300  $\mu\text{m}$  thick unaffected liver tissue (of PDAC metastases) explants cultured for two and five days at 37  $^{\circ}\text{C}$  in 5%  $\text{CO}_2$  in different culturing media; DMEM/F12 supplemented with 10% or 5% FBS and 1% PEST, WME supplemented with 10% or 5% FBS and 1% PEST. Positive cells show a brown cytoplasmic pattern (scale bar = 200  $\mu\text{m}$ ).

In conclusion, unaffected liver tissue explants cultured in WME medium with 10% FBS showed the highest metabolic activity, measured by the MTT assay, compared to other culturing conditions. On the other hand, tumour tissue retained comparable metabolic activity between different culturing conditions. H&E, Ki67 and clCasp3 IHC stainings of unaffected liver explants kept in different culturing conditions, did not reveal overt differences.

## **4.2. Tissue culture characterisation: viability, apoptosis, and cell type heterogeneity**

In order to further characterise the murine PCLM explant culture established in previous chapters, 300  $\mu$ m thick liver metastases sections were cultured for two and five days in WME medium with 10% FBS and 1% PEST (standard condition 2). These samples were subsequently analysed using H&E, Ki67 (proliferation marker), clCasp3 (apoptosis marker) and desmin (stromal cell marker) IHC stainings and *Alpi* (marker for more differentiated tumour cells) mRNA ISH, in order to test the viability and cellular heterogeneity compared to metastases *in vivo* that were directly fixed. Finally, murine PCLM explant culture was compared to a human PCLM sample (Fig. 18).

### **4.2.1. Cell survival**

Within the tumour tissue, heterogeneity of the tumour cells, from undifferentiated to differentiated morphology was observed. Necrotic areas were present, but less frequent, compared to initial experiments with manually cut PDAC explants (Fig. 17).



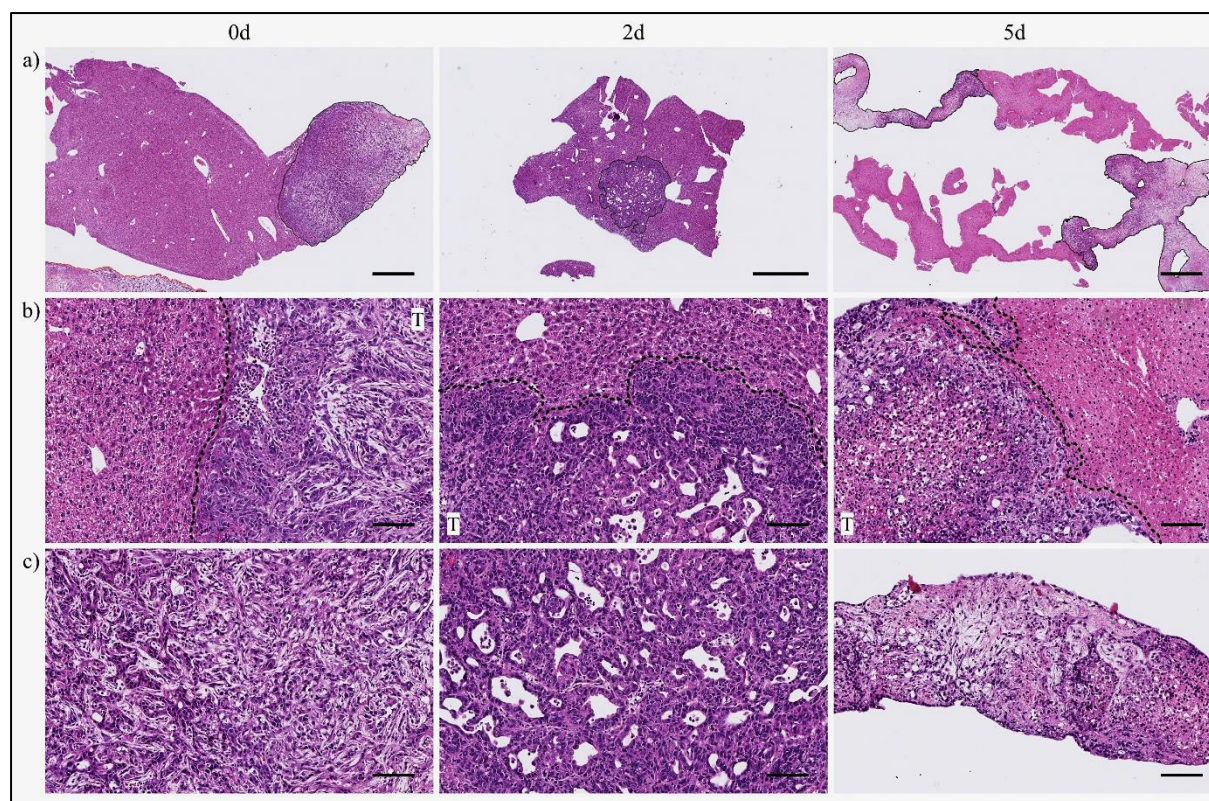


**Figure 17.** H&E staining on 300 µm thick PCLM explants cultured for zero, two and five days in the standard condition 2. (a) Whole explants (scale bar = 1000 µm). (b) Invasion front between tumour (T) and liver parenchyma (scale bar = 100 µm). Tumour tissue is encircled with a black dashed line (a, b). (c) Tumour tissue from the centre (scale bar = 100 µm).

The histology of murine PCLM explants cultured for five days resembled that of human patient samples (Fig. 18). In both murine and human metastases, the tumour cells invade the surrounding liver by establishing direct contact with the hepatocytes, which corresponds to the biologically aggressive “replacement” growth pattern.



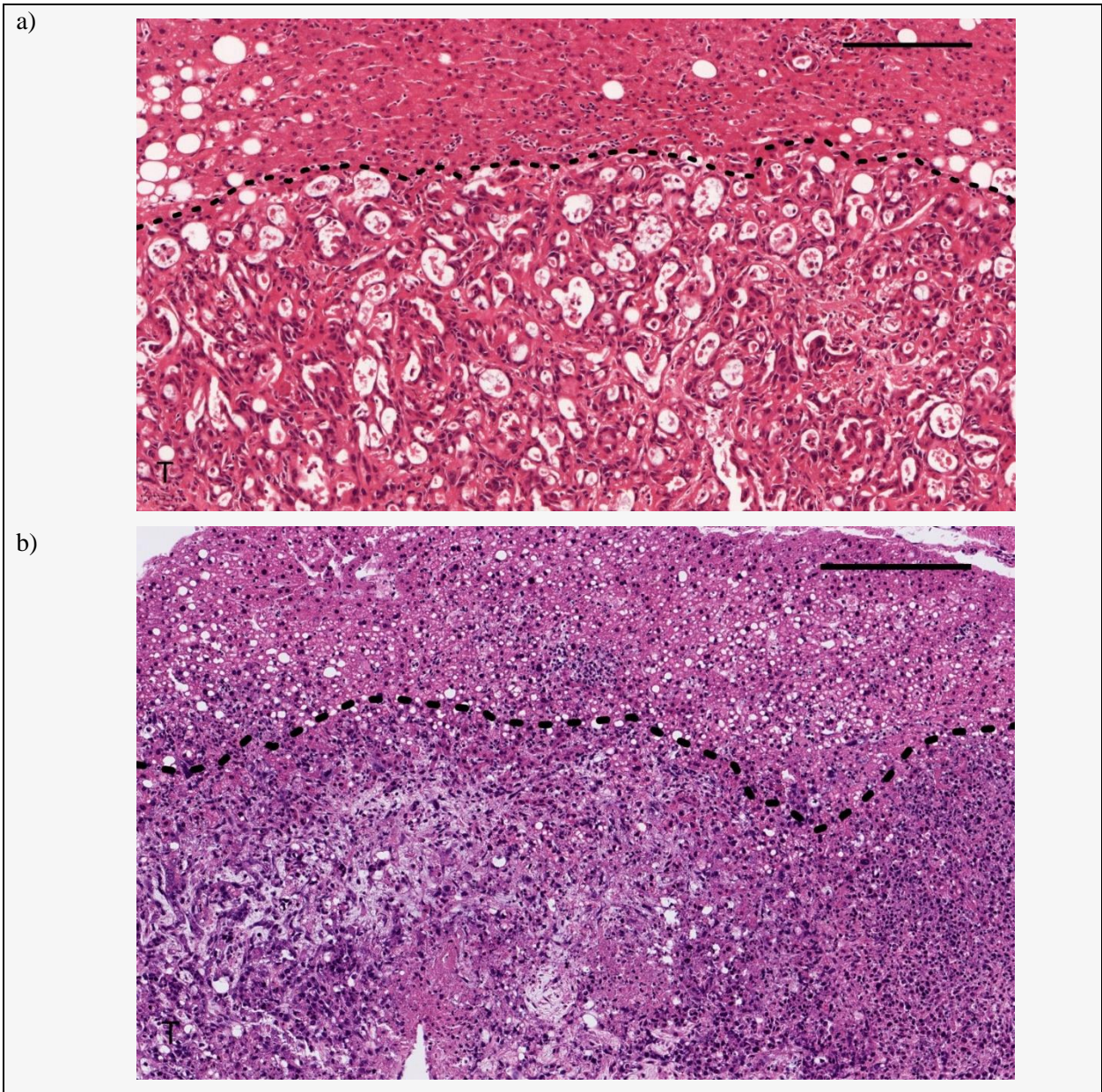


**Figure 18.** Comparison of general tumour tissue (T) morphology in a representative (a) human PDAC liver metastasis sample (courtesy of Carlos Fernández Moro) and b) murine PCLM explant cultured for five days in standard condition 2 (scale bar = 200  $\mu$ m).

Murine liver tissue contained Ki67 positive cells at all the analyzed time points of culturing, with the lowest amount after five days in culture (Fig. 19). Directly fixed tumour tissue contained 54.1 ( $\pm$  9.7) % Ki67 positive cells. The number of Ki67+ cells decreased over time to 8.7 ( $\pm$  4.4) % on day five (Fig. 20). In general, the number of Ki67+ cells in the tumour centre was lower than at the border (Fig. 19, not quantified).



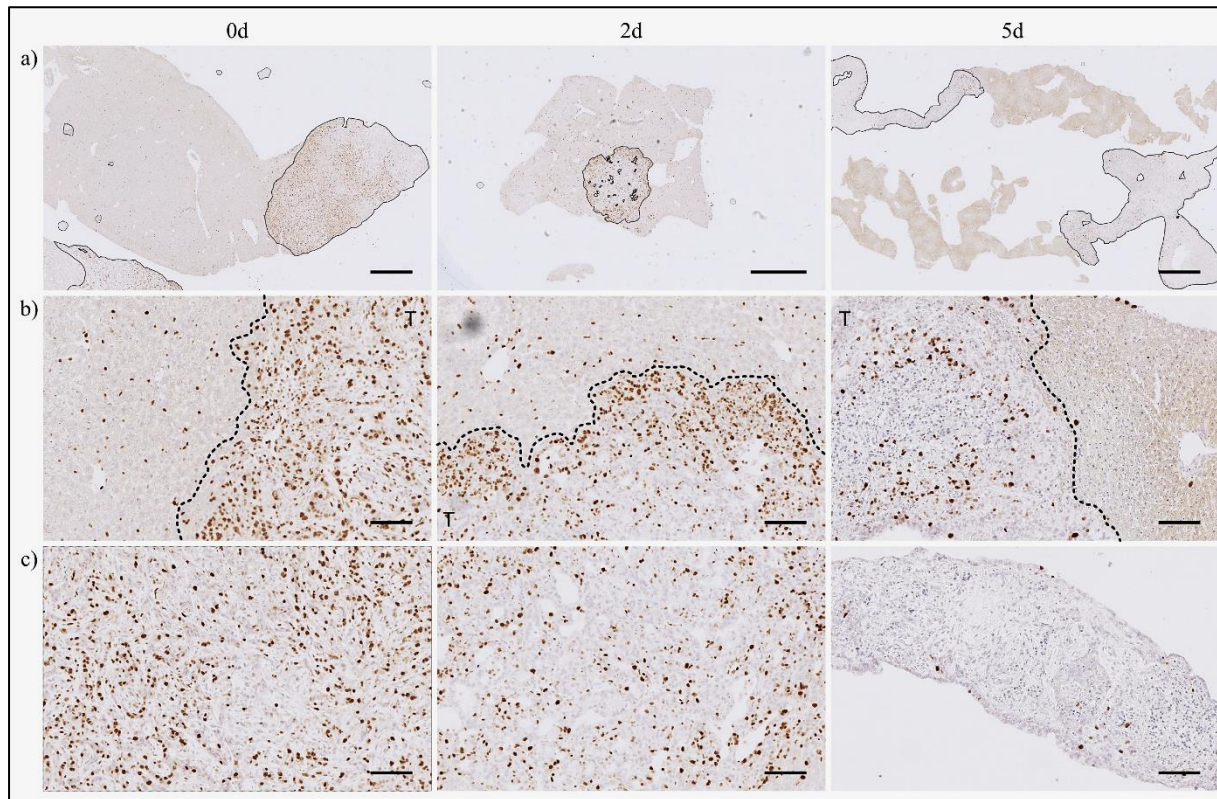


**Figure 19.** Ki67 (proliferation marker) immunohistochemistry staining on 300 µm thick PCLM explants cultured for two and five days in standard condition 2. Positive cells show a brown nuclear pattern. (a) Whole explants (scale bar = 1000 µm). (b) Invasion front between tumour (T) and liver parenchyma (scale bar = 100 µm). Tumour tissue is encircled with a black dashed line (a, b). (c) Tumour tissue from the centre (scale bar = 100 µm).



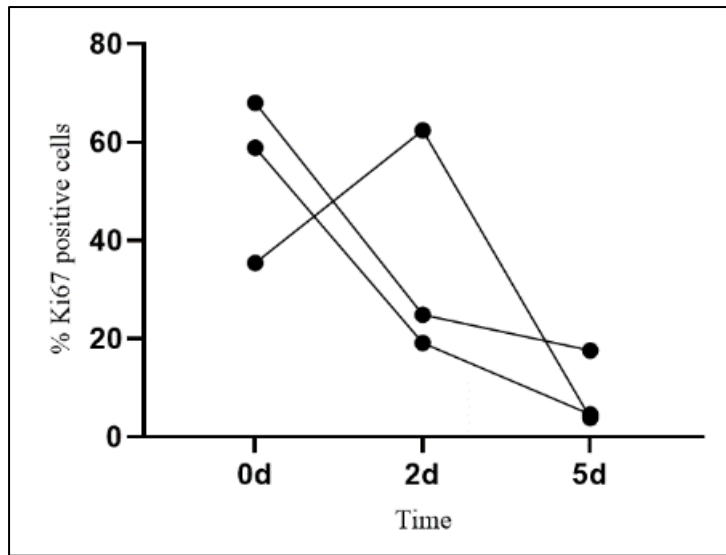


**Figure 20.** Ki67 IHC quantification for the whole tumour tissue area in PCLM explants cultured for up to five days in standard condition 2 (shown in Fig. 19). Each line represents one animal ( $n = 3$ ,  $r = \text{min. } 1$ ).

ClCasp3 positive cells were exclusively located inside the tumour area and not seen in the surrounding liver. Directly fixed samples (0d time point) contained a low number of apoptotic cells. However, based on observation of clCasp3 IHC staining, clCasp3 positive cell numbers increased after five days in culture (Fig. 21, not quantified).

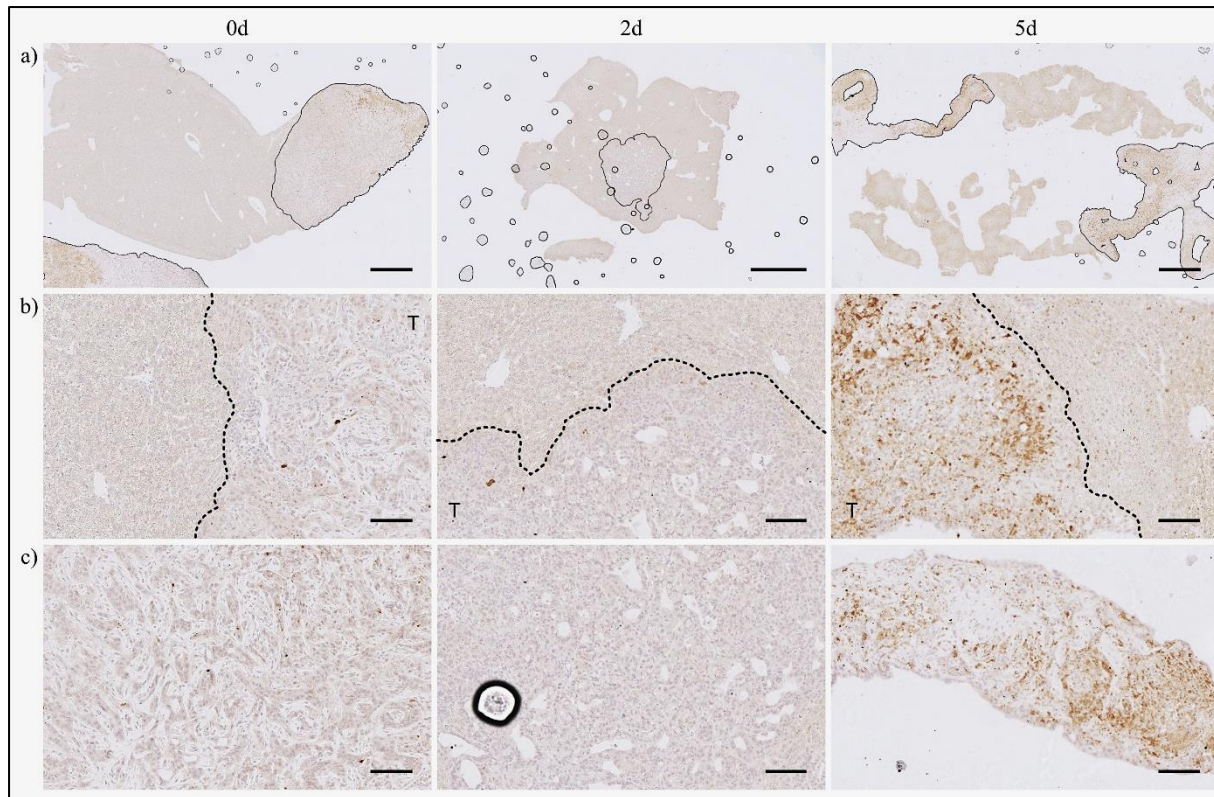


**Figure 21.** CIcasp3 (apoptosis marker) immunohistochemistry staining on 300 µm thick PCLM explants cultured for two and five days in standard condition 2. Positive cells show a brown cytoplasmic pattern. (a) Whole explants (scale bar = 1000 µm). (b) Invasion front between tumour (T) and liver parenchyma (scale bar = 100 µm). Tumour tissue is encircled with a black dashed line (a, b). (c) Tumour tissue from the centre (scale bar = 100 µm).

In conclusion, murine PCLM explants were viable, preserved their structural integrity and resembled the human tissue for up to five days in culture. Moreover, proliferating cells were present in both liver and tumour tissue during culturing, however, with a decrease after five days. Tumour tissue also contained apoptotic cells whose numbers increased with longer culturing time.

#### 4.2.2. Presence of different cell types

To analyse the cellular heterogeneity of murine PCLM explants, desmin IHC staining and *Alpi* mRNA ISH were performed. Desmin marks stromal cells, especially activated fibroblasts in the TME, and *Alpi* expression was identified as a marker for differentiated tumour cells, through single-cell RNA sequencing experiments by the host laboratory.

Desmin positive stromal cells were present in the tumour tissue of PCLM explants at zero time point and after two and five days of culturing (Fig. 22, not quantified). They seem to be less abundant in the tumour centre compared to the periphery.

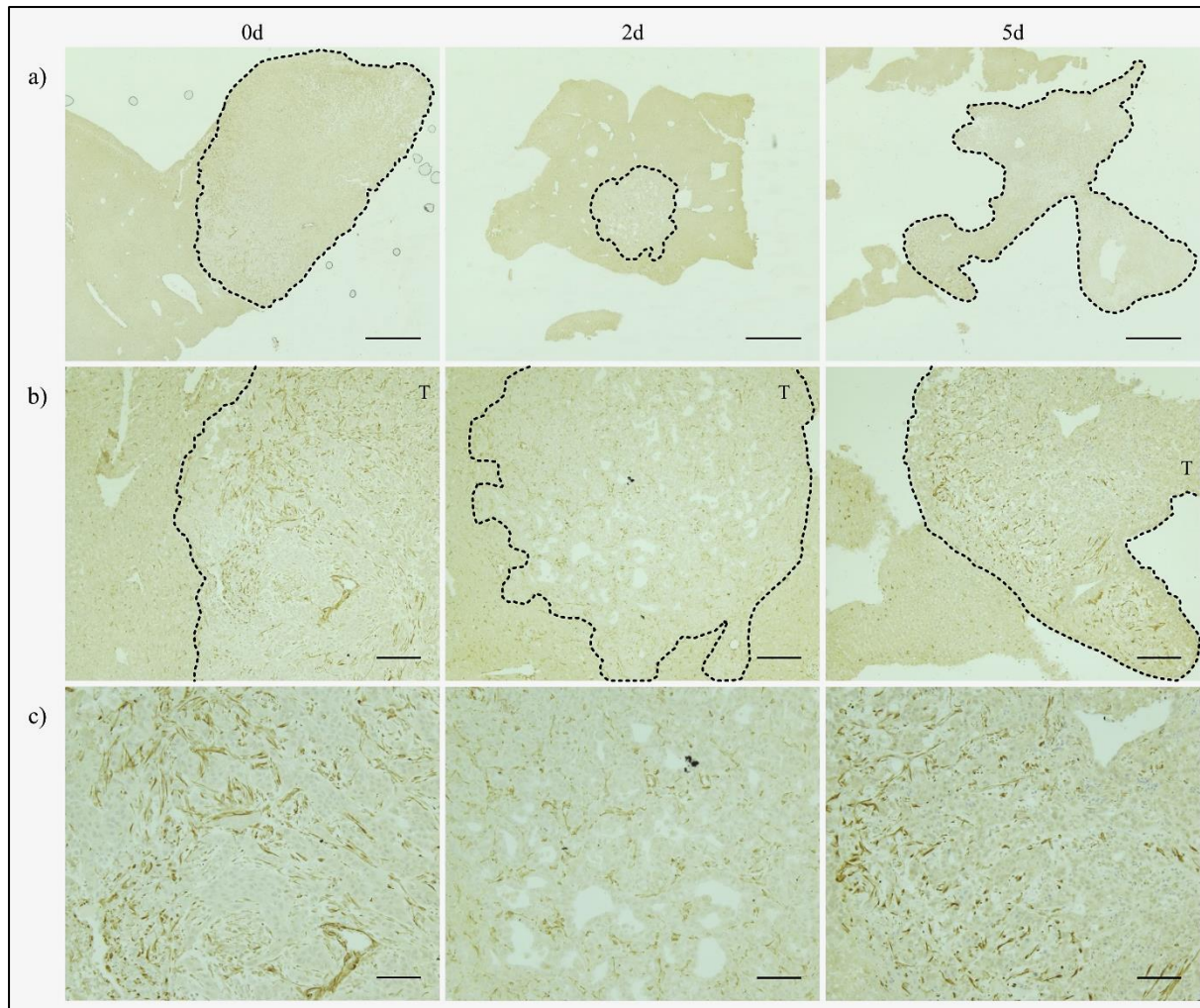


**Figure 22.** Desmin (stromal cell marker) immunohistochemistry staining on 300 µm thick PCLM explants cultured for two and five days in standard condition 2. Positive cells show a brown cytoplasmic pattern. (a) Whole explants (scale bar = 500 µm). (b) Invasion front between tumour (T) and liver parenchyma (scale bar = 100 µm). Tumour tissue is encircled with a black dashed line (a, b). (c) Tumour tissue from the centre (scale bar = 50 µm).



*Alpi* positive tumour cells were present in PCLM tissue sections at zero time point and after two and five days of culturing. However, the number of *Alpi* expressing cells decreased with increased culture length (Fig. 23, not quantified).

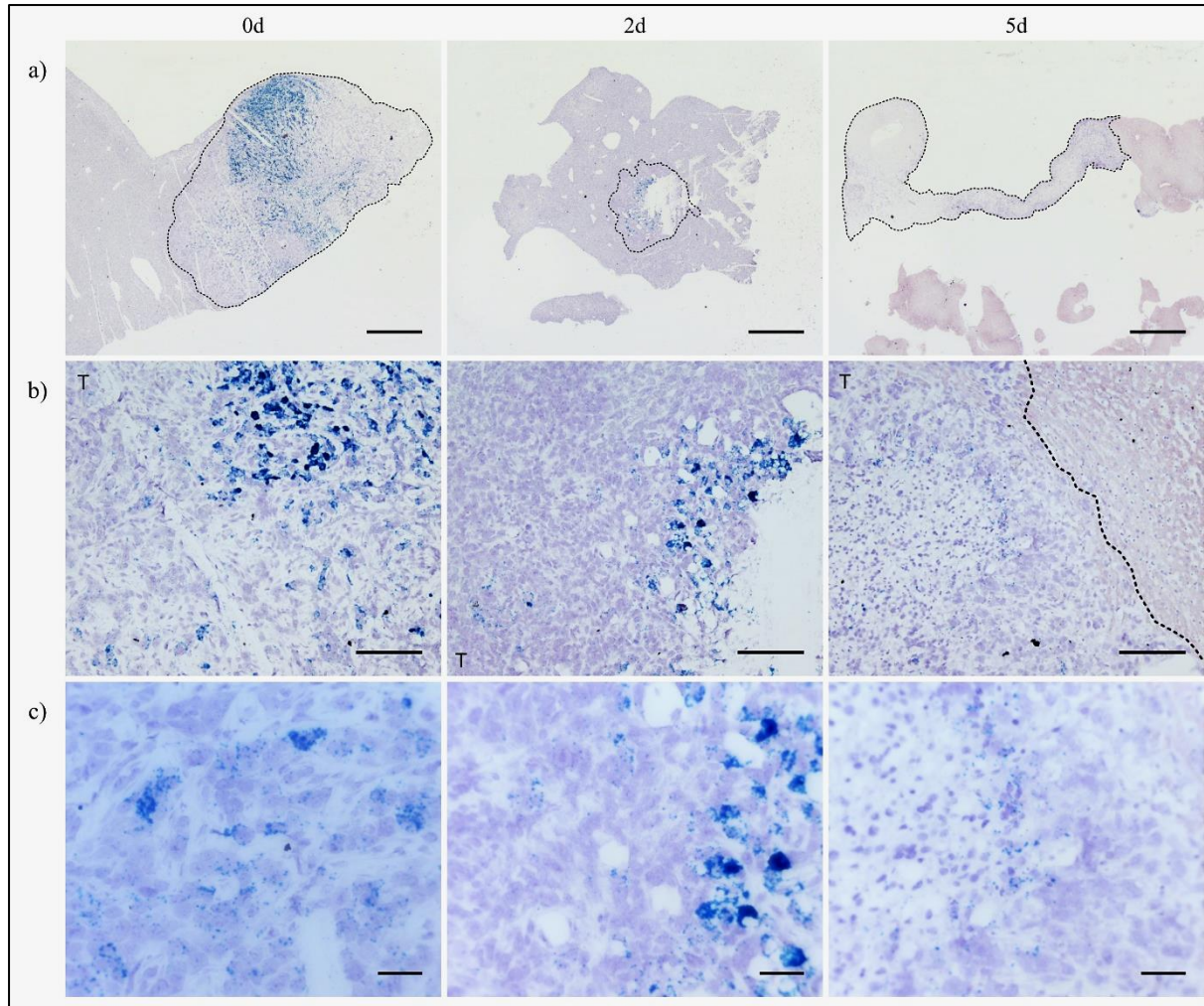


**Figure 23.** *Alpi* (a marker for differentiated tumour cells) mRNA in situ hybridisation on 300  $\mu\text{m}$  thick PCLM explants cultured for two and five days in standard condition 2. Positive cells contain blue dots. (a) 2.5x magnified (scale bar = 500  $\mu\text{m}$ ). Tumour tissue is encircled with a black dashed line (a). (b) 20x magnified (scale bar = 75  $\mu\text{m}$ ). (c) Tumour tissue from the centre (scale bar = 25  $\mu\text{m}$ ).

Both desmin positive stromal cells and *Alpi* positive, differentiated tumour cells, that were present in the directly fixed murine PCLM sections were also present after five days of culture.

### **4.3. Two-photon live-cell imaging**

Two-photon confocal live-cell imaging was used on optimised PCLM explant culture (300  $\mu\text{m}$  thick liver metastases sections cultured in WME medium with 10% FBS and 1% PEST at 37 °C in 5%  $\text{CO}_2$  – standard condition 2) to visualize and track cellular interactions between the tumour cells and liver parenchyma.

#### **4.3.1. Protocol optimisation**

While optimising the two-photon live-cell imaging protocol, the two main challenges encountered were photobleaching (Fig. 24) and focal drift (Fig. 26) of the explants. Several approaches have been taken to overcome these issues.

Photobleaching could be reduced by adjusting the laser wavelength and intensity. In addition, the auto bleach correction adjustment from ImageJ software was applied (Fig. 25).

Temperature fluctuations in the imaging incubator and using soft extracellular matrices such as collagen to embed the tissue sections were identified as potential causes of focal drift (Fig. 26). These were addressed by 1) leaving the explant in the microscope incubator for several hours, so the temperature balances out, before starting the imaging and 2) embedding the tissue sections in low melting point agarose.

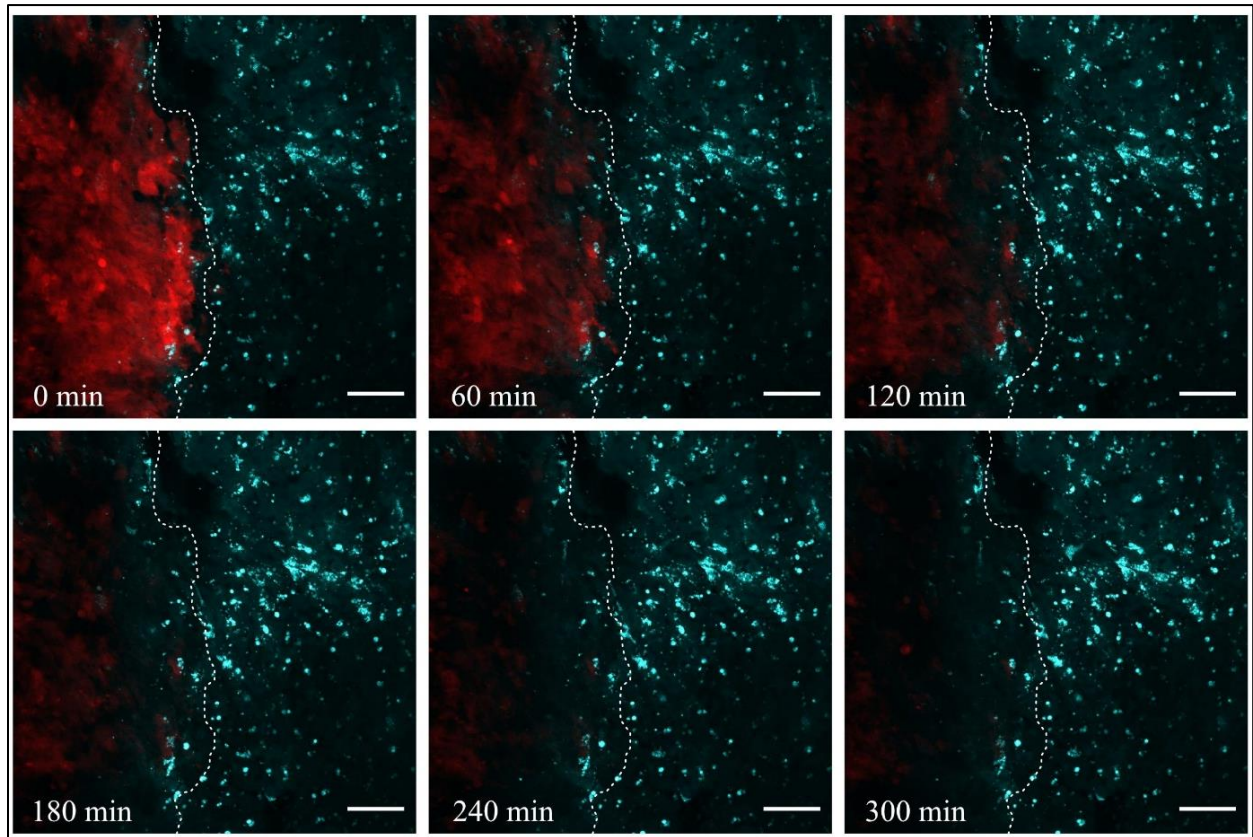


**Figure 24.** Photobleaching during two-photon time-lapse live-cell imaging on PCLM explants cultured in standard condition 2. Tumour cells (red) are marked with tdTomato fluorophore. The surrounding liver tissue (cyan) is visualized using second-harmonic generation. The invasion front between the tumour and the liver parenchyma is marked with a white dashed line (scale bar = 60  $\mu\text{m}$ ).



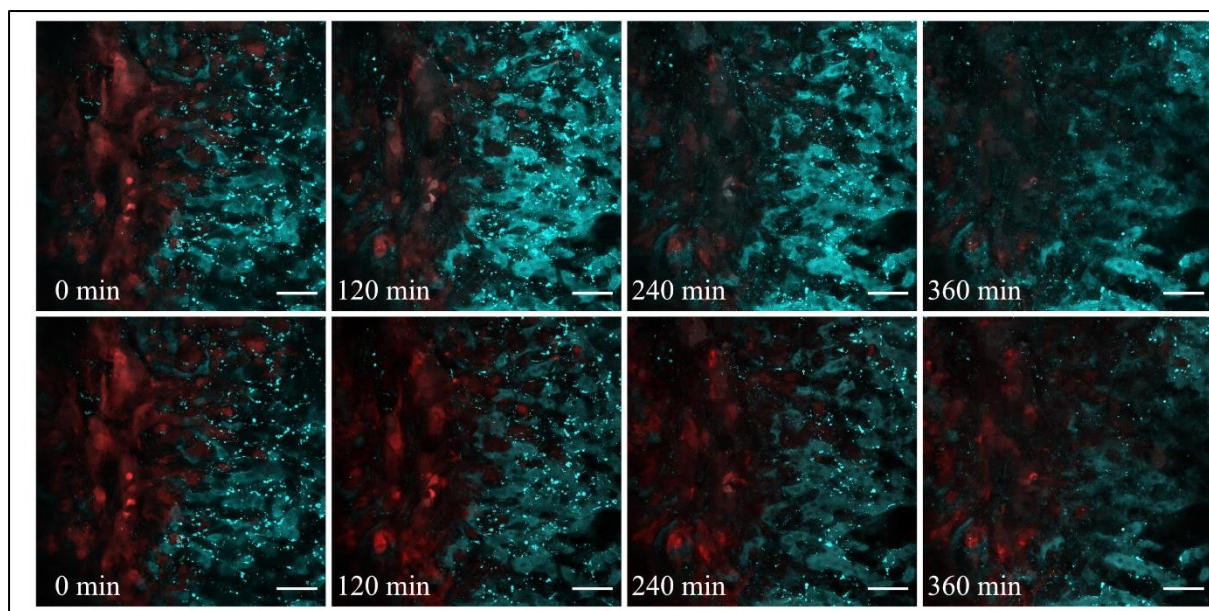


**Figure 25.** Bleach correction in ImageJ software done on two-photon time-lapse live-cell imaging of PCLM explants cultured in standard condition 2. Tumour cells (red) are marked with tdTomato fluorophore. The surrounding liver tissue (cyan) is detected using second-harmonic generation (scale bar = 60  $\mu\text{m}$ ).

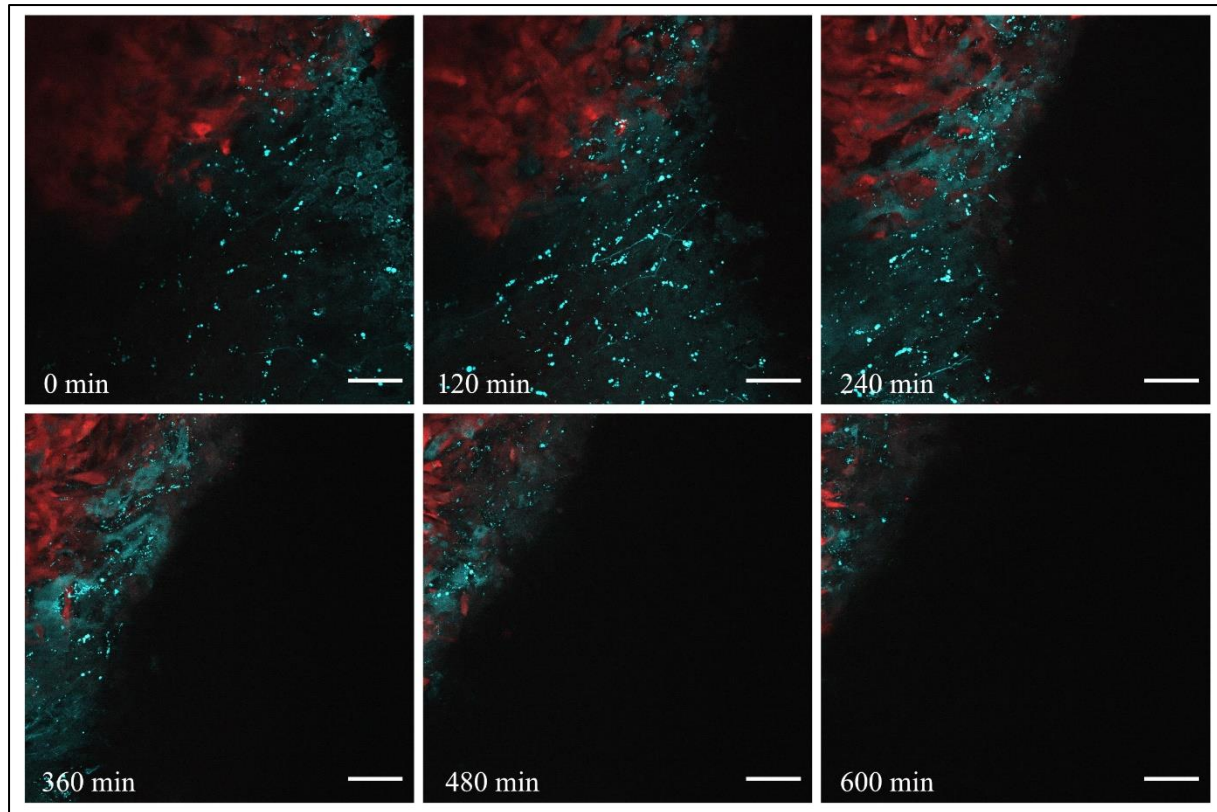


**Figure 26.** Focal drift during two-photon time-lapse live-cell imaging on PCLM explants cultured in standard condition 2. Tumour cells (red) are marked with tdTomato fluorophore. The surrounding liver tissue (cyan) is detected using second-harmonic generation (scale bar = 60 μm).



#### 4.3.2. Cellular movement

After optimising the time-lapse live-cell imaging set-up, PCLM explant cultures were used to detect cancer cell movement into the liver parenchyma (Figs. 27, 28).

Moreover, we visualized the movement of non-tumour cells at the invasion front between tumour and liver tissue (Fig. 29).

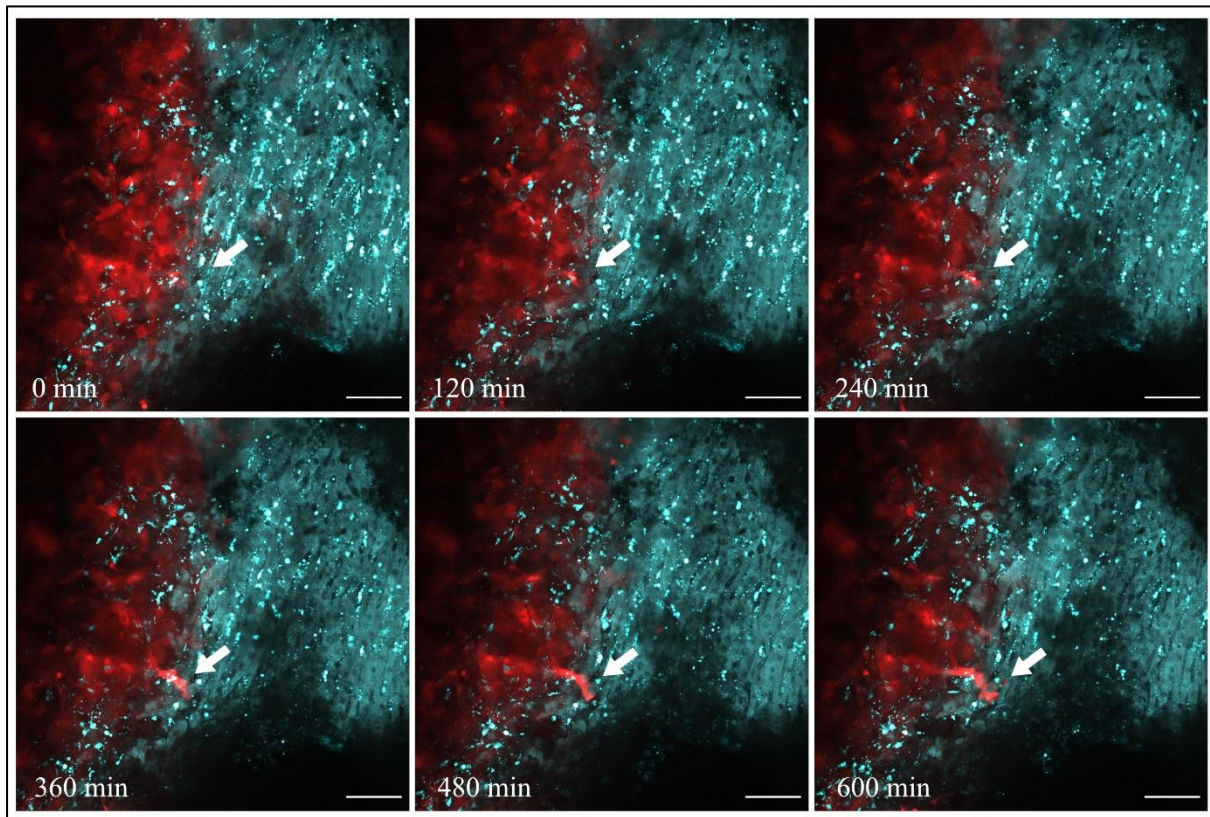


**Figure 27.** Cancer cell movement (marked with an arrow) during two-photon time-lapse live-cell imaging on PCLM explants cultured in standard condition 2. Tumour cells (red) are marked with tdTomato fluorophore. The surrounding tissue (cyan) is detected using second-harmonic generation (scale bar = 60  $\mu\text{m}$  ).

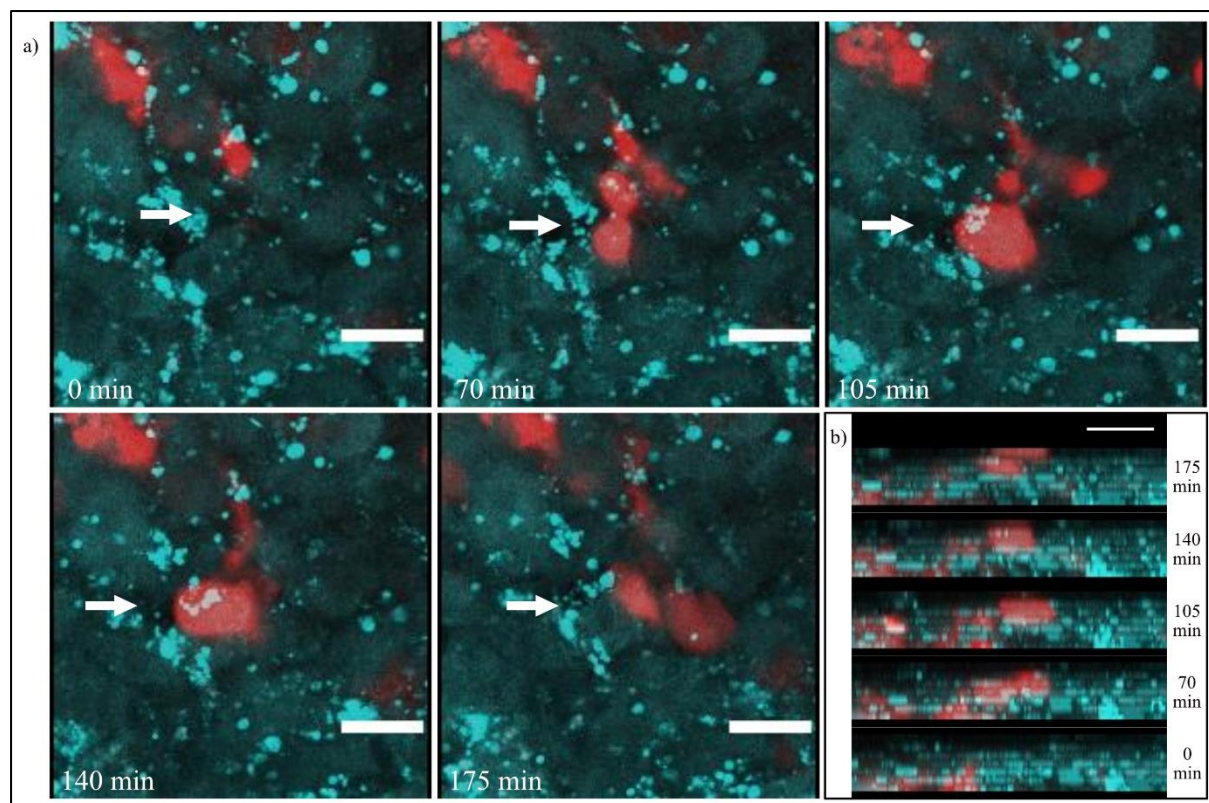


**Figure 28.** (a) Cancer cell movement (white arrow) in X, Y and Z direction during two-photon time-lapse live-cell imaging on PCLM explants cultured in standard condition 2. (b) Interpolation from different Z planes (made in ImageJ software).

Tumour cells (red) are marked with tdTomato fluorophore. The surrounding tissue (cyan) is detected using second-harmonic generation (scale bar = 40  $\mu\text{m}$ ).



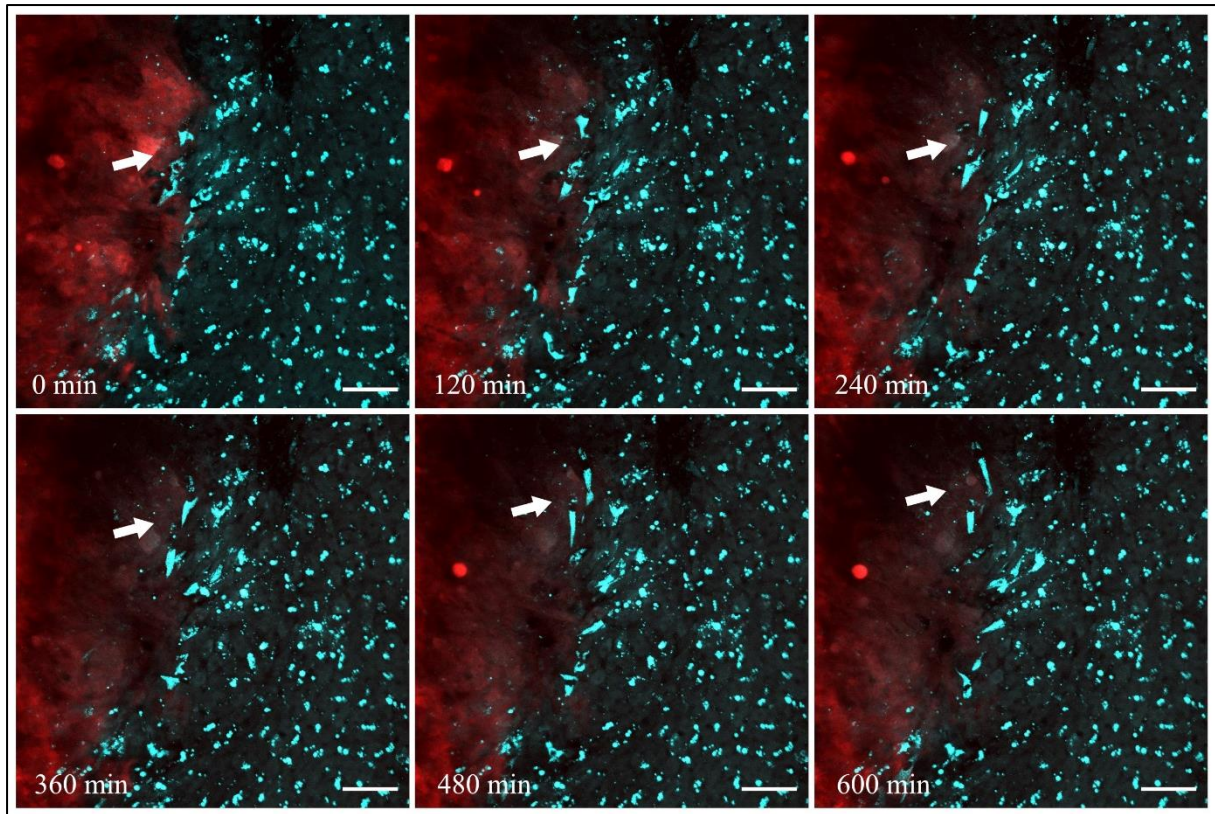


**Figure 29.** Cellular movement of non-tumour cells (white arrow) at the invasion front between the tumour and the liver parenchyma detected during two-photon time-lapse live-cell imaging on PCLM explants cultured in standard condition 2. Tumour cells (red) are marked with tdTomato fluorophore. The surrounding tissue (cyan) is detected using the second harmonic generation (scale bar = 60  $\mu$ m).

## 5. Discussion

In order to better understand the biology of PDAC (Garcia et al., 2020; Nelson et al., 2020) and to develop effective treatment options, there is a need to create appropriate cancer models (Garcia et al., 2020; Nelson et al., 2020; Kokkinos et al., 2021; Yu et al., 2021) that reflect cancer complexity and heterogeneity (Lim et al., 2018). The commonly used *in vivo* and *in vitro* models led to important discoveries in the last decades, however, they also pose various limitations (see Chapter 1.3). In recent years, several research groups developed patient derived PDAC organotypic cultures with promising results (Jiang et al., 2017; Lim et al., 2018; Misra and Moro et al., 2019; Kokkinos et al., 2021). They managed to preserve tissue viability (Lim et al., 2018; Misra and Moro et al., 2019; Kokkinos et al., 2021), morphology, TME (Jiang et al., 2017; Misra and Moro et al., 2019; Kokkinos et al., 2021) and genetic diversity (Kokkinos et al., 2021) for up to four (Misra and Moro et al., 2019), five (Lim et al., 2018), seven (Jiang et al., 2017) and twelve days (Kokkinos et al., 2021). Furthermore, Ghadari et al. utilised genome-wide transcriptome sequencing on patient derived PDAC explant culture and found only a limited number of gene expression changes, proving transcriptional stability of the tissue in culture (Ghadari et al., 2020).

The aim of my master thesis was to establish an organotypic culture of murine PCLM derived from an allograft transplantation model. The general workflow included 1) injection of KPC-T cells into the liver, 2) tissue extraction after ~4 weeks, 3) preparation of PCTS on a vibratome and 4) culturing the tissue slices on filter inserts for up to five days. The key steps in this protocol are transportation, slicing and culturing, all of which can induce stress and artifacts in tumour slices (Lim et al., 2018). Improving the viability and functionality of the tissue (Olinga et al. 1997; Lake and Price, 2013; Starokozhko et al. 2015; Starokozhko et al., 2017) enhances model reproducibility and validity (Johnson and Rabinovitch, 2012). So far, there is no consensus protocol for organotypic cultures (Granitzny et al., 2017) and since different tumours show different characteristics, it was necessary to modify culturing conditions for PDAC liver metastases specifically (Lim et al., 2018).

The first step was to induce PCLM allografts in mice using the ultrasound-guided injection of KPC-T cells into the liver. In theory, in this metastasis model, cancer cells skip several steps of the

metastatic cascade, including EMT, intravasation, migration through the circulation and extravasation. However, all animals injected in this way develop liver metastases, and, importantly, the resulting PCLM are histologically comparable to human PCLM. Alternative methods for PCLM inductions include injection of KPC-T cells into other anatomical sites, such as the tail vein, spleen and heart. The site of injection often dictates the location of metastasis formation. For instance, intravenous injection usually results in pulmonary metastasis, intrasplenic injections in liver metastases and intra-cardiac injections in systemic dissemination (Ayres Pereira and Chio, 2019).

It is important to note that the size of PDAC metastases, extracted approximately four weeks after the injection, varied between different animals (not shown). Potential reasons for this observation are difference in age, sex or weight between animals, the passaging number of KPC-T cells or the time between tumour cell injection and tissue isolation. Passaging of cells leads to genotypic and phenotypic drift resulting e.g. in cells that are more proliferative, aggressive and more prone to metastasize (Wegner et al., 2018; Yu et al., 2021). However, tumour growth is a multifaceted process that depends on many factors and some variability is expected even when using the animals of the same age and cells of the same passage number. Furthermore, variations induced by the circadian rhythm have been described earlier (van de Bovenkamp et al., 2005; Starokozhko et al., 2017). This may be another factor influencing tumour size in the described model, as tissue extraction at the same time of the day was not always possible.

Extracted tissue was kept on ice during transport and slice preparation until placed in culture. Cold temperatures prevent warm ischemia and consequent tissue deterioration (Graaf et al., 2007; Granitzny et al., 2017; Palma et al., 2019) and lead to higher tissue viability (Steaneva et al., 2018). Moreover, tissue was not kept outside the culture for > 5 hours, as a long time delay at this step could result in low viability (Lim et al., 2018; Wu et al., 2018).

Manually cut PCLM explants survived up to 96 hours in culture. Both liver and tumour tissue maintained their structural integrity and tissue morphology. Tumour tissue, at 96 hours in culture, was generally heterogeneous with apoptotic and necrotic regions as well as proliferating tumour cells. However, there are several reasons why the manual tissue cutting procedure was discontinued. Since it is difficult to produce tissue explants of similar size the reproducibility of the results obtained with these explants is lower than that of precision-cut explant cultures. Furthermore, there is a risk of separating tumour and liver tissue during scalpel sectioning. That is

especially problematic since the invasion front between the tumour tissue and liver parenchyma is of interest for studying tumour cell invasion into the liver.

First tissue slices, prepared manually by Otto Warburg in 1923, showed limited reproducibility and viability. Hence, their application in research started to increase only after the introduction of different automated tissue slicers (Graaf et al., 2007) such as the Krumdieck slicer (de Graaf et al., 2010; Fisher and Vickers, 2013), Brendel/Vitron slicer (Lake and Price, 2013) and vibrating-blade microtome or vibratome (Pearen et al., 2020). Therefore, automated sectioning, more specifically vibratome sectioning, was used in the remaining parts since it uses lateral blade vibration to minimise tissue tearing (Pearen et al., 2020). Furthermore, tissue thickness was optimized, since it influences nutrient and oxygen supply to all cell layers in the tissue (de Graaf et al., 2010; Fisher and Vickers, 2013) and consequently affect tissue viability (Guo et al., 2007; Fisher and Vickers, 2013) as well as live-cell imaging. Tissue thickness above 400  $\mu\text{m}$  can result in necrosis in the inner parts due to the lack of nutrients and oxygen. Tissue thickness below 100  $\mu\text{m}$  can result in a high ratio of damaged versus healthy cells (Sadasivan et al., 2015; Naipal et al., 2016). With the help of healthy liver tissue, we concluded that tissue sections of <250  $\mu\text{m}$  thicknesses were too damaged and hard to manipulate (results not shown). Hence, 300  $\mu\text{m}$  and 400  $\mu\text{m}$  thicknesses of unaffected liver and tumour tissue sections cultured in DMEM/F12 medium were compared using MTT assay. The MTT assay results showed that liver tissue sections of 300  $\mu\text{m}$  have significantly higher metabolic activity compared to 400  $\mu\text{m}$  tissue sections, while tumour sections did not show any significant difference. A probable explanation is that 400  $\mu\text{m}$  thick liver sections did not receive sufficient amounts of nutrient and oxygen and had lower viability in inner tissue regions. This result is in line with similar experiments showing that lower thicknesses (around 200-250  $\mu\text{m}$ ) were more beneficial for liver slices (de Graaf et al., 2010; Fisher and Vickers, 2013; Lake and Price, 2013; Palma et al., 2019). To further analyse unaffected liver tissue sections of different thicknesses H&E, Ki67 and clCasp3 IHC staining was performed. Explants of both thicknesses cultured for five days showed more damage as assessed by H&E stainings compared to uncultured sections and sections cultured for two days. This may be the result of tissue folding in the culture that complicated flat paraffin-embedded sectioning for immunohistochemistry. Both Ki67 and clCasp3 IHC stainings on cultured sections contained a strong background signal and scarce true signal. Since IHC results were not quantifiable, definitive conclusions could not be derived from these results.

After sectioning, precision-cut tissue sections were transferred to 6-well plates with filter inserts. These inserts enable constant diffusion of media and oxygen to tissue slices from beneath (Lim et al., 2018; Misra and Moro et al., 2019). On the contrary, PDAC tissue slices cultured on gelatine sponges soaked in culturing media have recently shown promising results (Kokkinos et al., 2021). In order to optimise the culturing conditions, we tested two different, widely used culturing media (DMEM/F12 and WME) and two different serum concentrations (10% and 5%) on 300 µm thick unaffected liver and tumour tissue sections using MTT assay. DMEM/F12 medium is commonly used with PDAC cell (Ehrenberg et al., 2019) and PDAC tissue cultures (Sivakumar et al., 2019), while Williams Medium E is often used with liver tissue cultures (Elferink et al., 2011, Huang et al., 2019; Bigaeva et al., 2019). MTT assay results showed that tumour tissue sections have similar metabolic activity in all culturing conditions, while unaffected liver tissue sections show significantly higher metabolic activity in 10% serum and in WME, compared to DMEM/F12 medium. There are several differences in DMEM/F12 (Gibco, REF 11320) and WME (Gibco, REF 32551) medium compositions that could contribute to these results. WME medium E contains certain vitamins like ascorbic acid, ergocalciferol, menadione sodium sulfate and vitamin A, that DMEM/F12 medium lacks. Of those, retinoids (vitamin A and its metabolites) are vital for normal liver integrity and are involved in several key processes such as fatty acid metabolism, iron metabolism, insulin resistance and 5' AMP-activated protein kinase (AMPK) activation (Shiota., 2017). To further analyse unaffected liver sections cultured in different media and serum concentrations we performed H&E, Ki67 and cIcasp3 IHC stainings. In all culturing conditions, tissue sections showed a higher degree of damage after five days of culture, as expected from previous experiments. Like in previous experiments, Ki67 and cIcasp3 IHC stainings contained a strong background signal. However, these IHC results were not quantified and therefore no certain conclusion can be given.

One to three hours after sectioning, the culture medium was exchanged as a preincubation step. That is recommended in the literature to stabilize the tissue (Carranza-Rosales et al., 2010) and to remove cell debris and enzymes from the cutting procedure (van Midwoud et al., 2011; Koch et al., 2014; Starokozhko et al., 2017). It was also shown that the intracellular adenosine triphosphate (ATP) concentration is restored during the preincubation step (de Bovenkamp et al., 2008; van Midwoud et al., 2011; Elferink et al., 2011; Koch et al., 2014; Vatakuti et al., 2016; Starokozhko et al., 2017).

Other aspects to consider for further optimising the murine PCLM culture set-up that have not been examined in this project include, for example, the impact of mitogenic factors in the culturing media, which could induce non-physiological conditions (Misra and Moro et al., 2019). Established PDAC explant cultures use supplements in the culturing media such as insulin (Lim et al., 2018; Misra and Moro et al., 2019; Kokkinos et al., 2021), epidermal growth factor (Lim et al., 2018) and hydrocortisone (Lim et al., 2018; Kokkinos et al., 2021). Moreover, dynamic cultures improve nutrient and oxygen exchange in the tissue and consequently increase tissue viability (Vickers et al., 2011; Paish et al., 2019). For instance, Naipal et al. found more proliferating cells in cultures exposed to a continuous movement as opposed to stationary culture (Naipal et al., 2016).

MTT assay, utilised as a validation assay in this research, is a colourimetric assay for assessing cell metabolic activity through the reduction of MTT into insoluble form formazan (Wu et al., 2018). Other assays, including viability and functionality test, could be used to further validate this model. Well-known viability tests include ATP level measurement (Starokozhko et al., 2017; Vickers et al., 2018, Gore et al., 2019), lactate dehydrogenase (LDH) leakage (Starokozhko et al., 2017; Zárýbnický et al., 2019) and glutathione (GSH) level measurement (Vickers et al., 2018). Commonly used functionality tests are albumin production measurement (Granitzny et al., 2017; Starokozhko et al., 2017; Paish et al., 2019), chemokine and cytokines measurement (Temann et al., 2017; Bigaeva et al., 2019) and urea production measurement (Hattersley et al., 2011).

After optimising the culturing setup, IHC and mRNA ISH were performed on PCLM explants, to characterise the model. Both tumour and liver tissue maintained their general architecture and cellular composition throughout five days of culturing. Tumour tissue showed fewer necrotic regions and no separation from liver tissue, compared to initial results with manually cut sections. Moreover, it resembled human PCLM in terms of tissue morphology, heterogeneity and differentiation. Tumour tissue, and liver tissue to a lower extent, contained proliferating cells after five days in culture. However, the percentage of proliferating cells in the tumour tissue significantly decreased after five days of culturing, from ~ 54% (before cultivation, day 0) to ~9%. This result is similar to the one of Misra and Moro et al., which was based on culturing well-differentiated patient derived PDAC tumour tissue for up to four days (Misra and Moro et al., 2019). On the other hand, Lim et al. found no significant changes in Ki67 expression in patient derived PDAC explant culture until five days of culturing (Lim et al., 2018). Moreover, it appears that the tumour tissue



located closer to the liver contained more proliferating cells than the tumour centre. Tumour tissue in directly fixed samples and samples cultured for two days contained cIcasp3 positive cells. However, the frequency of apoptosis notably increased after five days of culturing. Interestingly, Lim et al. detected a significant increase in apoptosis after one day of culture, and no other significant changes until nine days of culture (Lim et al., 2018).

Furthermore, we performed desmin (stromal cell marker) IHC staining and *Alpi* (more differentiated tumour cell marker) mRNA ISH to test for the presence of different cell types. We found that stromal cells are present after five days in culture in a comparable amount to directly fixed sections. More differentiated tumour cells are present after five days in culture, however, in lower numbers compared to directly fixed samples.

As a proof-of-principle, live-cell confocal imaging on murine PCLM explant culture was performed and used to detect tumour cell invasion into the liver. It was crucial to find the optimal imaging set-up, including laser wavelength and power, detection wavelengths, detector gain, offset and digital gain, to minimize photobleaching. However, the degree of sample variability regarding photobleaching was still very high. Therefore, ImageJ software was utilised to correct for it. Another challenge during live-cell imaging optimisation was focal drift. This could be improved by leaving the sample for a few hours in the inbuilt incubator until the temperature completely stabilized to 37 °C before starting the time-lapse imaging. Furthermore, the ECM used to stabilize the tissue sections was changed to further stabilize the explant during imaging. 80% collagen was too soft and often resulted in focal drift. However, 4% low melting point agarose seemed to improve the results by diminishing or eliminating focal drift.

Based on these optimisations, we succeeded in detecting the movement of different cell types, including cancer cells and stromal cells. These results could be of importance in future experiments. For instance, changes in cancer cell movement could be analysed in response to different treatment options.

Together, the results demonstrate that murine PCLM explant culture, as established and characterised here, maintains morphological integrity, tissue viability and cellular heterogeneity of the *in vivo* state, and resembles human tissue for up to five days. Tumour tissue retains stromal cells and more differentiated tumour cells. Moreover, tumour cells and surrounding stromal cells

move between the tissue compartments during culturing. This model, therefore, recapitulates many important characteristics of PCLM and could be used to study the biology of this disease and potentially for the development of new therapeutic approaches, with a focus on the liver-tumour interface. Furthermore, it could lower the number of animals needed for the research, since many tissue sections prepared from the same animal could serve as replicates. Organotypic cultures enable easy straightforward drug testing since they are an open system (Lim et al., 2018). This explant culture can be analysed with live-cell imaging, and as such, it enables real-time mechanistic studies. However, it does come with several limitations. It does not possess vascular or lymphatic circulation, hence the immune microenvironment of organotypic slices is limited (Jiang et al., 2017). Since tumour tissue is very heterogeneous tissue sections prepared from one tumour do not contain the same composition of different regions present *in vivo* state (Lim et al., 2018; Misra and Moro et al., 2019). As a result, tissue sections from different tumour regions could respond differently to certain treatments (Jiang et al., 2017).

Finally, PCLM explant culture models could be prepared with patient samples as well, similar to patient derived PDAC explant cultures established in recent years (Jiang et al., 2017; Lim et al., 2018; Misra and Moro et al., 2019; Kokkinos et al., 2021). However, resected patient tissue has a limited volume that allows the preparation of only a limited number of sections, making large-scale drug screenings challenging (Lim et al., 2018). Besides, in around 80-85% of PDAC patients, diagnosis is done via needle biopsy specimens, as tumours are not resectable by surgery (Lim et al., 2018; Kokkinos et al., 2021). In these cases, it should be possible to prepare an organotypic culture from biopsy specimens (Lim et al., 2018).

## 6. Conclusions

- The optimal settings for murine PDAC liver metastases explant model were identified as 300  $\mu\text{m}$  thick precision-cut tissue slices cultured in William's Medium E with GlutaMAX (Gibco, REF 32551) supplemented with 10% fetal bovine serum (Sigma-Aldrich, F9665) and 1% of Penicillin-Streptomycin (PEST) antibiotics (Cytiva, HyClone™, Cat No: SV30010)
- Murine PCLM explants preserve their structural integrity and morphology during five days of culturing and recapitulate central aspects of human metastases. They resemble the human patient tissue. During culturing the number of proliferating cells is gradually decreasing, while the number of apoptotic cells is gradually increasing. Furthermore, these explants preserve their cellular heterogeneity and contain stromal cells as well as more differentiated tumour cells after five days in culture.
- This model can be utilised to study tumour cell movement using time-lapse two-photon confocal microscopy.

## References

Aguirre, A.J. and Collisson, E.A., 2017. Advances in the genetics and biology of pancreatic cancer. *The Cancer Journal*, 23(6), pp.315-320.

Ayres Pereira, M. and Chio, I.I.C., 2019. Metastasis in pancreatic ductal adenocarcinoma: Current standing and methodologies. *Genes*, 11(1), p.6.

Barbazán, J., Alonso-Alconada, L., Elkhatib, N., Geraldo, S., Gurchenkov, V., Glentis, A., van Niel, G., Palmulli, R., Fernández, B., Viaño, P. and Garcia-Caballero, T., 2017. Liver metastasis is facilitated by the adherence of circulating tumor cells to vascular fibronectin deposits. *Cancer research*, 77(13), pp.3431-3441.

Bazzichetto, C., Conciatori, F., Luchini, C., Simionato, F., Santoro, R., Vaccaro, V., Corbo, V., Falcone, I., Ferretti, G., Melisi, D. and Scarpa, A., 2020. From genetic alterations to tumor microenvironment: the Ariadne's string in pancreatic cancer. *Cells*, 9(2), p.309.

Bigaeva, E., Gore, E., Simon, E., Zwick, M., Oldenburger, A., de Jong, K.P., Hofker, H.S., Schlepütz, M., Nicklin, P., Boersema, M. and Rippmann, J.F., 2019. Transcriptomic characterization of culture-associated changes in murine and human precision-cut tissue slices. *Archives of toxicology*, 93(12), pp.3549-3583.

Borazanci, E., Dang, C.V., Robey, R.W., Bates, S.E., Chabot, J.A. and Von Hoff, D.D., 2017. Pancreatic cancer: "a riddle wrapped in a mystery inside an enigma". *Clinical Cancer Research*, 23(7), pp.1629-1637.

Brodts, P., 2016. Role of the microenvironment in liver metastasis: from pre-to prometastatic niches. *Clinical Cancer Research*, 22(24), pp.5971-5982.

Brosens, L.A., Hackeng, W.M., Offerhaus, G.J., Hruban, R.H. and Wood, L.D., 2015. Pancreatic adenocarcinoma pathology: changing “landscape”. *Journal of gastrointestinal oncology*, 6(4), p.358.

Bulle, A. and Lim, K.H., 2020. Beyond just a tight fortress: contribution of stroma to epithelial-mesenchymal transition in pancreatic cancer. *Signal Transduction and Targeted Therapy*, 5(1), pp.1-12.

Carranza-Rosales, P., Santiago-Mauricio, M.G., Guzmán-Delgado, N.E., Vargas-Villarreal, J., Lozano-Garza, G., Ventura-Juárez, J., Balderas-Rentería, I., Morán-Martínez, J. and Gandolfi, A.J., 2010. Precision-cut hamster liver slices as an ex vivo model to study amoebic liver abscess. *Experimental parasitology*, 126(2), pp.117-125.

Ciner, A.T., Jones, K., Muschel, R.J. and Brodt, P., 2021. The unique immune microenvironment of liver metastases: challenges and opportunities. *Seminars in Cancer Biology*, 71, pp. 143-156.

Clark, A.M., Ma, B., Taylor, D.L., Griffith, L. and Wells, A., 2016. Liver metastases: Microenvironments and ex-vivo models. *Experimental Biology and Medicine*, 241(15), pp.1639-1652.

Clarke, M.A. and Fisher, J., 2020. Executable cancer models: successes and challenges. *Nature Reviews Cancer*, 20(6), pp.343-354.

Costa-Silva, B., Aiello, N.M., Ocean, A.J., Singh, S., Zhang, H., Thakur, B.K., Becker, A., Hoshino, A., Mark, M.T., Molina, H. and Xiang, J., 2015. Pancreatic cancer exosomes initiate pre-metastatic niche formation in the liver. *Nature cell biology*, 17(6), pp.816-826.

Deer, E.L., González-Hernández, J., Coursen, J.D., Shea, J.E., Ngatia, J., Scaife, C.L., Firpo, M.A. and Mulvihill, S.J., 2010. Phenotype and genotype of pancreatic cancer cell lines. *Pancreas*, 39(4), pp.425-435.

De Graaf, I.A., Olinga, P., De Jager, M.H., Merema, M.T., De Kanter, R., Van De Kerkhof, E.G. and Groothuis, G.M., 2010. Preparation and incubation of precision-cut liver and intestinal slices for application in drug metabolism and toxicity studies. *Nature protocols*, 5(9), pp.1540-1551.

Elferink, M.G.L., Olinga, P., Van Leeuwen, E.M., Bauerschmidt, S., Polman, J., Schoonen, W.G., Heisterkamp, S.H. and Groothuis, G.M.M., 2011. Gene expression analysis of precision-cut human liver slices indicates stable expression of ADME-Tox related genes. *Toxicology and applied pharmacology*, 253(1), pp.57-69.

Fisher, R.L. and Vickers, A.E., 2013. Preparation and culture of precision-cut organ slices from human and animal. *Xenobiotica*, 43(1), pp.8-14.

Fokas, E., O'Neill, E., Gordon-Weeks, A., Mukherjee, S., McKenna, W.G. and Muschel, R.J., 2015. Pancreatic ductal adenocarcinoma: From genetics to biology to radiobiology to oncoimmunology and all the way back to the clinic. *Biochimica et Biophysica Acta (BBA)-Reviews on Cancer*, 1855(1), pp.61-82.

Frappart, P.O. and Hofmann, T.G., 2020. Pancreatic Ductal Adenocarcinoma (PDAC) Organoids: The Shining Light at the End of the Tunnel for Drug Response Prediction and Personalized Medicine. *Cancers*, 12(10), p.2750.

Garcia, P.L., Miller, A.L. and Yoon, K.J., 2020. Patient-derived xenograft models of pancreatic cancer: Overview and comparison with other types of models. *Cancers*, 12(5), p.1327.

Ghaderi, M., Moro, C.F., Elduayen, S.P., Hultin, E., Verbeke, C.S., Björnstedt, M. and Dillner, J., 2020. Genome-wide transcriptome profiling of ex-vivo precision-cut slices from human pancreatic ductal adenocarcinoma. *Scientific Reports*, 10(1), pp.1-8.

Graaf, I.A.D., Groothuis, G.M. and Olinga, P., 2007. Precision-cut tissue slices as a tool to predict metabolism of novel drugs. *Expert opinion on drug metabolism & toxicology*, 3(6), pp.879-898.

De Graaf, I.A., Olinga, P., De Jager, M.H., Merema, M.T., De Kanter, R., Van De Kerkhof, E.G. and Groothuis, G.M., 2010. Preparation and incubation of precision-cut liver and intestinal slices for application in drug metabolism and toxicity studies. *Nature protocols*, 5(9), p.1540.

Granitzny, A., Knebel, J., Schaudien, D., Braun, A., Steinberg, P., Dasenbrock, C. and Hansen, T., 2017. Maintenance of high quality rat precision cut liver slices during culture to study hepatotoxic responses: Acetaminophen as a model compound. *Toxicology in Vitro*, 42, pp.200-213.

Guo, Y., Wang, H. and Zhang, C., 2007. Establishment of rat precision-cut fibrotic liver slice technique and its application in verapamil metabolism. *Clinical and Experimental Pharmacology and Physiology*, 34(5-6), pp.406-413.

Haeno, H., Gonen, M., Davis, M.B., Herman, J.M., Iacobuzio-Donahue, C.A. and Michor, F., 2012. Computational modeling of pancreatic cancer reveals kinetics of metastasis suggesting optimum treatment strategies. *Cell*, 148(1-2), pp.362-375.

Hall, J.E., 2015. Pocket Companion to Guyton & Hall Textbook of Medical Physiology E-Book. Elsevier Health Sciences.

Hattersley, S.M., Greenman, J. and Haswell, S.J., 2011. Study of ethanol induced toxicity in liver explants using microfluidic devices. *Biomedical microdevices*, 13(6), pp.1005-1014.

Haykal, M.M., Nahmias, C., Varon, C. and Martin, O.C., 2020. Organotypic Modeling of the Tumor Landscape. *Frontiers in Cell and Developmental Biology*, 8, p.1406.

Hessmann, E., Buchholz, S.M., Demir, I.E., Singh, S.K., Gress, T.M., Ellenrieder, V. and Neesse, A., 2020. Microenvironmental determinants of pancreatic cancer. *Physiological reviews*, 100(4), pp.1707-1751.

Hingorani, S.R., Wang, L., Multani, A.S., Combs, C., Deramaudt, T.B., Hruban, R.H., Rustgi, A.K., Chang, S. and Tuveson, D.A., 2005. Trp53R172H and KrasG12D cooperate to promote

chromosomal instability and widely metastatic pancreatic ductal adenocarcinoma in mice. *Cancer cell*, 7(5), pp.469-483.

Houg, D.S. and Bijlsma, M.F., 2018. The hepatic pre-metastatic niche in pancreatic ductal adenocarcinoma. *Molecular cancer*, 17(1), pp.1-18.

Huang, X., Cai, H., Ammar, R., Zhang, Y., Wang, Y., Ravi, K., Thompson, J. and Jarai, G., 2019. Molecular characterization of a precision-cut rat liver slice model for the evaluation of antifibrotic compounds. *American Journal of Physiology-Gastrointestinal and Liver Physiology*, 316(1), pp.G15-G24.

Hwang, C.I., Boj, S.F., Clevers, H. and Tuveson, D.A., 2016. Preclinical models of pancreatic ductal adenocarcinoma. *The Journal of pathology*, 238(2), pp.197-204.

Iacobuzio-Donahue, C.A., 2012. Genetic evolution of pancreatic cancer: lessons learnt from the pancreatic cancer genome sequencing project. *Gut*, 61(7), pp.1085-1094.

Jain, M., Venkataraman, J., Varghese, J., Vij, M., Reddy, M.S. and Rela, M., 2020. Explant liver evaluation decodes the mystery of cryptogenic cirrhosis!. *JGH Open*, 4(1), pp.39-43.

Jiang, X., Seo, Y.D., Chang, J.H., Coveler, A., Nigjeh, E.N., Pan, S., Jalikis, F., Yeung, R.S., Crispe, I.N. and Pillarisetty, V.G., 2017. Long-lived pancreatic ductal adenocarcinoma slice cultures enable precise study of the immune microenvironment. *Oncoimmunology*, 6(7), p.e1333210.

Johnson, S. and Rabinovitch, P., 2012. Ex vivo imaging of excised tissue using vital dyes and confocal microscopy. *Current protocols in cytometry*, 61(1), pp.9-39.

Kenerson, H.L., Sullivan, K.M., Seo, Y.D., Stadel, K.M., Ussakli, C., Yan, X., Lausted, C., Pillarisetty, V.G., Park, J.O., Riehle, K.J. and Yeh, M., 2020. Tumor slice culture as a biologic surrogate of human cancer. *Annals of Translational Medicine*, 8(4).



Khan, A.A., Liu, X., Yan, X., Tahir, M., Ali, S. and Huang, H., 2021. An overview of genetic mutations and epigenetic signatures in the course of pancreatic cancer progression. *Cancer and Metastasis Reviews*, pp.1-28.

Koch, A., Saran, S., Tran, D.D.H., Klebba-Färber, S., Thiesler, H., Sewald, K., Schindler, S., Braun, A., Klopffleisch, R. and Tamura, T., 2014. Murine precision-cut liver slices (PCLS): a new tool for studying tumor microenvironments and cell signaling ex vivo. *Cell Communication and Signaling*, 12(1), pp.1-13.

Kokkinos, J., Sharbeen, G., Haghighi, K.S., Ignacio, R.M.C., Kopecky, C., Gonzales-Aloy, E., Youkhana, J., Timpson, P., Pereira, B.A., Ritchie, S. and Pandzic, E., 2021. Ex vivo culture of intact human patient derived pancreatic tumour tissue. *Scientific reports*, 11(1), pp.1-15.

Kong, K., Guo, M., Liu, Y. and Zheng, J., 2020. Progress in animal models of pancreatic ductal adenocarcinoma. *Journal of Cancer*, 11(6), p.1555.

Kos, K. and de Visser, K.E., 2021. Neutrophils create a fertile soil for metastasis. *Cancer Cell*.

Krempley, B.D. and Yu, K.H., 2017. Preclinical models of pancreatic ductal adenocarcinoma. *Chinese clinical oncology*, 6(3), pp.25-25.

Lafaro, K.J. and Melstrom, L.G., 2019. The paradoxical web of pancreatic cancer tumor microenvironment. *The American journal of pathology*, 189(1), pp.44-57.

Lake, B.G. and Price, R.J., 2013. Evaluation of the metabolism and hepatotoxicity of xenobiotics utilizing precision-cut slices. *Xenobiotica*, 43(1), pp.41-53.

Lim, C.Y., Chang, J.H., Lee, W.S., Lee, K.M., Yoon, Y.C., Kim, J. and Park, I.Y., 2018. Organotypic slice cultures of pancreatic ductal adenocarcinoma preserve the tumor microenvironment and provide a platform for drug response. *Pancreatology*, 18(8), pp.913-927.

Lippi, G. and Mattiuzzi, C., 2020. The global burden of pancreatic cancer. *Archives of Medical Science: AMS*, 16(4), p.820.

Mejia, I., Bodapati, S., Chen, K.T. and Díaz, B., 2020. Pancreatic adenocarcinoma invasiveness and the tumor microenvironment: from biology to clinical trials. *Biomedicines*, 8(10), p.401.

Mielgo, A. and Schmid, M.C., 2020. Liver tropism in cancer: the hepatic metastatic niche. *Cold Spring Harbor perspectives in medicine*, 10(3).

Milette, S., Sicklick, J.K., Lowy, A.M. and Brodt, P., 2017. Molecular pathways: targeting the microenvironment of liver metastases. *Clinical Cancer Research*, 23(21), pp.6390-6399.

Misra, S., Moro, C.F., Del Chiaro, M., Pouso, S., Sebestyén, A., Löhr, M., Björnstedt, M. and Verbeke, C.S., 2019. Ex vivo organotypic culture system of precision-cut slices of human pancreatic ductal adenocarcinoma. *Scientific reports*, 9(1), pp.1-16.

Morris, J.P., Wang, S.C. and Hebrok, M., 2010. KRAS, Hedgehog, Wnt and the twisted developmental biology of pancreatic ductal adenocarcinoma. *Nature Reviews Cancer*, 10(10), pp.683-695.

Naipal, K.A., Verkaik, N.S., Sánchez, H., van Deurzen, C.H., den Bakker, M.A., Hoeijmakers, J.H., Kanaar, R., Vreeswijk, M.P., Jager, A. and van Gent, D.C., 2016. Tumor slice culture system to assess drug response of primary breast cancer. *BMC cancer*, 16(1), pp.1-13.

Nelson, S.R., Zhang, C., Roche, S., O'Neill, F., Swan, N., Luo, Y., Larkin, A., Crown, J. and Walsh, N., 2020. Modelling of pancreatic cancer biology: Transcriptomic signature for 3D PDX-derived organoids and primary cell line organoid development. *Scientific reports*, 10(1), pp.1-12.

Paish, H.L., Reed, L.H., Brown, H., Bryan, M.C., Govaere, O., Leslie, J., Barksby, B.S., Garcia Macia, M., Watson, A., Xu, X. and Zaki, M.Y., 2019. A Bioreactor technology for modeling fibrosis in human and rodent precision-cut liver slices. *Hepatology*, 70(4), pp.1377-1391.

Palma, E., Doornebal, E.J. and Chokshi, S., 2019. Precision-cut liver slices: a versatile tool to advance liver research. *Hepatology international*, 13(1), pp.51-57.

Paoli, C. and Carrer, A., 2020. Organotypic Culture of Acinar Cells for the Study of Pancreatic Cancer Initiation. *Cancers*, 12(9), p.2606.

Pearen, M.A., Lim, H.K., Gratte, F.D., Fernandez-Rojo, M.A., Nawaratna, S.K., Gobert, G.N., Olynyk, J.K., Tirnitz-Parker, J.E. and Ramm, G.A., 2020. Murine precision-cut liver slices as an ex vivo model of liver biology. *JoVE (Journal of Visualized Experiments)*, (157), p.e60992.

Rampetsreiter, P., Casanova, E. and Eferl, R., 2011. Genetically modified mouse models of cancer invasion and metastasis. *Drug Discovery Today: Disease Models*, 8(2-3), pp.67-74.

Sadasivan, S.K., Siddaraju, N., Khan, K.M., Vasamsetti, B., Kumar, N.R., Haridas, V., Reddy, M.B., Baggavalli, S., Oommen, A.M. and Rao, R.P., 2015. Developing an in vitro screening assay platform for evaluation of antifibrotic drugs using precision-cut liver slices. *Fibrogenesis & tissue repair*, 8(1), pp.1-9.

Sakamoto, H., Attiyeh, M.A., Gerold, J.M., Makohon-Moore, A.P., Hayashi, A., Hong, J., Kappagantula, R., Zhang, L., Melchor, J.P., Reiter, J.G. and Heyde, A., 2020. The evolutionary origins of recurrent pancreatic cancer. *Cancer Discovery*, 10(6), pp.792-805.

Sarantis, P., Koustas, E., Papadimitropoulou, A., Papavassiliou, A.G. and Karamouzis, M.V., 2020. Pancreatic ductal adenocarcinoma: Treatment hurdles, tumor microenvironment and immunotherapy. *World Journal of Gastrointestinal Oncology*, 12(2), p.173.

Sewald, K. and Braun, A., 2013. Assessment of immunotoxicity using precision-cut tissue slices. *Xenobiotica*, 43(1), pp.84-97.

Shi, H., Li, J. and Fu, D., 2016. Process of hepatic metastasis from pancreatic cancer: biology with clinical significance. *Journal of cancer research and clinical oncology*, 142(6), pp.1137-1161.

Shiota, G., 2017. Retinoids in liver function. In *Liver Pathophysiology* (pp. 705-713). Academic Press.

Sivakumar, R., Chan, M., Shin, J.S., Nishida-Aoki, N., Kenerson, H.L., Elemento, O., Beltran, H., Yeung, R. and Gujral, T.S., 2019. Organotypic tumor slice cultures provide a versatile platform for immuno-oncology and drug discovery. *OncoImmunology*, 8(12), p.e1670019.

Søreide, K., Primavesi, F., Labori, K.J., Watson, M.M. and Stättner, S., 2019. Molecular biology in pancreatic ductal adenocarcinoma: implications for future diagnostics and therapy. *European Surgery*, 51(3), pp.126-134.

Sperb, N., Tsesmelis, M. and Wirth, T., 2020. Crosstalk between Tumor and Stromal Cells in Pancreatic Ductal Adenocarcinoma. *International journal of molecular sciences*, 21(15), p.5486.

Stamataki, Z. and Swadling, L., 2020. The liver as an immunological barrier redefined by single-cell analysis. *Immunology*, 160(2), pp.157-170.

Starokozhko, V., Abza, G.B., Maessen, H.C., Merema, M.T., Kuper, F. and Groothuis, G.M., 2015. Viability, function and morphological integrity of precision-cut liver slices during prolonged incubation: Effects of culture medium. *Toxicology In Vitro*, 30(1), pp.288-299.

Starokozhko, V., Vatakuti, S., Schievink, B., Merema, M.T., Asplund, A., Synnergren, J., Aspegren, A. and Groothuis, G.M., 2017. Maintenance of drug metabolism and transport functions in human precision-cut liver slices during prolonged incubation for 5 days. *Archives of toxicology*, 91(5), pp.2079-2092.

Stopa, K.B., Kusiak, A.A., Szopa, M.D., Ferdek, P.E. and Jakubowska, M.A., 2020. Pancreatic Cancer and Its Microenvironment—Recent Advances and Current Controversies. *International journal of molecular sciences*, 21(9), p.3218.

Storz, P., 2017. Acinar cell plasticity and development of pancreatic ductal adenocarcinoma. *Nature reviews Gastroenterology & hepatology*, 14(5), pp.296-304.

Temann, A., Golovina, T., Neuhaus, V., Thompson, C., Chichester, J.A., Braun, A. and Yusibov, V., 2017. Evaluation of inflammatory and immune responses in long-term cultured human precision-cut lung slices. *Human vaccines & immunotherapeutics*, 13(2), pp.351-358.

Tomás-Bort, E., Kieler, M., Sharma, S., Candido, J.B. and Loessner, D., 2020. 3D approaches to model the tumor microenvironment of pancreatic cancer. *Theranostics*, 10(11), p.5074.

Van Dam, P.J., Van Der Stok, E.P., Teuwen, L.A., Van den Eynden, G.G., Illemann, M., Frentzas, S., Majeed, A.W., Eefsen, R.L., Van Den Braak, R.R.C., Lazaris, A. and Fernandez, M.C., 2017. International consensus guidelines for scoring the histopathological growth patterns of liver metastasis. *British Journal of Cancer*, 117(10), pp.1427-1441.

Van de Bovenkamp, M., Groothuis, G.M., Draaisma, A.L., Merema, M.T., Bezuijen, J.I., van Gils, M.J., Meijer, D.K., Friedman, S.L. and Olinga, P., 2005. Precision-cut liver slices as a new model to study toxicity-induced hepatic stellate cell activation in a physiologic milieu. *Toxicological Sciences*, 85(1), pp.632-638.

Van Midwoud, P.M., Merema, M.T., Verweij, N., Groothuis, G.M. and Verpoorte, E., 2011. Hydrogel embedding of precision-cut liver slices in a microfluidic device improves drug metabolic activity. *Biotechnology and bioengineering*, 108(6), pp.1404-1412.

Vatakuti, S., Pennings, J.L., Gore, E., Olinga, P. and Groothuis, G.M., 2016. Classification of cholestatic and necrotic hepatotoxicants using transcriptomics on human precision-cut liver slices. *Chemical research in toxicology*, 29(3), pp.342-351.

Vickers, A.E., Fisher, R., Olinga, P. and Dial, S., 2011. Repair pathways evident in human liver organ slices. *Toxicology in Vitro*, 25(7), pp.1485-1492.

Vickers, A.E., Ulyanov, A.V. and Fisher, R.L., 2018. Progression of Repair and Injury in Human Liver Slices. *International journal of molecular sciences*, 19(12), p.4130.

Vidal-Vanaclocha, F., Crende, O., de Durango, C.G., Herreros-Pomares, A., López-Doménech, S., González, Á., Ruiz-Casares, E., Vilboux, T., Caruso, R., Durán, H. and Gil, A., 2020, August. Liver prometastatic reaction: Stimulating factors and responsive cancer phenotypes. In *Seminars in Cancer Biology*. Academic Press.

Wegner, C.S., Hauge, A., Andersen, L.M.K., Huang, R., Simonsen, T.G., Gaustad, J.V. and Rofstad, E.K., 2018. Increasing aggressiveness of patient-derived xenograft models of cervix carcinoma during serial transplantation. *Oncotarget*, 9(30), p.21036.

Westra, I.M., Pham, B.T., Groothuis, G.M.M. and Olinga, P., 2013. Evaluation of fibrosis in precision-cut tissue slices. *Xenobiotica*, 43(1), pp.98-112.

Whatcott, C.J., Diep, C.H., Jiang, P., Watanabe, A., LoBello, J., Sima, C., Hostetter, G., Shepard, H.M., Von Hoff, D.D. and Han, H., 2015. Desmoplasia in primary tumors and metastatic lesions of pancreatic cancer. *Clinical cancer research*, 21(15), pp.3561-3568.

Williamson, T., Sultanpuram, N. and Sendi, H., 2019. The role of liver microenvironment in hepatic metastasis. *Clinical and translational medicine*, 8(1), pp.1-7.



Wu, X., Roberto, J.B., Knupp, A., Kenerson, H.L., Truong, C.D., Yuen, S.Y., Bremmelis, K.J., Tuefferd, M., Chen, A., Horton, H. and Yeung, R.S., 2018. Precision-cut human liver slice cultures as an immunological platform. *Journal of immunological methods*, 455, pp.71-79.

Ying, H., Dey, P., Yao, W., Kimmelman, A.C., Draetta, G.F., Maitra, A. and DePinho, R.A., 2016. Genetics and biology of pancreatic ductal adenocarcinoma. *Genes & development*, 30(4), pp.355-385.

Yonezawa, S., Higashi, M., Yamada, N. and Goto, M., 2008. Precursor lesions of pancreatic cancer. *Gut and liver*, 2(3), p.137.

Yu, Y., Yang, G., Huang, H., Fu, Z., Cao, Z., Zheng, L., You, L. and Zhang, T., 2021. Preclinical models of pancreatic ductal adenocarcinoma: challenges and opportunities in the era of precision medicine. *Journal of Experimental & Clinical Cancer Research*, 40(1), pp.1-13.

Zárybnický, T., Matoušková, P., Ambrož, M., Šubrt, Z., Skálová, L. and Boušová, I., 2019. The selection and validation of reference genes for mRNA and microRNA expression studies in human liver slices using RT-qPCR. *Genes*, 10(10), p.763.

Zheng, X., Carstens, J.L., Kim, J., Scheible, M., Kaye, J., Sugimoto, H., Wu, C.C., LeBleu, V.S. and Kalluri, R., 2015. Epithelial-to-mesenchymal transition is dispensable for metastasis but induces chemoresistance in pancreatic cancer. *Nature*, 527(7579), pp.525-530.

## Curriculum vitae

Born in 1996 in Zagreb (Croatia), I attended the first two grades of high school at First Gymnasium, and the second two at Fifth Mathematical Gymnasium, both in Zagreb. I enrolled in undergraduate studies in Molecular biology (2015), and in graduate studies in Molecular biology (2018), at the Faculty of Science, University of Zagreb. Besides my studies, I did internships in various research topics including evolutionary genetics (Dr. Tomislav Domazet Lošo) at Ruđer Bošković Institute, plant physiology (Ass. Prof. Dr. Željka Vidaković Cifrek), molecular ecology (Dr. Lucija Šerić Jelaska), cartilage regeneration (Ass. Prof. Dr. Inga Marijanović) at Faculty of Science, University of Zagreb. I received the Rector's Award for the research "The effect of mechanical stress on model plant *Arabidopsis thaliana* (L.) Heynh". I did a summer internship at Lab for Animal Evolutionary Ecology at Institut for Evolution and Biodiversity, University of Munster (2018) (project: The effects of individual host experiences and microbiota on pathogen evolution, Prof. dr. Joachim Kurtz) and at Lab for Signalling and cellular heterogeneity in cancer at Karolinska Institutet, Stockholm (2019) (topic: Tumour-microenvironment interactions in gastrointestinal cancers, Dr. med. Marco Gerling), where I did my master thesis research.

I was a demonstrator for two years (2017-18) at Zoology and Physics courses for molecular biology students. I participated in several workshops on Night of Biology. I was a member of the Biology Students Association (BIUS), where I was co-leading the Coleoptera Section. I volunteered as a reviewer at the 5th Croatian tournament of young naturalists organised by the Youth Research Centre. I participated in several conferences; Student congress of neuroscience 'Neuri' 2019, Rijeka (oral presentation: Neuronal differentiation in developing and adult brain), Students' Symposium in Biology and Life Sciences 2019, Zagreb (oral presentation: The effect of mechanical stress on model plant *Arabidopsis thaliana* (L.) Heynh; and part of the organising committee), SymBioSE 2019, Glasgow (poster presentation: Predation on the winter moth *Operophtera brumata* by carabid beetles, centipedes and spiders) and SymBioSE 2020, Groningen, Virtual (oral presentation: The story of winner and loser cells). I have written two review articles for Gyrus (Croatian neuroscience journal run and published by students): "Human brain development" and "Viruses that affect the human brain" that have been accepted for publication.

I was awarded the Zagreb scholarship for excellence from 2017 to 2020 for academic achievements.

Currently, I am working as a Research Assistant in the group for Signalling and cellular heterogeneity in cancer, topic: Breast cancer cells-of-origin and tumour heterogeneity, mentor: Leander Blass.

### Publications:

Andrews, N., Serviss, J.T., Geyer, N., Andersson, A.B., Dzwonkowska, E., Šutevski, I., Heijboer, R., Baryawno, N., Gerling, M. and Enge, M., 2021. An unsupervised and broadly applicable method for physical cell interaction profiling of complex tissues. *Nature Methods* (Accepted, 03.2021.)